Technical Implementation Plan for the VLA Sky Survey

Steven T. Myers, Casey Law, Claire Chandler, Mark Lacy

1. Overview

This working document details the Technical Implementation Plan (TIP) for the VLA Sky Survey (VLASS).

The main Survey Science proposal "The Jansky Very Large Array Sky Survey (VLASS)" contains the science justification and overall description of the survey. This supplementary document describes in more detail the technical issues, project plan, and risks associated with the proposed VLASS.

Version Note: current draft reflects Pilot Survey implementation and updates for the PDR

Version Milestones:

2016-08-25 — draft for the Preliminary Design Review in Sep 2016.

2015-10-02 — draft reflects the revisions to the survey following the Community Review in March 2015.

2015-02-02 — version submitted to Community Review

1.1. High-Level Goals and Requirements

In the original proposal and TIP, the only high-level goals called out were:

- Observe and image the sky with Declination $\delta > -40^\circ$ (33885 square degrees)
- Observe each area of sky three times (epochs) with 32 months (average) between passes
- Produce continuum images with Stokes I rms noise goal of 120μJy for a single epoch
- Produce continuum images with Stokes I rms noise goal of 69μJy for a 3 combined epochs of data

In this updated TIP, we have augmented this with additional goals and requirements to make the boundaries and risks clearer. These are the specifications that have science impact, and are "owned" (for compliance and change control purposes) by the VLASS Project Scientist and the Survey Science Group (SSG). These now consist of:

1. *Goal:* Observe and image the sky with Declination $\delta > -40^\circ$ (33885 square degrees); *Requirement:* Observe and image at least 90% of the sky with Declination $\delta > -40^\circ$ (30496 square degrees).
2. *Goal:* Observe each area of sky three times (epochs) with 32 ($\pm$5) months between passes; *Requirement:* For the area of sky observed, at least 90% must be observed with 3 epochs with with 32 ($\pm$5) months between passes.
3. *Goal:* Produce Quick-Look continuum images with Stokes I theoretical rms noise goal of $\leq$ 120μJy; *Requirement:* Produce Quick-Look continuum images with Stokes I rms noise of $\leq$ 200μJy (+67%) over 80% of the observed sky.

4. *Goal:* Produce single-epoch continuum images with Stokes I theoretical rms noise goal of $\leq 120\mu$Jy; *Requirement:* Produce single-epoch continuum images with Stokes I rms noise of $\leq 168\mu$Jy (+40%) over 90% of the observed sky.

5. *Goal:* Produce multi-epoch continuum images with Stokes I theoretical rms noise goal of 69μJy for 3 full epochs combined; *Requirement:* Produce multi-epoch continuum images with Stokes I rms noise of $\leq 97\mu$Jy (+40%) for 3 full epochs combined over 90% of the sky with 3 full epochs available.

6. *Goal:* Flux density scale (Stokes IQU) calibration accuracy shall be better than 5% over 90% of the observed area; *Requirement:* Flux density scale (Stokes IQU) calibration accuracy shall be better than 10% over 90% of the observed area.

7. *Goal:* Linear Polarized flux density (Stokes Q and U with respect to Stokes I) residual leakage on-axis calibration shall be better than 0.25% over 90% of the observed area; *Requirement:* Linear Polarized flux density (Stokes Q and U with respect to Stokes I) residual leakage on-axis calibration shall be better than 0.75% over 90% of the observed area.

8. *Goal:* Linear Polarization Angle calibration (EVPA= 0.5 $\tan^{-1}(U/Q)$) shall be better than 1° over 90% of the observed area; *Requirement:* Linear Polarization Angle calibration (EVPA= 0.5 $\tan^{-1}(U/Q)$) shall be better than 2° over 90% of the observed area.

9. *Goal:* Geometric mean of the synthesized beam major and minor axis FWHMs to be < 3-arcsec over 90% of the observed area. *Requirement:* Geometric mean of the synthesized beam major and minor axis FWHMs to be < 3-arcsec over 60% of the observed area.

Continuum noise goals are given in terms of "theoretical" noise (i.e. the thermal noise expected in an image given the SEFD over the band at the given elevation and available unflagged visibilities and channels), while requirements are in terms of realized image properties over areas taking into account losses to RFI, failure, and presence of bright sources. It is implied that the spectral cubes made from the same data perform in the same manner scaled by the expected sensitivity in the given bandwidth. The Linear Polarization calibration goals and requirements are upon the calibration measurement and transfer using on-axis observations of calibrators, not upon the final OTFM image properties.

Note that there are other goals and requirements on the delivery of basic data products presented in § 4.1 and Table 13.

2. Sensitivity, Angular Resolution, & Overheads

The following assumptions about the sensitivity, angular resolution, and calibration and slewing overheads are used to calculate the parameters of the survey.

2.1. Point-Source Sensitivity Assumptions

The point-source sensitivity of the Jansky VLA for mosaicking is computed using the procedure given in the "Guide to VLA Observing: Mosaicking"[1] and described below. For continuum (Stokes I) at S-band

[1] `https://science.nrao.edu/facilities/vla/docs/manuals/obsguide/modes/mosaicking`

(2–4 GHz) we assumed in the proposal a raw (on-sky) Survey Speed (SS) of

$$SS = 23.83 \left(\frac{\sigma_I}{120\,\mu\mathrm{Jy/beam}} \right)^2 \mathrm{deg}^2\,\mathrm{hr}^{-1} \tag{1}$$

for an assumed image rms of σ_I (μJy/beam).

2.1.1. Survey Speed

For a large OTF region covered, the raw survey speed SS is calculated from

$$SS = \frac{\Omega_B}{t_{calc}} \tag{2}$$

where t_{calc} is the exposure time at the desired rms imaging depth over the bandwidth assumed, and Ω_B is the effective mosaic beam area. For a Gaussian beam with full-width half-maximum (FWHM) θ_P,

$$\Omega_B = \frac{\pi}{8\,\ln 2}\,\theta_P^2 = 0.5665\,\theta_P^2 \tag{3}$$

and is the area under the square of the Primary Beam (see Mosaicking Guide).

Original Calculation: We used for t_{calc} the exposure time at the desired rms imaging depth as returned by the VLA Exposure Time Calculator[2] (ECT). For the VLASS single-pass continuum depth of 120μJy/beam, the ECT gives t_{calc} = 5.36sec. This assumes 25 antennas available, 1500 MHz of usable bandwidth (after RFI excision) centered at 3 GHz, dual polarization, natural weighting, medium elevation, and worst case summer observing. In the original TIP, the assumed primary beam width of $\theta_P = 15'$ at 3 GHz which was approximate for the classic VLA, giving a Survey Speed of 23.8 deg^2/hour.

Effective Wideband Mosaic Beam Area: The beam width and area are, however, not simply calculated at mid-band (3 GHz). The mosaic imaging process weights the data explicitly by assigned weights (normally related to the rms noise) and implicitly by the beam area at each frequency (as the effective integration time for a channel is proportional to the beam area). This effect was pointed out by Condon (2015) and can simply be calculated through an effective MFS weighted mean beam area over the frequency channels k

$$\bar{\Omega}_B = \frac{\sum_k w_k \Omega_{Bk}}{\sum_k w_k} \tag{4}$$

where for uniform weights w_k =const. and uniform frequency coverage over the band we can approximate by the integral

$$\bar{\Omega}_B = \frac{1}{\nu_{max} - \nu_{min}} \int_{\nu_{min}}^{\nu_{max}} d\nu\,\Omega_B(\nu). \tag{5}$$

Assuming the beam FWHM scales inversely by frequency, then

$$\bar{\Omega}_B = \frac{\nu_0^2}{\nu_{min}\,\nu_{max}}\,\Omega_B(\nu_0) \qquad\qquad \Omega_B(\nu) = \Omega_B(\nu_0)\,\left(\frac{\nu_0}{\nu}\right)^2 \tag{6}$$

or equivalently $\bar{\Omega}_B = \Omega_B(\bar{\nu})$ where $\bar{\nu} = \sqrt{\nu_{min}\,\nu_{max}}$ is the geometric mean frequency. For full S-band ν_{min} =2GHz, ν_{max} =4GHz, and $\nu_{mid} = (\nu_{min} + \nu_{max})/2$ =3GHz then

$$\bar{\Omega}_B = \frac{9}{8}\,\Omega_B(\nu_{mid} = 3\mathrm{GHz}) \qquad\qquad \bar{\theta}_P = \sqrt{\frac{9}{8}}\,\theta_P(\nu_{mid} = 3\mathrm{GHz}) \tag{7}$$

[2] https://science.nrao.edu/facilities/vla/docs/manuals/propvla/determining

(this holds for any 2:1 band relative to the mid-band FWHM).

For the upgraded Jansky VLA, new wide-band feed horns were installed, including the new S-band system. In EVLA Memo 195 (Perley 2016) the measured sizes and polynomial fits to the primary beam over S-band are given, see Fig. 1. What is apparent from this is that the primary beams are narrower than those assumed previously and varying over the band, with the product $\theta_P \nu_{\rm GHz}$ in the range 40.6′–42.9′. At band center, these values give $\theta_P = 13.97'$ at 3 GHz, which is 7% narrower than that assumed in the original TIP and original proposal.

For our new measured $\theta_P = 13.97'$ at 3 GHz, the effective primary beam width we should use for mosaic sensitivity is $\bar{\theta}_P = 14.82'$, which is only 1.2% below the nominal VLA value of 15′ used originally to calculate speeds. We conclude that the survey speed need not be reduced due to the measured beam size, although formally we expect a value closer to

$$SS = \frac{\bar{\Omega}_B}{t_{calc}} = \frac{0.5665\,\bar{\theta}_P^2}{t_{calc}} = 23.21\,\mathrm{deg}^2/\mathrm{hr} \tag{8}$$

for $t_{calc} = 5.36$s from the ECT.

Weighted Wideband Mosaic Beam Area: The ECT currently uses older values estimated for the System Equivalent Flux Density (SEFD) of the array antennas in S-band. Recently, new measured values over the band have been obtained (E. Momjian, Aug. 2016). The S-band SEFD varies over the band with an average of around 350 Jy, lower at the upper end and increasing towards 2GHz. If we use Eq. 4 with a weight $w_k = \sigma_k^{-2}$ where σ_k is the rms noise proportional to the SEFD. If we carry the noise calculation for the mosaic all the way through, we find

$$\bar{\sigma}^{-2} \propto \sum_k \Omega_{Bk}\,\sigma_k^{-2} \propto \Omega_B(\bar{\nu})\,\bar{\nu}^2 \sum_k \nu_k^{-2}\,\sigma_k^{-2} \tag{9}$$

for our beam FWHM scaling inversely by frequency, which in turn suggests that we use the effective weighted SEFD

$$\bar{\mathrm{SEFD}}^{-2} = \frac{1}{N_k} \sum_k \nu_k^{-2}\,\mathrm{SEFD}_k^{-2} \tag{10}$$

which for our measured SEFD spectrum gives $\bar{\mathrm{SEFD}} = 350.73$ Jy. We can then compute the required integration time independent of the ECT

$$t_{calc} = \left(\frac{\bar{\mathrm{SEFD}}}{\sigma_{calc}\,\eta}\right)^2 \frac{1}{4\,N_{bl}\,\Delta\nu} \qquad N_{bl} = \frac{N_{ant}\,(N_{ant}-1)}{2}. \tag{11}$$

For $\sigma_{calc} = 120\mu$Jy, $\eta = 0.92$, $\Delta\nu = 1500$MHz, and $N_{ant} = 26$ (pilot survey testing indicates we can reasonably relax the number of expected antennas from 25 to 26) giving $t_{calc} = 5.18$sec giving a survey speed of $SS = 23.9\mathrm{deg}^2/\mathrm{hr}$ for our weighted beam of $\bar{\theta}_P = 14.8'$.

Summary: The new calculations using the weighted beam and measured weighted SEFD indicate that we can use the original survey speed of $SS = 23.8\mathrm{deg}^2/\mathrm{hr}$, although there is sensitivity to bandwidth loss to RFI and loss of an additional antenna from the array.

Risk: Low We choose to use the previous nominal survey speed of 23.83 deg^2/hour, which was employed in the Pilot observations. However, there are many factors such as number of available antennas and RFI free bandwidth that will have much larger effect on the achieved sensitivity and uniformity, so adoption of this nominal survey speed will have negligible impact on the survey performance in comparison. Full analysis of the Pilot Survey will establish the realized sensitivity.

Table 4: **Polynomial Fits for S-Band**

Freq. MHz	A_0	A_2 $\times 10^{-3}$	A_4 $\times 10^{-7}$	A_6 $\times 10^{-10}$	HWHM	Freq. MHz	A_0	A_2 $\times 10^{-3}$	A_4 $\times 10^{-7}$	A_6 $\times 10^{-10}$	HWHM
2052	1.000	-1.429	7.52	-1.47	21.10	3052	1.000	-1.467	8.05	-1.70	20.87
2180	1.000	-1.389	7.06	-1.33	21.38	3180	1.000	-1.497	8.38	-1.80	20.66
2308						3308	1.000	-1.504	8.37	-1.77	20.58
2436	1.000	-1.377	6.90	-1.27	21.45	3436	1.000	-1.521	8.63	-1.88	20.49
2564	1.000	-1.381	6.92	-1.26	21.42	3564	1.000	-1.505	8.37	-1.75	20.57
2692	1.000	-1.402	7.23	-1.40	21.29	3692	1.000	-1.521	8.51	-1.79	20.44
2820	1.000	-1.433	7.62	-1.54	21.09	3820	1.000	-1.534	8.57	-1.77	20.33
2948	1.000	-1.433	7.46	-1.42	21.03	3948	1.000	-1.516	8.30	-1.66	20.43

Typical rms residual is 0.4%. Typical errors in the four coefficients are .002, .010, .15, and .06 in the units given in the table. The units for HWHM are Arcmin-GHz.

Fig. 1.— The JVLA primary beam measured half-width and polynomial coefficients tabluated over the S-band from EVLA Memo 195 (Perley 2016).

2.1.2. Useable bandwidth

A key parameter that factors into the sensitivity is the amount of useable bandwidth from 2–4 GHz. Standard JVLA guidelines and the VLA Exposure Calculator Tool recommend a value of 1500 MHz, and therefore this is what we used in Equation 2, and was employed to calculate the required observing time to reach a given depth. However, the exact amount of RFI affected frequency space is not yet carefully quantified, and also depends upon direction (antenna pointing direction in Azimuth and Elevation in many cases) and time of day.

As a case in point, the Stripe-82 surveys referenced throughout this TIP (12A-371 PI: Kulkarni, and 13B-370, PI: Hallinan) employed fairly brutal excision, throwing away whole spectral windows. The effective bandwidth used for the imaging of these datasets was around 1350 MHz. If the VLASS employed this level of bandwidth reduction, then we would require an 11% increase in required observing time to reach the specified depths of the survey, or would incur a 5.4% penalty in achieved rms imaging sensitivity. On the other hand, even one extra antenna (26 versus the assumed 25) would provide an effective time increase of 8.3% which gets back most of this loss. In addition, it is worth noting that for many S-band continuum experiments that are run through the production pipeline, only two 128 MHz spectral windows are lost. The effective bandwidth is a function of position on the sky and time of day of observation.

Risk: Medium. We consider this to be medium risk for the VLASS. This is one of the key issues to be resolved in the Test and Development Program (§ 10).

2.1.3. Sensitivity Loss at Low Elevation

The VLA exhibits sensitivity loss at low elevations, in the S-band primarily due to an increase in system temperature from spillover from the over-illuminated secondary. In the calculations used to estimate the required integration time, we have used measured values for this noise increase provided by Rick Perley (private communication).

A more detailed explanation of the sensitivity and observing time calculations are available in an online iPython Notebook.[3]

[3] `http://goo.gl/znDX0i`

2.2. Angular Resolution

The Observational Status Summary (OSS)[4] for the VLA lists the angular resolution (FWHM) for S-band (at 3GHz) as $2.1''$ in B-configuration. This applies to long tracks at high declination using *uniform* weighting (equivalent to a fully filled uv-plane out to the maximum baseline). The current advice given to users in the OSS is "The listed resolutions are appropriate for sources with declinations between -15 and 75 degrees...The approximate resolution for a naturally weighted map is about 1.5 times the numbers listed for $\theta_{\rm HPBW}$. The values for snapshots are about 1.3 times the listed values." These values are derived from the 1995 PhD thesis of Dan Briggs[5] based on classic VLA tests using the narrow continuum bandwidths then available. More careful examination of Briggs' thesis suggests that the resolution for naturally-weighted snapshots is 1.4 times the numbers listed for uniformly-weighted, long track observations in the OSS.

The above standard numbers for uniform weighting, coupled with the Briggs factor of 1.4 for naturally weighted snapshots, imply that we should obtain a naturally weighted resolution of $2.9''$. These are expected to be valid for regions with $-15^\circ < \delta < 75^\circ$, fields outside this range will have degraded resolution (unless observed in a hybrid configuration).

It is not clear how applicable the Briggs thesis numbers are to the wideband JVLA observations proposed here, and so this issue will be further investigated as part of the Test & Development Program (§ 10.1.2). In particular, the Briggs thesis found that "super-uniform" weighting of snapshots would yield a rms sensitivity 1.11 times the naturally weighted values, with an increase of the beam size of only 1.2 times that for uniform weighting. If this holds for VLASS continuum imaging, this would yield resolution of $2.5''$ at an rms image sensitivity level 1.11 times the natural weighting values quoted for the survey components in § 3.

It is the baseline plan to use Briggs weighting with a "robust" parameter $r = 1$ for the Basic Data Products, with differently-weighted images falling under Enhanced Data Products (see below).

2.2.1. Case Study: SDSS Stripe-82 at $\delta = 0^\circ$

In the 13B-370 Stripe-82 B-configuration data[6], we found (at Declination $\delta = 0^\circ$) snapshot synthesized beam sizes (FWHM) of around $3.4'' \times 2.3''$ for natural weighting, with a geometric mean beam size of $2.8''$. This is encouragingly close to the expected values based on the Briggs study. In a small sub-mosaic in a relatively empty part of the sky imaging tests gave geometric mean PSF sizes of $2.6''$ (Briggs robust $r = 1.0$) down to $2.2''$ ($r = 0.5$) with image rms of $81\,\mu$Jy ($r = 1.0$) and $79\,\mu$Jy ($r = 0.5$) respectively. Note that $r = 0.5$ gives slightly better rms due to better sidelobe suppression from the sources that are in the field. Using the assumptions of sensitivity for VLASS (1500MHz bandwidth, survey speed as in Eq. 1) and the survey speed used for the Stripe-82 observations ($10.6\,{\rm deg}^2/{\rm hr}$), we would expect a "naturally weighted" image rms of $80\,\mu$Jy. Thus we conclude that using the naturally weighted survey speed sensitivity given by Equation 1 and listed in the proposal and in the next section is valid, within uncertainties given by the issues raised in § 2.1.2 and the calibration of the Stripe-82 data.

---

[4] `https://science.nrao.edu/facilities/vla/docs/manuals/oss/performance/resolution`

[5] `http://www.aoc.nrao.edu/dissertations/dbriggs/`

[6] SB `13B-370.sb28581653.eb28626177.56669.781848645835`

2.3. Overhead Assumptions

In the estimates for total observing time, the assumption is made that there is a overhead for slewing, setup, and calibration applies to the components of the survey. For example, for general VLA observing, we recommend use of a 25% overhead, where integration times are to be multiplied by 1.25 in order to arrive at the "clock time" needed to execute observations. In practice, the overhead will depend on exactly how the survey components are scheduled and how much calibration is required, and what calibration can be shared between blocks.

Below we present two case studies based on an actual schedule and on a simple model respectively. Based on these studies, we fully expect to be able to meet (or come in under) the global 25% overhead for (i) observing blocks of 6 hours or longer, and (ii) short blocks that can share calibration with other blocks observed around the same time, (iii) blocks of 3 hours or longer that are fixed-time scheduled. More detailed verification of overheads, including full calibration, are scheduled as part of the Test Plan.

2.3.1. Case Study 1: Stripe-82

As an example, the S-band Stripe-82 observations of program 13B-370 (Hallinan et al.) were observed using dynamic scheduling and independent 3-hour blocks with 2.25 hours of on-target observing, and thus had a 33% overhead. This particular base schedule were self-contained, and included standard calibrators 3C48 (for flux density and polarization angle) and 3C84 (low-polarization leakage calibrator). The observations were made in On-The-Fly Mosaic (OTFM) mode, with the OTFM scans comprising 15 stripes to cover the Declination range, with each stripe covering 36min (9 degrees) in RA. At the scan rate chosen, each stripe took 9.25 min to get 9 min on-source integration (3% scan overhead). Groups of two stripes were interspersed with calibrator scans (with a singlet stripe left over in the block). There were extra observations of calibrators from adjacent blocks included to help link the blocks. This was a fairly conservative strategy, but control of calibration errors was important for the program.

Starting with the actual SBs used for the observations, a number of example SBs were constructed under a range of different assumptions. The overheads ranged from 24% to as low as 14% under different less conservative criteria. See Table 1 for results from the example schedule construction exercise.

Table 1: Overheads for Example Scheduling Blocks

Duration (hours)	**Dwell (hours)**	**Overhead**	**Dynamic?**	**Notes**
3.0	2.25	33%	yes	(1)
2.75	2.25	22%	no	(2)
5.6	4.5	24%	yes	(3)
5.25	4.5	17%	no	(2)
7.7	6.75	14%	no	(2)

Table Notes: (1) 13B-370 original schedule, multiple gain calibrators, calibration every 20min; (2) single gain calibrator, calibration every 30min; (3) multiple calibrators, calibration every 20min.

All blocks contained full calibration. Note that whether an example is "dynamic" or not depends on whether this SB could be submitted over a significant range of LST and thus includes extra padding for

possibly longs slews or wraps. If it needed a narrow range of starting LST then it was deemed to be essentially a fixed time schedule.

2.3.2. Case Study 2: A simplified model

We now present a simplified model of overheads in SBs, guided by the first case study above. In this model we assume:

- a fixed startup overhead (to slew to first source) of 10 min.
- a fixed time on per calibrator observation of 2 min.
- for each hour of on-source integration, a number N of 2 min. calibration scans (e.g. N=2 or N=3)
- a fixed flux density and polarization calibration (on a low polarization source) of 15 min.
- (if needed, an additional fixed polarization leakage calibration of 15 min with 3 scans at different PA with 5 min. per scan)

Thus in this model, there is a fixed overhead of 27 minutes, plus a possible additional overhead of 15 minutes for the polarization calibration, so the fixed per-block overhead is either 30 minutes or 45 minutes (rounded).

These assumptions are meant to be appropriate for large areas over a range of Declinations, where slew times to calibrators may vary. Small areas (e.g. far southern regions that must be observed at transit and are far from calibrators) may or may not conform to this model.

Assuming our calibration every 20 min (N=3), and allowing for a single leakage scan on an unpolarized source (or use of the phase calibrators for PA coverage of a polarized source), then we obtain the overheads in Table 2. The overhead for calibration every 30 min. (N=2) is about 3% lower in all cases.

Table 2: Overheads for Simplified Model A — Calibration every 20min, single leakage scan

On-source time (hours)	**Duration (hours)**	**Overhead**
3.0	3.75	25%
4.0	4.75	19%
6.0	7.05	18%
10.0	11.45	15%

If we add the additional 15 min. fixed overhead for 3 leakage scans, then we obtain the overheads in Table 3. The overhead for calibration every 30 min. (N=2) is again about 3% lower for all cases.

In the original VLASS proposal, we used Simplified Model B as a conservative estimate of overheads for the VLASS, and assumed a 17% overhead for the ALL-SKY element of the survey.

2.3.3. Case Study 3: Formal Model

For a more detailed Survey Design, we introduce a similar scheme modified for our SB length choice. In this model we assume:

Table 3: Overheads for Simplified Model B — Calibration every 20min, 3 leakage scans

On-source time (hours)	Duration (hours)	Overhead
3.0	4.00	33%
4.0	5.00	25%
6.0	7.30	22%
10.0	11.70	17%

1. START (T_{START}): a fixed startup overhead (to slew to first source, do SETUP scan) of duration T_{START},
2. FLUX (T_{FLUX}): a fixed flux density and polarization calibration (angle if high polarization, leakage if low polarization source), of duration of duratin T_{FLUX}. This (or the POL source) serves as bandpass/delay calibrator,
3. POL (T_{POL}): a fixed polarization angle and/or leakage calibration (whichever is not covered by the flux density calibrator), of duration (including slew from previous source) T_{POL}. This is an alternate bandpass calibrator if needed (if using ALTPOL, this is one of the different PA scans instead). Not needed if the GCAL and FLUX sources suffice for leakage and angle calibration.
4. CAL1 (T_{CAL1}): a fixed initial scan on the gain/phase calibrator, including slew to calibrator and to the first OTF position, of duration t_{CAL1}. Note: if bright enough and observed over a good range of parallactic angles, can serve as the leakage calibrator also. In some cases might serve as a polarization angle calibrator.
5. OBS (N X Δt_{GCAL}): each Δt_{GCAL} =15–30m block of target observing contains $\Delta t_{GCAL} - t_{GCAL}$ on-source and one gain calibrator scan of duration t_{GCAL},
6. ALTPOL (T_{ALTPOL}): optional — a polarization leakage calibration of 1 or 2 additional scans of one of the other calibrators, with T_{ALTPOL} =2–10m depending on what source is used.

In this model, there is a total fixed calibration (FCAL) for each block containing this full calibration of $T_{FCAL} = T_{START} + T_{FLUX} + T_{POL} + T_{CAL1}(+T_{ALTPOL})$. We estimate this to be in the range 20–36m for our calculations below. Note that scenario Z to get 20m fixed calibration duration requires locating

Table 4: Scenarios for fixed overhead duration T_{FCAL}.

Scenario	T_{FCAL} (min)	T_{START} (min)	T_{FLUX} (min)	T_{POL} (min)	T_{CAL1} (min)	T_{ALTPOL} (min)
X	30	10	2	9	9	0
Y	25	10	2	6	7	0
Z	20	8	2	5	5	0
P	15	8	3	0	4	0

the first source in mid-wrap South to reduce the starting slew needed, and having nearby POL and target areas, and thus is probably only achievable over limited number of tiles. Scenario P assumes you can use the GCAL source for polarization leakage (or angle, whichever is not covered by FLUX) and minimal slews, and probably represents the best case.

The OTF scanning itself is subject to overheads, given by the time needed to move from the end of one row and move to and get up to speed scanning the next row. In the current OPT (April 2016) an extra duration t_{OTF} of around 16–18 seconds is required. This greatly increases the final overhead versus the on-target time in OTF for even longer block durations and OTF scan lengths. We think the overheads should be 6 seconds or less. The total overhead factor is given by

$$f_{OTF} = \frac{T_{OTF} + t_{OTF}}{T_{OTF}} \qquad T_{OTF} = \theta_{OTF}/\dot{\theta} \tag{12}$$

where the OTF stripe duration on-sky T_{OTF} is calculated from the OTF stripe length θ_{OTF} and the scan speed $\dot{\theta}$. See Table 5 for representative values expressed as percent over unity. Thus, if we are limited to 18s

Table 5: Overheads for OTF scanning (OTF-OH) including OTF scan turnaround costs t_{OTF}, for OTF scan lengths assuming a scan speed of $\dot{\theta} = 3.3'/\mathrm{s}$ to get the scan durations T_{OTF}.

OTF stripe length θ_{OTF} **(deg)**	**stripe duration** T_{OTF} **(sec)**	**OTF-OH** ($t_{OTF} = 18$**s**)	**OTF-OH** ($t_{OTF} = 6$**s**)
8.0	145	12.4%	4.1%
10.0	182	9.9%	3.3%
12.0	218	8.3%	2.8%
15.0	273	6.6%	2.2%
20.0	364	4.9%	1.6%

of OTF scan turnaround, then we are limited to OTF-OH of 6.6% or worse for scan distances of 15° or less. If we can reduce the turnaround to 6s or better, then we can achieve OTF-OH of 3.3% or better for scan distances of 10° or more. We will assume that we can turnaround in 6s for the purposes of our overhead calculation.

Another recurring overhead is that due to the gain calibrator (GCAL) of duration t_{GCAL} (1–2m) inserted at a given interval Δt_{GCAL} (15–30m). These overheads are shown in Table 6. Note that the GCAL scan

Table 6: Gain Calibration Overheads (GCAL-OH) recurring at a given interval Δt_{GCAL} between calibration, for various calibration scan durations t_{GCAL} (1–2m).

GCAL Interval Δt_{GCAL} **(min)**	**GCAL-OH** ($t_{GCAL} =$**60s**)	**GCAL-OH** ($t_{GCAL} =$**90s**)	**GCAL-OH** ($t_{GCAL} =$**120s**)
15.0	7.1%	11.1%	15.4%
18.0	5.9%	9.1%	12.5%
20.0	5.3%	8.1%	11.1%
30.0	3.4%	5.3%	7.1%

durations t_{GCAL} should incorporate the slew back to the next row in OTF in addition to the slew to the calibrator from the previous OTF.

The fixed flux and polarization calibration plus the first gain calibration scan in our simple model above provides a "fixed" calibration (FCAL) baseline. Assuming a single leakage scan on an unpolarized source, this is nominally 30min using the assumptions above, but could be in the range 20–36m. This gives a fixed overhead depending on block duration (or total duration sharing the same fixed calibration). These are tabulated in Table 7.

Table 7: Fixed overheads for various assumed fixed calibration (FCAL) durations T_{FCAL}. "Block Duration" T_{BLK} refers to the length of a single self-contained SB or the sum of SB lengths that can share a single fixed calibration.

Block Duration T_{BLK} **(hrs)**	**FCAL-OH** (T_{FCAL} **=15m)**	**FCAL-OH** (T_{FCAL} **=20m)**	**FCAL-OH** (T_{FCAL} **=25m)**
4.0	6.7%	9.1%	11.6%
6.0	4.3%	5.9%	7.5%
8.0	3.2%	4.3%	5.5%
10.0	2.6%	3.4%	4.3%
12.0	2.1%	2.9%	3.6%
18.0	1.4%	1.9%	2.4%
24.0	1.1%	1.4%	1.8%

To obtain the final overall overhead, we must multiply the other overheads expressed as a factor $f = 1$ + OH (e.g. $f_{OTF} = 1.033$ for OTF-OH=3.3%), with:

$$f_{TOT} = f_{FCAL} \cdot f_{GCAL} \cdot f_{OTF} = \frac{T_{BLK}}{T_{BLK} - T_{FCAL}} \frac{\Delta t_{GCAL}}{\Delta t_{GCAL} - t_{GCAL}} \frac{T_{OTF} + t_{OTF}}{T_{OTF}} \tag{13}$$

We obtain the final overheads in Table 8 using representative choices from the above tables enumerated in Table 9.

Table 8: Final total overheads for different scenarios.

Block Duration T_{BLK} **(hrs)**	**TOT-OH CASE A**	**TOT-OH CASE B**	**TOT-OH CASE C**	**TOT-OH CASE D**
4.0	16.7%	20.3%	20.7%	28.1%
6.0	14.1%	17.5%	17.2%	23.4%
8.0	12.9%	16.3%	15.4%	21.1%
12.0	11.7%	15.1%	13.8%	18.9%
24.0	10.6%	13.9%	12.2%	16.8%

Table 9: Scenarios for calculating overheads. All these cases assume a t_{OTF} =6s turnaround and a OTF stripe length of 10° at nominal scan speed $\dot{\theta} = 3.3'/\mathrm{s}$.

Case	**FCAL Duration** T_{FCAL} **(min)**	**GCAL Interval** Δt_{GCAL} **(min)**	**GCAL Duration** t_{GCAL} **(sec)**
A	15	18	60
B	15	18	90
C	20	15	60
D	25	15	90

In the VLASS proposal and TIP reviewed by the Community Review Panel, the ALL-SKY component for the full survey was assumed to incur an overhead of 17%, while for the pilot design we assumed a 20% overhead. If we observe in self-contained 4 hour blocks and insert a 90s gain calibration every 15m with 25m

fixed calibration (CASE D) then the overhead will be 28.1%, or 21.0% if we reduce the gain calibration scans to 60s and the fixed calibration to 20m (CASE C), reaching 20.3% for 90s gain calibration scans every 18m with only 15m of fixed calibration at start (CASE B). Note that CASE A for a 4-hour block and overhead under 17% is possible in fortuitous circumstance, as shown by test schedules on COSMOS, but is a lower limit on overheads for our purposes. Sharing calibration between multiple 4-hour SB is highly desirable. If we were to use longer 8-hour blocks, then using a 90s gain calibration every 18m with 15m fixed calibration (CASE B) will give a 16.3% overhead, under the target value of 17% for the survey proposal.

For the VLASS Pilot observations, which use 4-hour SBs, an average overhead of 21% has been realized in practice, and the overhead for a test 8-hour SB was 16.3%. For the calculation of observing time required we assume an overhead of 19%, using a combination of 4 and 8-hour SBs.

Risk: Low Although overhead has a large impact on the time it takes to do the survey, unlike other issues it is totally under our control. The Survey Pilot will inform us on the required durations that go into the model and more accurately assess the overheads in real SBs. Choices will be made on block length based on operational considerations, and the ability to observe with longer co-calibrated blocks could be implemented in the pipeline.

2.4. On-The-Fly Mosaicking (OTFM)

We now describe the technical issues and formulae related to using On-The-Fly Mosaicking (OTFM) to carry out the VLASS.

2.4.1. Scanning in RA or Dec

The VLA implementation of OTF scanning employs uniform scan rates in Right Ascension (RA) and Declination (DEC), with the coordinates of the start and end points and effective duration determining the rates in RA and DEC. This means that OTF scan "stripes" must be either in constant RA or constant DEC to enforce uniform dwell time on a given point in the sky. Furthermore, this uniformity requires the same separation between OTF stripe "rows" ($\theta_{row} = 7.25'$ as defined in the TIP) which in turn means that our scanning should be in RA at constant DEC δ. Therefore, for the VLASS, we will scan in RA with rows separated by θ_{row} in DEC at a fixed on-the-sky rate $\dot{\theta}$ which means the effective RA rate will be given by $\dot{\theta_\alpha} = \dot{\theta}/\cos\delta$. In the OPT, this will be effected by choosing a number of phase center steps n_{step} such that the scanning time $\Delta t = t_{dump}\, n_{step} = \Delta\alpha/\dot{\theta_\alpha}$.

2.4.2. Scan Rate and Row Separation

The scan rate $\dot{\theta}$ for a large OTF region covered using rows separated by θ_{row} is

$$\dot{\theta} = \frac{SS}{\theta_{row}} \tag{14}$$

where the survey speed SS is calculated as above.

Below, we present a plot of the OTF mosaic uniformity as a function of θ_{row}/θ_P. This is shown in Figure 3 and tabulated in Table 10 below, using the beamwidths from Fig. 1 (Table 4 of Perley 2016). For

Table 10: Peak-to-peak difference in uniformity of mosaic sensitivity over S-band for different row spacings.

Frequency (GHz)	θ_P	$\theta_{row} = 7.5'$	$\theta_{row} = 7.2'$	$\theta_{row} = 6.67'$
3.00	$13.97'$	0.43%	0.28%	0.12%
3.56	$11.56'$	3.0%	2.1%	1.0%
3.95	$10.34'$	6.8%	5.1%	2.8%

example, a conservative spacing would be to use $6.67'$ ($400''$) which gives 9 rows per degree (see § 2.4.6 below).

These results assume an ideal linear mosaic with no cutoff on the beam response with which fields are added in. The cyan dashed curve in Figure 3 shows the uniformity if one imposes a cutoff at a beam level similar to that used in the NVSS imaging. This shows a "plateau" in the uniformity at the 2% level for rows spacings favored above. Thus one should not expect to do better than this and the most conservative row spacings are likely not needed. For completeness, Figure 4 shows the corresponding minimum and maximum rms in the mosaic for the two cases.

From Equation 14 we see that reducing the row separation will increase the scan speed, which will cause beam smearing on the scale of the visibility integration time. This effect is described below. For a survey speed of $SS = 23.83$ deg^2/hour, and a visibility integration time of $t_{dump} = 0.45$ sec, we derive the beam smearing values shown in Table 11. The value of the smearing at the beam center represents a loss

Table 11: Ratio of the smeared beam to the ideal Gaussian beam calculated at the beam center, assuming a survey speed $SS = 23.83$ deg^2/hour and a visibility integration time of $t_{dump} = 0.45$ sec.

Frequency (GHz)	θ_P	$\theta_{row} = 7.5'$ $\dot{\theta} = 3.177'$/s	$\theta_{row} = 7.2'$ $\dot{\theta} = 3.310'$/s	$\theta_{row} = 6.67'$ $\dot{\theta} = 3.573'$/s
3.00	$13.97'$	0.9976	0.9974	0.9969
3.56	$11.56'$	0.9965	0.9962	0.9955
3.95	$10.34'$	0.9956	0.9952	0.9944

of signal-to-noise ratio, as the inverse of this will need to be applied to restore flux density correctness. As shown in the table, this is a small effect for these scan speeds and integration times so this is not a significant consideration in choice of row separation.

2.4.3. Dump Times and Data Rates

The Survey Speed (SS) defined above is the sky area covered per unit time to reach a given continuum image rms sensitivity. For an On-the-Fly Mosaic (OTFM) this translates to a Scanning Rate ($\dot{\theta}$) in arcmin/second at which the telescopes move while taking data. There are limitations on how fast one can scan, mostly dependent on the data rates resulting from the need to support short data dump times during fast scanning.

A critical limitation is that the correlator dump time must be fast enough to temporally resolve the amplitude envelopes of sources as they move through the primary beam pattern. The minimum dump time is in turn limited by the output data rate, which should not exceed 25 MB/s in order to limit the archiving

requirements. The VLA produces data at a rate $R_{\rm data}$ of:

$$R_{\rm data} = 45 * (n_{\rm spw} * n_{\rm ch} * n_{\rm pol}/16384)/t_{\rm dump}. \tag{15}$$

Conservatively assuming that all 16 subbands are useful (2 GHz bandwidth), each with 64 2MHz channels and 4 polarization products, the VLASS will produce 11.25 MB per dump. For a data rate limit of 25 MB/s, the shortest full-VLASS dump time is 0.45s for the nominal VLASS configuration bringing back the full 2048 MHz bandwidth ($n_{\rm spw} = 16$). Thus,

$$t_{{\rm dump},min} = 0.45\,(n_{\rm spw}/16)\,{\rm sec} \tag{16}$$

Risk: Low We have taken extensive test and Pilot data using 0.45sec dumps (as well as 0.25sec dumps at twice the rate).

2.4.4. OTFM Smearing

Because the telescopes are in constant motion during a OTFM stripe, a visibility will exhibit the effects of the primary beam movement during that integration time. This is purely and amplitude error, as the phase center of the array is fixed on this (or a longer) timescale. Furthermore, unless there are antenna to antenna variations in the scanning (which are equivalent to pointing errors), this is purely an overall amplitude error and not antenna or baseline based.

Consider a Gaussian primary beam

$$B(x,y) = {\rm e}^{-\frac{x^2+y^2}{2s^2}} = 2^{\frac{x^2+y^2}{(\theta_{pb}/2)^2}} \tag{17}$$

where s is the Gaussian dispersion of the beam and θ_{pb} is the FWHM ($\theta_{pb}^2 = 8\ln 2\, s^2$). For an integration taken over the interval from $t_0 - \Delta t/2$ to $t_0 + \Delta t/2$ at OTFM scanning rate $\dot\theta$ in the x-direction, a visibility centered at an offset point x_0, y_0 in the primary beam will see an averaged beam value of

$$B_{avg}(x_0,y_0) = \int_{x_0-\Delta x/2}^{x_0+\Delta x/2} {\rm d}x\, B(x,y_0) \tag{18}$$

where $\Delta x = \dot\theta\,\Delta t$. Thus, the effective beam is the primary beam smeared in the scan direction. For our Gaussian beam,

$$B_{avg}(x_0,y_0) = {\rm e}^{-\frac{y_0^2}{2s^2}} \int_{x_0-\Delta x/2}^{x_0+\Delta x/2} {\rm d}x\, {\rm e}^{-\frac{x^2}{2s^2}}. \tag{19}$$

We can use the standard erf integral definition

$${\rm erf}(x) \equiv \frac{2}{\sqrt{\pi}} \int_0^x {\rm d}t\, {\rm e}^{-t^2} \tag{20}$$

to find that

$$B_{avg}(x_0,y_0) = \frac{s}{\Delta x}\sqrt{\frac{\pi}{2}}\,{\rm e}^{-\frac{y_0^2}{2s^2}}\,\left[{\rm erf}\left(\frac{x_0+\Delta x/2}{\sqrt{2}\,s}\right) - {\rm erf}\left(\frac{x_0-\Delta x/2}{\sqrt{2}\,s}\right)\right] \tag{21}$$

or in terms of θ_{pb} the ratio to the unsmeared beam is

$$\frac{B_{avg}(x_0,y_0)}{B(x_0,y_0)} = \frac{\theta_{pb}}{\Delta x}\sqrt{\frac{\pi}{16\,\ln 2}}\,\left[{\rm erf}(z_{up}) - {\rm erf}(z_{low})\right]. \tag{22}$$

where

$$z_{up} = \frac{x_0 + \Delta x/2}{\sqrt{2}\,s} = 2\sqrt{\ln 2}\,\frac{x_0 + \Delta x/2}{\theta_{pb}} \quad (23)$$

$$z_{low} = \frac{x_0 - \Delta x/2}{\sqrt{2}\,s} = 2\sqrt{\ln 2}\,\frac{x_0 - \Delta x/2}{\theta_{pb}} \quad (24)$$

$$(25)$$

and is plotted in Figure 2.

The net effect of this smearing is an overall reduction of S/N by the value at $x_0 = 0$. The beam given by normalizing Equation 21 could be used to optimally weight the integrations to make the mosaic, but the overall loss still affects the S/N. The ultraconservative value of $\Delta x/\theta_{pb} < 0.1$ was chosen so that the maximum error (which will show up when you use the unsmeared beam for the mosaic imaging) at any place $|x/\theta_{pb}| < 0.8$ in the beam would be less than 0.5%. One could probably also do well with $\Delta x/\theta_{pb} < 0.2$ for which the overall S/N loss is less than 1% and the effective beam area over the plotted range is around 2% or less.

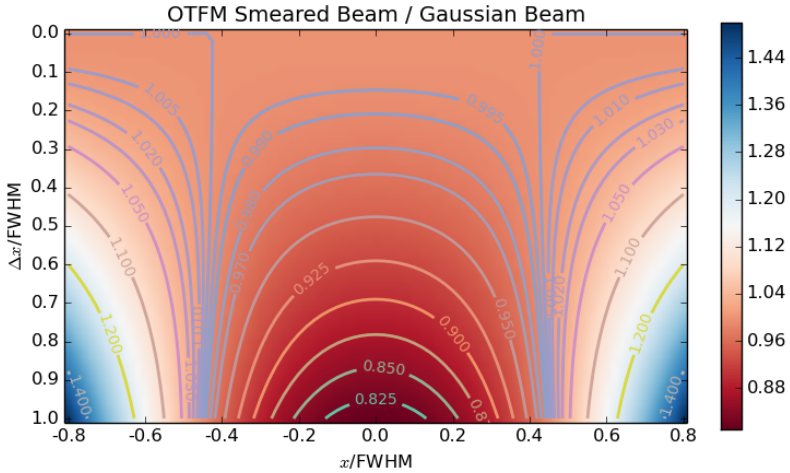

Fig. 2.— The values of B_{avg}/B as a function of the x displacement in the beam (x-axis) and the integration step size $\Delta x/\theta_{pb}$ (y-axis) as given by Equation 22.

2.4.5. OTFM Uniformity

OTFM is carried out by scanning a "stripe" or "row" across a region separated by θ_{row} in the perpendicular direction (in this case scanning in RA at constant Dec, with stripes separated in the Dec direction).

The row separation is set by some allowed limit to the non-uniformity in effective noise level in the resulting mosaic. Here we present the calculations of this effect.

Reconstructing a mosaic from a set of offset measurements is carried out by a linear weighted sum of these values either in the image or uv plane. This is equivalent to the sum

$$F = \frac{1}{Z} \sum_i w_i \frac{f_i}{b_i} \qquad\qquad Z = \sum_i w_i \tag{26}$$

where the f_i are the measured values from image (or gridded uv equivalent) i at offset x_i, y_i for the sky position of interest and $b_i = B(x_i, y_i)$ the values of the beam for those offsets (Z represents the sum of weights). For optimal weighting, the $w_i = (b_i/\sigma_i)^2$ where σ_i is the rms noise for the image i at the pixel that is relevant. Thus,

$$Z = \sum_i \frac{b_i^2}{\sigma_i^2} \tag{27}$$

and

$$F = \frac{1}{Z} \sum_i \frac{b_i}{\sigma_i^2} f_i. \tag{28}$$

Using standard propagation of Gaussian errors, the rms in the weighted average F is

$$\sigma_F^2 = \frac{1}{Z^2} \sum_i \left(\frac{b_i}{\sigma_i^2}\right)^2 \sigma_i^2 = \frac{1}{Z^2} \sum_i \frac{b_i^2}{\sigma_i^2} = \frac{1}{Z} \tag{29}$$

so the calculation of the mosaic rms simply comes down to calculation the sum of mosaic weights Z.

This function was calculated numerically and the results are shown as the solid black curve in Figure 3. The normalized maximum deviation is defined as

$$\frac{\Delta\sigma}{\sigma} = 2.0 \frac{\sigma_{max} - \sigma_{min}}{\sigma_{max} + \sigma_{min}} \tag{30}$$

where σ_{max} and σ_{min} are the maximum and minimum rms noise in the reconstructed mosaic assuming uniform intrinsic noise per pointing.

These results assume an ideal linear mosaic with no cutoff on the beam response with which fields are added in. The cyan dashed curve in Figure 3 shows the uniformity if one imposes a cutoff at a beam level similar to that used in the NVSS imaging. This shows a "plateau" in the uniformity at the 2% level for rows spacings favored above. Thus one should not expect to do better than this and the most conservative row spacings are likely not needed. For completeness, Figure 4 shows the corresponding minimum and maximum rms in the mosaic for the two cases.

2.4.6. Choice of row separation

The nominal separation given in the TIP presented to the review panel of $\theta_{row} = 7.25'$ was derived by setting a uniformity specification of 1% or better at 3.6GHz assuming $\theta_P = 12.5'$. However, this value does not produce an integer number of rows over a convenient span (say integer number of degrees). It would be beneficial for the tiling if it were to do so. In addition, recent beam mapping observations have measured the S-band beam to be narrower than previously assumed (§ 2.1 and Fig. 1), indicating that correspondingly narrower row separations are needed to limit the error to the same extent as discussed above in § 2.4.2.

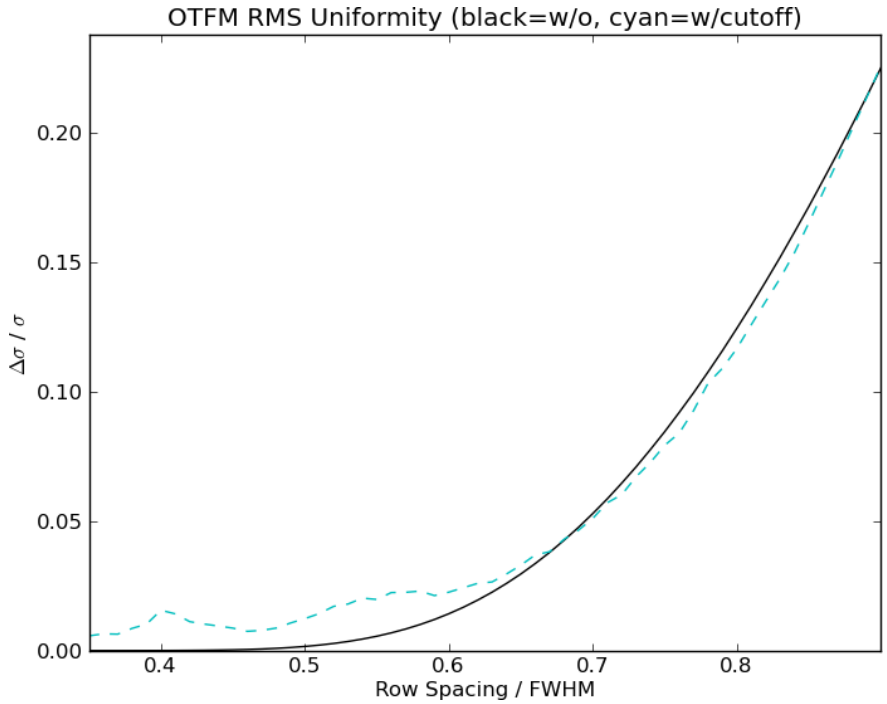

Fig. 3.— Uniformity of linear mosaic as peak-to-peak differences as function of θ_{row}/θ_P. The ideal case without any radius cutoff on fields included in the mosaic is shown as the black solid curve. If a cutoff at a radius at which the Gaussian beam falls to $g = 0.17$ ($R_g = 0.8\,\theta_P$) is imposed, you get the dashed cyan curve, which deviates from the ideal case at low and high separations. Note that around $\theta_{row}/\theta_P \approx 0.55$–$0.65$ the cyan curve plateaus with a non-uniformity of around 2%. Realistically, one cannot expect a uniformity better than this using normal imaging procedures.

Obvious options are to use $6.67'$, $7.2'$, or $7.5'$ instead. Implications of these changes on the scan speed and mosaic errors using the values in Table 10 and discussion in § 2.4.2 are:

- $\theta_{row} = 6\farcm67$: There are 9 rows in 1° for a total of 810 in the North, and an additional 360 rows in the South to get to $\delta = -40°$, plus one at the equator, giving a total of 1171 rows in the survey. The scan rate would be $\dot{\theta} = 3.573'$/sec for a survey speed of $SS = 23.83$ deg^2/hour.
  - *Uniformity:* This θ_{row} gives a mosaic uniformity deviation of 1.0% at 3.56 GHz, and 2.8% at 3.95 GHz.
  - *Beam Smearing:* For 0.45 second integrations the beam error at beam center is 0.5% at 3.56 GHz, and 0.6% at 3.95 GHz.
  - *Assessment:* This is a conservative choice giving good mosaic uniformity equivalent to the choice in the original TIP for the old beam and $\theta_{row} = 7.25'$. It has a correspondingly higher scan rate which may affect pointing and tracking performance.
- $\theta_{row} = 7\farcm2$: There are 25 rows in 3° for a total of 750 rows in the 90 degrees of the North, and an additional 333 (formally 333.33) rows in the South to get to $\delta = -40°$ plus one at the equator, giving a total of 1084 rows in the survey. The scan rate would be $\dot{\theta} = 3.310'$/sec.

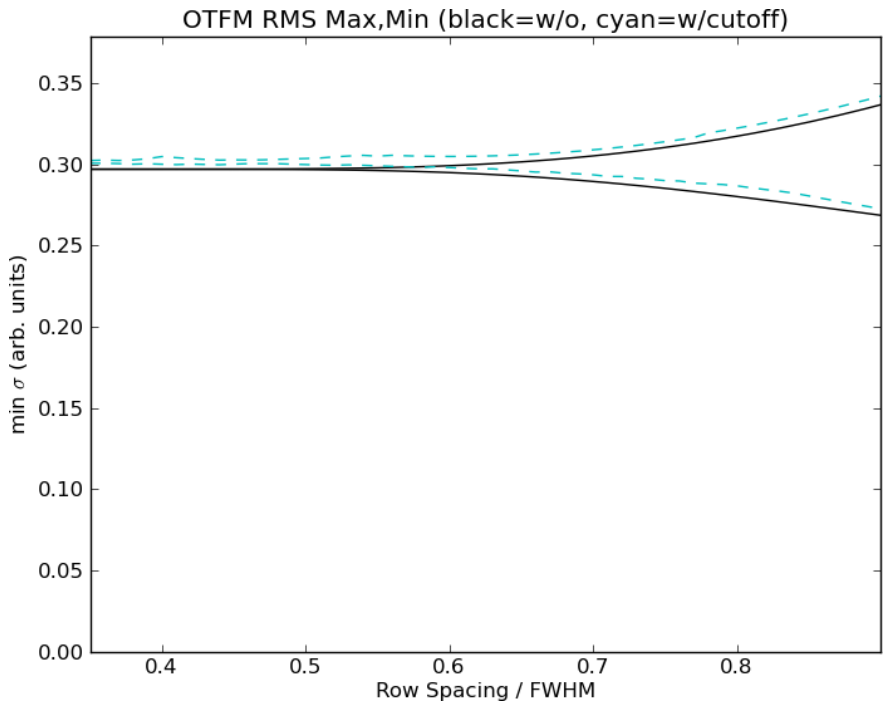

Fig. 4.— For the uniformity calculations plotted in previous figure, the corresponding minimum and maximum rms in the mosaic (in arbitrary overall units). The curves are the same with the solid black for the ideal linear mosaic case and the dashed cyan curve for the imposed cutoff in the beam.

  - *Uniformity:* This θ_{row} gives a mosaic uniformity deviation of 2.1% at 3.56 GHz, and 5.1% at 3.95 GHz.
  - *Beam Smearing:* For 0.45 second integrations the beam error at beam center is 0.4% at 3.56 GHz, and 0.5% at 3.95 GHz.
  - *Assessment:* The uniformity errors are about a factor of two worse than for $\theta_{row} = 6.67'$ but probably still acceptable for most science cases.

- $\theta_{row} = 7\farcm5$: There are 8 rows per degree for a total of 720 rows in the North, one on the equator, and 320 rows to $\delta = -40°$ giving a total of 1041 rows in the survey. The scan rate would be $\dot{\theta} = 3.177'$/sec.
  - *Uniformity:* This θ_{row} gives a mosaic uniformity deviation of 3.0% at 3.56 GHz, and 6.8% at 3.95 GHz.
  - *Beam Smearing:* For 0.45 second integrations the beam error at beam center is 0.3% at 3.56 GHz, and 0.4% at 3.95 GHz.
  - *Assessment:* The uniformity errors are about a factor of three worse than for $\theta_{row} = 6.67'$ but this choice provides the slowest scan speeds.

At the SSG telecon on 23-May-2016, the results of a poll of interested SSG members was announced. The majority choice was for $\theta_{row} = 7\farcm2$. We subsequently adopted this value for the Survey Pilot observations, and propose to use this for the full survey.

Risk: Low This row separation gives adequate perfomance, and other factors such as RFI, loss of antennas, and presence of bright sources dominate the uniformity level of the survey.

2.5. Cadences for Transients & Variability

One of the headline science goals of the VLASS is the exploration of the dynamic radio sky on timescales of days to years. There is some latitude with which the scheduling of the VLASS can influence the sensitivity to transient and variable phenomena through the selection of cadences for fields.

The VLASS will be carried out in 3 total epochs (each area is observed three times) over the six configuration cycles spanning 7 years. The most straightforward approach is to divide the sky into two (equal observing time) sets of regions, say N and S (possibly, but not necessarily, referring to North and South), and alternate between them each cycle, e.g. NSNSNS. In this scheme there is a 32-month cadence between epochs. For known transient classes at 2–4 GHz this means that each epoch is essentially independent and will observe fresh cases of these transients on the sky. In the Test & Development plan (in § 10.1.4) we propose to investigate optimal schemes. For example, an alternate approach might be to introduce two cadences, e.g. NNSNSS where both 16-month and 32-month separations are measured.

Below we give a model that can be used to optimize cadences for different classes of transients.

2.5.1. A Toy Model for Transient Yield for the VLASS

The following describes a "toy model" for slow transients used to estimate the survey yields in the various scenarios.

We assume a transient is a square wave burst of duration T_{trans} going off at an full-sky rate (per year) of R_{trans}, giving a "snapshot" yield per epoch of $N_{sky} = R_{trans}\,T_{trans}$ visible on-sky at any given time, computed at a survey flux density limit of $S_{lim} = 1$ mJy/beam. We will assume Euclidean source counts, $N(>S) = N_{sky}(S/S_{lim})^{-1.5}$. Note, this is the analog of the "Equivalent Width" for a transient light curve.

Assume that the observations comprise N_{ep} snapshot epochs separated by cadence T_{cad} spanning $T_{span} = (N_{ep} - 1)\,T_{cad}$. The survey covers a fractional area of the sky F_{sky}. Each epoch of the survey has a $10\,\sigma$ detection limit of $S_{lim} = 10\,S_{rms}$.

The primary reference for the yields is the preprint by Metzger, Williams, & Berger (2015; hereafter MWB15)[7]. Note that this paper appeared as we were finalizing the proposal for the Community Review, and we were unable to fully incorporate its contents into the proposal. Furthermore, the "VLASS" referred to by MWB15 was for the old (pre-Dec 2014) VLASS-Wide definition (WIDE) for a 4-epoch survey covering 10^4 deg^2. The parameters for the MWB15 assumed WIDE and our proposed VLASS are:

	N_{ep}	F_{sky}	T_{cad}	T_{span}	S_{rms}
WIDE:	4	0.242	12 mos.	36 mos.	0.10 mJy/beam per epoch
VLASS:	3	0.821	32 mos.	64 mos.	0.12 mJy/beam per epoch

[7] arXiv:1502.01350

MWB15 use a Monte-Carlo approach with complicated (realistic) light curves, but our toy model should get the scaling approximately correct.

Case-I: *"Shorter" transients* — If the transients have timescales less than the cadence ($T_{trans} \ll T_{cad}$), each epoch is an independent snapshot, and the survey yield Y_{short} is given by

$$Y_{short} = F_{sky}\, N_{sky}\, (S/S_{lim})^{-1.5}\, N_{ep} \tag{31}$$

so that

$$\begin{array}{lllll} \text{WIDE:} & Y_{short}/N_{sky} & = & 0.242 \times 1.0^{-1.5} \times 4 & = & 0.968 \\ \text{VLASS:} & Y_{short}/N_{sky} & = & 0.821 \times 1.2^{-1.5} \times 3 & = & 1.873 \end{array}$$

and thus $Y_{short}(\text{VLASS})/Y_{short}(\text{WIDE}) = 1.93$. The yields for transients given by MWB15 for VLASS are therefore almost $2\times$ those presented in that paper.

Case-II: *"Longer" transients* — If the transients have timescales much longer than the survey span, as do the MWB15 models for NS-NS mergers (NSM) and TDE, then the fraction of transients within T_{span} of either end of its duration must be considered, and thus

$$\begin{aligned} Y_{long} &= F_{sky}\, N_{sky}\, (S/S_{lim})^{-1.5}\, (2\, T_{span}/T_{trans}) && (32) \\ &= F_{sky}\, (S/S_{lim})^{-1.5}\, 2\, T_{span}\, R_{trans} && (33) \end{aligned}$$

and so

$$\begin{array}{lllll} \text{WIDE:} & Y_{long}/R_{trans} & = & 0.242 \times 1.0^{-1.5} \times 3\,\text{yrs.} & = & 0.726 \\ \text{VLASS:} & Y_{long}/R_{trans} & = & 0.821 \times 1.2^{-1.5} \times 5.26\,\text{yrs.} & = & 3.285 \end{array}$$

In this case, $Y_{long}(\text{VLASS})/Y_{long}(\text{WIDE}) = 4.52$, and our proposed VLASS will yield more than $4\times$ more "longer" transients than MWB15 predict for WIDE.

The expected yields for various types of transients presented by MWB15, for various surveys and survey designs, are given in Table 12. The upshot is that yields for the proposed VLASS are significantly enhanced over those given by MWB15 for the old WIDE in Fig. 4 of their paper, and now in most cases are comparable to (or better than) those given for ASKAP VAST-DEEP. See MWB15 for an explanation of the specifics of these classes of transients. Note that MWB15 used specific models taken from the literature. However, there is significant variation among available models that were not explored by those authors. Thus, these rates and yields should be taken to have free parameters that would be constrained by our survey. In addition, MWB15 did not consider Type-II radio supernovae, which will be the most common slow transient observed (see Figure 5 of the final VLASS proposal). Note also that the yields presented by MWB15 for the other classes of transients are lower than those in Figure 5 of the proposal, presumably due to the filtering applied by requiring that the transients be found only within the survey itself with a factor of 2 change between epochs (e.g., present at 10σ in at least one epoch, and a $2\times$ brightness change or a 5σ upper limit in at least one other epoch). Obviously, more detailed calculations using all available information (e.g., the identification of the host and location of the transient within the host, use of the FIRST survey in the relevant area) and some relaxed assumptions can be made and so we feel this will be a lower limit to the transient yields for these models.

Table 12: Yields for various transient types and survey scenarios

Class	**WIDE**	**VLASS**	**VAST-DEEP**
"Shorter" transients:			
LGRB On-axis	2	4	1
LGRB $\theta_{obs} = 0.2$	4	8	4
LGRB $\theta_{obs} = 0.4$	8	16	12
LGRB $\theta_{obs} = 0.8$	2	4	13
SGRB On-axis	1	2	2
SGRB $\theta_{obs} = 0.4$	0.6	1.2	1
"Longer" transients:			
NSM Magnetar	5	22.5	22
TDE On-axis	0.8	3.6	0.8
TDE Off-axis	6	27	20

2.6. Source Spectrum, Angular Size & Sensitivity

The basic calculations for the wideband continuum sensitivity presented in § 2.1 are valid for sources unresolved by the VLA in a given configuration, and with a spectrum that is either constant or linearly varying with frequency. Sources that break one or both of these assumptions will have an apparent brightness in the VLASS that is different from their flux density at band center. We deal with these two effects below.

2.6.1. Source Spectrum & Sensitivity

If the spectral energy distribution (SED) of a radio source were constant or a linear function of frequency, and the VLA sensitivity were constant over the band, then the measured signal-to-noise ratio for the measured wideband continuum intensity of a source would be given by the ratio of the flux density at band center to the rms noise over the band. However, this is not really the case for actual radio sources, or for the sensitivity of the JVLA S-band system.

The SED of a radio source is generally taken to be a power-law as a function of frequency

$$S(\nu) = S_0 \left(\frac{\nu}{\nu_0}\right)^{\alpha} \tag{34}$$

where α is the spectral index and S_0 is the flux density at the reference frequency ν_0. For example, the flux density of an average radio source with $\alpha = -0.7$ measured at the VLASS band center of 3 GHz is 0.587 times the flux density measured at the FIRST/NVSS frequency of 1.4 GHz. When we make a continuum image (of an unresolved source) we form the band-weighted average

$$\bar{S} = \frac{1}{Z} \int_{\nu_{min}}^{\nu_{max}} d\nu \, w(\nu) \, S(\nu) \qquad Z = \int_{\nu_{min}}^{\nu_{max}} d\nu \, w(\nu) \tag{35}$$

where Z is the normalization factor (integral of the weights w). Note that the rms noise is also a band averaged quantity

$$\bar{\sigma}^2 = \frac{1}{Z} \int_{\nu_{min}}^{\nu_{max}} d\nu \, w(\nu) \, \sigma^2(\nu) \tag{36}$$

where $\sigma(\nu)$ is the rms image noise (in flux density rms units) as a function of frequency. The calculations that lead to Equation 1 assumed a particular form of the VLA system equivalent flux density (SEFD) in the online calculator, and a (constant) assumed integration time on source. For the wide bandwidth of the VLASS, the effective integration time given a fixed mosaic survey speed SS is a function of frequency over the band and is inversely proportional to the beam area at that frequency, so

$$\sigma(\nu)^2 = \sigma^2(\nu_0) \, \frac{\Omega_B(\nu_0)}{\Omega_B(\nu)} = \sigma^2(\nu_0) \, \left(\frac{\nu}{\nu_0} \right)^2 \tag{37}$$

which strongly favors the lower end of the band. The true performance of the JVLA over S-band (versus the assumed sensitivity) is a Test & Development target. For now we will assume that this is a known function.

We first consider the uniform case where $w = 1$ with uniform frequency coverage between ν_{min} and ν_{max}. In this case $Z = \Delta\nu = \nu_{max} - \nu_{min}$. Then it is straightforward to show for the power-law model (Eq. 34) that

$$\bar{S}_{unif} = \frac{1}{Z} \int_{\nu_{min}}^{\nu_{max}} d\nu \, S_0 \, \left(\frac{\nu}{\nu_0} \right)^{\alpha} \tag{38}$$

$$= S_0 \, \frac{\nu_0^{-\alpha}}{\alpha + 1} \, \frac{\nu_{max}^{\alpha+1} - \nu_{min}^{\alpha+1}}{\Delta\nu} \tag{39}$$

$$\tag{40}$$

for all $\alpha \neq -1$ (for $\alpha = -1$ the integral becomes a logarithmic function). Note that for a flat spectrum source $\alpha = 0$ we recover the constant flux density S_0. For other values of the spectral index we can define an equivalent frequency ν_{eq} for which

$$S(\nu_{eq}) = S_0 \, \left(\frac{\nu_{eq}}{\nu_0} \right)^{\alpha} = \bar{S}_{unif} \tag{41}$$

which gives

$$\nu_{eq} = \left[\frac{1}{\alpha + 1} \, \frac{\nu_{max}^{\alpha+1} - \nu_{min}^{\alpha+1}}{\Delta\nu} \right]^{\frac{1}{\alpha}} \tag{42}$$

for $\alpha \neq 0$ (as well as $\alpha \neq 1$). For $\alpha = 1$ this gives $\nu_{eq} = 0.5 \, (\nu_{min} + \nu_{max})$ the average frequency in the band. For other reasonable values we obtain an equivalent frequency close to but below the mean frequency. For example, for a typical radio source $\langle\alpha\rangle = -0.7$ and the full S-band frequency range one finds $\nu_{eq} \approx 2.9\,\mathrm{GHz}$. Thus, average sources are slightly brighter than one might expect by just using the mid-band frequency of 3 GHz (0.601 times the 1.4 GHz flux density, versus the 0.587 factor we found above).

A more careful calculation involves using optimal weights as well as a more realistic model for the noise part of the signal-to-noise ratio. There are two effects: the system noise which for JVLA gets worse at the lower frequencies, and the effective mosaic time-on-source which gets better at the lower frequencies where the primary beam is larger. At this time no detailed calculation can be done due to lack of system noise curves, and thus for the purposes of this proposal we assume those effects cancel out, leaving a roughly uniform $\sigma(\nu)$.

2.6.2. Source Angular Size and Surface Brightness Sensitivity

To predict the sensitivity of the VLASS to extended sources such as star forming galaxies and extended AGN-related emission regions, we have to take into account the match between the resolution of the VLASS and the size of the source.

Surface brightness in the radio regime is typically given in Rayleigh-Jeans equivalent brightness temperature T_b (in K), or in flux density per unit solid angle S/Ω (in MJy/sr or mJy/sq.arcsec). These are related by

$$T_b = \frac{c^2}{2k_b\,\nu^2}\,\frac{S}{\Omega} = 32.6\,\mathrm{K}\,\left(\frac{S/\Omega}{\mathrm{MJy/sr}}\right)\,\left(\frac{\nu}{1\,\mathrm{GHz}}\right)^{-2} \tag{43}$$

where $k_b = 1380\,\mathrm{Jy\,K^{-1}\,m^2}$ is Boltzmann's constant in radio astronomy units (where brightnesses are typically reported as Jy/beam). For a Gaussian source of peak flux density S_p and angular (beam or source) size full-width half-maximum θ_F,

$$\Omega = \frac{\pi}{4\,\ln\,2}\,\theta_F^2 = 1.1331\,\theta_F^2 \tag{44}$$

we get

$$T_b = 1223\,\mathrm{K}\,\left(\frac{S_p}{1\,\mathrm{mJy}}\right)\,\left(\frac{\theta_F}{1''}\right)^{-2}\,\left(\frac{\nu}{1\,\mathrm{GHz}}\right)^{-2}. \tag{45}$$

Thus, the 1.4 GHz FIRST survey flux density limit of $150\,\mu$Jy/beam ($\theta_F = 5.4''$) corresponds to a $T_b = 3.21$ K limit, while the 3 GHz VLASS ALL-SKY limit of $69\,\mu$Jy/beam ($\theta_F = 2.5''$) corresponds to $T_b = 1.50$ K. Where brightness temperatures and limits are given in the proposal, they were calculated using the above formulation.

However, the emission targeted by the VLASS is either not thermal in origin, or does not follow a Rayleigh-Jeans relation. The predominant extragalactic radio sources of interest have a non-thermal synchrotron emission spectrum, while thermal bremsstrahlung emission from the Galaxy typically shows a flat spectrum in the radio bands. The power-law spectrum for these cases is discussed in the previous sub-section and given by Equation 34. A Rayleigh-Jeans thermal spectrum is equivalent to a power-law flux density spectrum with $\alpha = 2$. Likewise, a non-thermal power-law spectrum is equivalent to a power-law thermal spectrum

$$T_b(\nu) = T_b(\nu_0)\,\left(\frac{\nu}{\nu_0}\right)^{\beta} \qquad\qquad \beta = \alpha - 2 \tag{46}$$

with $\alpha = -0.7$ corresponding to $\beta = -2.7$.

For the VLASS, it is most convenient to describe radio sources with these spectra with some total flux density (e.g. mJy) and characteristic angular size, rather than some peak brightness (e.g. mJy/beam). To quantify the yield of the VLASS for such science, the brightness limits of the survey to these sources must be calculated. To do this, the method used for finding sources must also be factored in.

The most straightforward approach is to look for peaks above some threshold, typically above some peak brightness limit, e.g. $5\,\sigma$, set by the rms image noise level. The PSF width θ_F (a Gaussian "synthesized" or "restoring" beam FWHM used in the imaging) is convolved with the sky brightness of the source, which then appears more extended. The peak brightness is thus reduced by the apparent area. A Gaussian source of total flux density S and intrinsic FWHM ϕ_F will show up in the image with a peak brightness

$$S_p = S\,\left(\frac{\theta_F^2}{\phi_F^2 + \theta_F^2}\right) \tag{47}$$

in usual units (Jy/beam etc.). Thus, a face-on (circular) star-forming galaxy disk at $z \sim 2$ might have an apparent angular size of $\phi_F = 3.1''$ (5 kpc), which will appear in the VLASS ($\theta_F = 2.5''$) with $S_p/S = 0.394$ (disregarding whether such a galaxy is actually bright enough to detect). These are the factors used in the main proposal to calculate the source yields. Note that more edge-on disks will not be as adversely affected, with factors approaching the square-root of those calculated above.

This angular size penalty is harsh, going as the square of the sizes of the PSF to the convolved source size. This, however, can be partly mitigated by employing matched filtering in the source finding. In the example above, the input image could be convolved with a Gaussian of size θ_c, where $\theta_c^2 \approx \phi_F^2$ producing a finding image with resolution matched to the angular size of the source and detecting the full flux density S. However, there is a penalty in the noise of the convolved map (after renormalization to conserve flux) with the increase in the convolved image variance given by the inverse of the peak dilution factor above, or the square root of this for the rms noise

$$\sigma_c = \sigma \left(\frac{\phi_F^2 + \theta_F^2}{\theta_F^2} \right)^{1/2} \tag{48}$$

where σ is the rms noise in the input image. This filtering gives a net gain over the unfiltered peak finding algorithm, falling only roughly linearly with the ratio of source size to PSF rather than the square. Note that this image convolution filtering is equivalent to imaging with a uv-taper applied. In our above example, the reduction of S/N due to the filtered noise increase to measure a $3.1''$ galaxy would be $\sigma/\sigma_c = 0.628$. In principle, this could significantly increase the source yields over those given in the proposal. There is certainly some limit to how large a source can be recovered this way, based on the (wideband) uv-coverage of the array. This simple calculation is probably applicable to source sizes out to ten times the PSF size.

The price of this matched filtering is the added complexity to devise and use a multi-scale source finder. Development and testing of this is probably beyond the scope of our Test & Development plan unless contributed effort is provided by the community. If such a source finder were provided and worked efficiently, it could be used for the final catalogs, most likely as a Enhanced Data Product (§ 4.2).

Note that the most effective approach to increasing the sensitivity to extended (few arcsecond) sources would be to observe roughly 25% of the time in a more extended configuration such as the C-configuration ($8.6''$ resolution at 3 GHz) — this would essentially reduce the penalty in signal-to-noise ratio to only 0.5 in peak brightness for sources of angular sizes out to around 3 arcseconds and 0.25 at 9 arcseconds, even without matched filter source-finding. This should be considered as an option if extra sensitivity to faint extended sources becomes a strong science driver.

2.6.3. Measurement of the Source Spectrum

One of the science goals of the VLASS is to measure the frequency spectrum of source emission across the 2–4 GHz band. This can be done using various techniques: by imaging the data in spectral channels across the band and fitting source spectra to the cubes, by uv-plane model fitting to the channelized visibilities, or by constructing multiple Taylor-term images using "Multi-frequency Synthesis" (MFS) as a part of the continuum imaging. We plan to use the last of these as a main data product of VLASS, and we now derive the sensitivity limits to this measurement. Note that the other approaches should have comparable performance.

In MFS, one uses a frequency dependent gridding kernel to appropriately combine the visibilities to form images corresponding to the Taylor expansion of the frequency spectrum. We now analyze a toy model

for this process that represents the salient characteristics of the algorithm. We assume the source follows a power-law spectral energy distribution (Equation 34). The Taylor expansion of the spectrum with α as a function of frequency is

$$S(\nu,\alpha) = S_0 + \alpha \left.\frac{dS}{d\alpha}\right|_{\alpha=0} + \ldots \tag{49}$$

where for our power-law

$$\frac{dS}{d\alpha} = \frac{d}{d\alpha}\, S_0\, e^{\alpha \ln(\nu/\nu_0)} = S(\nu)\, \ln(\nu/\nu_0). \tag{50}$$

The series expansion of the logarithm is

$$\ln(\nu/\nu_0) = \left(\frac{\nu}{\nu_0} - 1\right) - \frac{1}{2}\left(\frac{\nu}{\nu_0} - 1\right)^2 + \ldots = \left(\frac{\nu-\nu_0}{\nu_0}\right) - \ldots \tag{51}$$

Thus, to first order, expanding about $\alpha = 0$,

$$S(\nu,\alpha) = S_0 \left[1 + \alpha \left(\frac{\nu-\nu_0}{\nu_0}\right) + \ldots\right] \tag{52}$$

and it is apparent if we integrated these first two terms over the frequency band setting for convenience $\nu_0 = 0.5\,(\nu_{min} + \nu_{max})$ and $\Delta\nu = (\nu_{max} - \nu_{min})$, we find

$$\begin{aligned} M_0 &= \frac{1}{\Delta\nu}\int_{\nu_{min}}^{\nu_{max}} d\nu\, S(\nu,\alpha) && (53)\\ &\simeq \frac{1}{\Delta\nu}\int_{\nu_{min}}^{\nu_{max}} d\nu\, S_0 \left[1 + \alpha\left(\frac{\nu-\nu_0}{\nu_0}\right)\right] && (54)\\ &= S_0 && (55) \end{aligned}$$

as the integral over the kernel in the second term to zero. Likewise, we can form the next order integral

$$\begin{aligned} M_1 &= \frac{1}{\Delta\nu}\int_{\nu_{min}}^{\nu_{max}} d\nu \left(\frac{\nu-\nu_0}{\nu_0}\right) S(\nu,\alpha) && (56)\\ &\simeq \frac{1}{\Delta\nu}\int_{\nu_{min}}^{\nu_{max}} d\nu\, S_0 \left[\left(\frac{\nu-\nu_0}{\nu_0}\right) + \alpha\left(\frac{\nu-\nu_0}{\nu_0}\right)^2\right] && (57)\\ &= \frac{\alpha\, S_0}{\Delta\nu}\int_{\nu_{min}}^{\nu_{max}} d\nu \left(\frac{\nu-\nu_0}{\nu_0}\right)^2 && (58)\\ &= \frac{\alpha\, S_0\, \nu_0^2}{\Delta\nu^2}\int_{-1/2}^{1/2} dx\, x^2 \qquad x = \frac{\nu-\nu_0}{\Delta\nu} && (59)\\ &= \frac{\alpha\, S_0\, \nu_0^2}{12\,\Delta\nu^2} && (60) \end{aligned}$$

where in this case the first term vanishes in the integral. Thus, the unity weighted integral M_0 (Taylor term "`tt0`") measures the intensity S_0, while the frequency weighted integral M_1 (Taylor term "`tt1`") measures $\alpha\, S_0$, in particular

$$\alpha \approx \frac{12\,\Delta\nu^2}{\nu_0^2}\,\frac{M_1}{M_0}. \tag{61}$$

Note that there are higher order corrections to this, so one needs more careful simulation testing on MFS recovery of spectral index, but this formula captures the essence of the method.

The next ingredient is the error estimates on these integrals. We assume that the S in the integral is now a measurement with a uniform (zero-mean Gaussian) noise given by the spectral noise power density σ_ν. Thus,

$$\sigma_{M0}^2 = \frac{1}{\Delta\nu^2} \int_{\nu_{min}}^{\nu_{max}} d\nu\, \sigma_\nu^2 \tag{62}$$

$$= \frac{\sigma_\nu^2}{\Delta\nu}, \tag{63}$$

$$\equiv \sigma_I^2 \tag{64}$$

where we define σ_I as the (measured) rms intensity image noise, and

$$\sigma_{M1}^2 = \frac{1}{\Delta\nu^2} \int_{\nu_{min}}^{\nu_{max}} d\nu \left(\frac{\nu - \nu_0}{\nu_0}\right)^2 \sigma_\nu^2 \tag{65}$$

$$= \frac{\Delta\nu_0^2}{12\,\nu_0^2} \frac{\sigma_\nu^2}{\Delta\nu} \tag{66}$$

$$= \frac{\Delta\nu_0^2}{12\,\nu_0^2} \sigma_I^2 \tag{67}$$

Using standard propagation of errors on the ratio in Equation 61, we get

$$\frac{\sigma_\alpha^2}{\alpha^2} \approx \frac{\sigma_{M0}^2}{M_0^2} + \frac{\sigma_{M1}^2}{M_1^2} \tag{68}$$

$$= \frac{\sigma_I^2}{S_0^2} \left[1 + \frac{\Delta\nu^2}{12\,\nu_0^2} \left(\frac{12\,\nu_0^2}{\alpha\,\Delta\nu^2}\right)^2\right] \tag{69}$$

$$= \frac{\sigma_I^2}{S_0^2} \left[1 + \frac{12\,\nu_0^2}{\alpha^2\,\Delta\nu^2}\right] \tag{70}$$

$$\tag{71}$$

or

$$\sigma_\alpha^2 \approx \frac{\sigma_I^2}{S_0^2} \left[\alpha^2 + \frac{12\,\nu_0^2}{\Delta\nu^2}\right]. \tag{72}$$

Since $\alpha^2 < 1$ for the usual range $-1 < \alpha < 1$, the second term dominates. Thus,

$$\sigma_\alpha \approx \frac{\sigma_I}{S_0} \sqrt{12}\, \frac{\nu_0}{\Delta\nu}. \tag{73}$$

For the ideal full S-band VLASS $\Delta\nu = 2$ GHz, $\nu_0 = 3$ GHz, and thus

$$\sigma_\alpha \approx 5.2\, \frac{\sigma}{S_0} \tag{74}$$

and thus in order to obtain a spectral index uncertainty of $\sigma_\alpha < 0.1$ a source bright enough in intensity such that $S_0/\sigma_I > 52$ is needed, or approximately $10\times$ the $5\,\sigma$ noise cutoff on object finding.

Note: this derivation based on MFS agrees with the calculation based upon least squares fitting given by Condon (2015).

2.7. Polarimetry

A key science goal of the VLASS is the production of images in the linear polarization Stokes parameters Q and U. Wideband continuum imaging in Q and U will be compromised by depolarization induced by Faraday Rotation. Therefore, the spectral cubes at higher frequency resolution than the full-band 2–4GHz will need to be employed to construct the "continuum" polarization maps.

There are 3 types of polarization products to be produced:

1. Fine spectral cubes — frequency resolution 8-16 MHz
2. Coarse spectral cubes — frequency resolution 128 MHz
3. Full-band continuum images — frequency span 2–4 GHz (2 GHz bandwidth)

The first two spectral cube products can be created directly through standard clean. However, the final continuum polarization image will need to be processed in a different way.

2.7.1. Fine Spectral Cubes for Polarization

The highest possible spectral resolution is the native 2 MHz in the visibility data. At the low end of the band at 2 GHz this corresponds to a wavelength resolution of $\Delta\lambda = 0.15$mm or a Faraday resolution of $\Delta\lambda^2 = 4.5 \times 10^{-5}\,\mathrm{m}^2$. This is higher resolution than required for the survey, where target rotation measure spans to 1000–10000 rad/m^2 are desirable. A resolution of 10 MHz, which at 2 GHz corresponds to $\Delta\lambda = 0.75$mm or $\Delta\lambda^2 = 2.9 \times 10^{-4}\,\mathrm{m}^2$, will be sufficient. For ease of computation, multiples of 2 MHz are desirable, so fine cubes with resolution of 8 or 16 MHz are our best options.

2.7.2. Coarse Spectral Cubes for Polarization

For the bulk of the sky, spectral resolutions of 128 MHz with $\Delta\lambda = 9.6$mm or $\Delta\lambda^2 = 2.9 \times 10^{-3}\,\mathrm{m}^2$ will suffice given galactic rotation measures in the range 10–200 rad/m^2.

2.7.3. Wide-band Continuum Images for Polarization

If the full 2–4 GHz bandwidth, spanning wavelengths from 15cm to 7.5cm, were used in continuum polarimetry, then the Faraday span would be $\Delta\lambda^2 = 0.017\,\mathrm{m}^2$. This would cause significant depolarization in the presence of modest galactic rotation measures of 50 rad/m^2. Therefore, it will be necessary to construct these images for Q and U in such a way that Faraday Rotation effects can be mitigated.

Ideally, with the narrow band (fine or coarse grained) polarization spectrum known, the Faraday rotation to the source emission could be determined and removed, allowing rotation of the Q and U Stokes values to a reference frequency. In this case, we would store for every pixel:

- The bulk rotation measure RM (in rad/m^2)

- The values of Q and U de-rotated to a reference frequency/wavelength (3 GHz/10cm, or infinite frequency/zero wavelength), e.g. using the complex polarization $P = Q + iU$ with

$$P(\lambda) = P(\lambda_0)\, \mathrm{e}^{i2\chi} \qquad\qquad \chi = \mathrm{RM}\, \lambda^2 \tag{75}$$

- The wide-band continuum Stokes values recorded would then be constructed by imaging with weighted sums of the de-rotated finer grain complex polarization values over channels k:

$$\bar{P}(\lambda_0) = \sum_k w_k\, P(\lambda_k)\, \mathrm{e}^{-i2\chi_k} \qquad\qquad \chi_k = \mathrm{RM}\, \lambda_k^2 \tag{76}$$

  The choice of weighting functions w_k will need to be determined based on design study and optimized for polarization science utility and efficiency of processing. Two choices of interest are (a) uniform weighting to get an averaged Q and U over the band, and (b) weighting by intensity to get an averaged Q/I and U/I over the band.

It is not practical for BDP to do full Faraday synthesis to account for multiple rotation measures with emission at different Faraday depths along the line of sight. A single RM may be practical, particularly if restricted to pixels where the Stokes I is above some threshold. However, ensuring robustness of this determination, e.g. by fitting to the coarse cubes, is currently beyond what can be promised for BDP. Fitting of science-ready RM and Faraday parameters and construction of de-rotated continuum polarization is an EDP.

3. Survey Structure

The VLASS, as defined following the Community Review in March 2015, is an ALL-SKY survey covering 33885 square degress to a combined depth of 69 μJy/beam image rms (120 μJy/beam per epoch in each of 3 epochs). The observing time proposed for the ALL-SKY component, including overhead, was 5436 hours.

Note: The VLASS as proposed at the time of the Community Review also contained a Tier-2 DEEP survey component. The review panel recommended dropping this from the survey, and it will not be considered further in this version of the TIP.

3.1. ALL-SKY

The VLASS ALL-SKY covers the entire sky visible to the VLA north of Declination $-40°$, 33885 square degrees (82.14% of the sky). The observations for ALL-SKY will be carried out using On-The-Fly Mosaicking (OTFM). The scan rate will be adjusted depending on declination (elevation) to provide uniform sensitivity, requiring an extra 9% net integration time over the entire area. A given area of sky will be passed over three times during the survey duration, making this a 3-epoch transient survey at 120μJy/beam rms per epoch. The ALL-SKY area includes the areas of the Galactic plane and bulge visible to the VLA.

The summary statistics of the VLASS ALL-SKY are:

- B-configuration (2.5″ resolution)
- total visible sky area of 33885 square degrees, $\delta > -40°$
- per epoch continuum image rms (Stokes I) $\sigma_I \geq 120\, \mu$Jy/beam

- net survey speed is 23.832 $\deg^2$/hr at this depth
- effective integration time required is 1421.8 hours per epoch (4265.4 hours total for 3 epochs)
- a given area of sky is observed in 3 cycles (each cycle half the ALL-SKY area is observed), mean cadence is 32 months between epochs

In the original TIP we also assumed:

- multiply by factor 1.09 for sensitivity loss at low elevation for low declinations (§ 2.1.3), requiring 4649.3 hours total true integration to reach uniform sensitivity over entire area
- total of 5440 hours observing required with 17% overhead
- observations are spread through the duration of the survey comprising 6 configuration cycles, rounded to 5436 hours total (906 hours per cycle)

For the PDR, we revise these based on the new overhead calculations above, we use an overhead of 19% assuming a mix of 4 and 8 hour blocks. To compensate, recognizing the full uniformity is not practical or required, we relax the increased time at Southern declinations. Finally, we now explicitly include a 3% contingency for repeating failed observations during the cycle. The revised time request is:

- multiply by factor 1.056 for sensitivity loss at low elevation for low declinations (§ 2.1.3), requiring 4504.3 hours total true integration to provide closer to uniform sensitivity over the entire area
- total of 5360 hours observing required with 19% overhead
- an explicit contingency of 3% for repeat of failed blocks, yielding a total of 5520 hours (920 hours per cycle)

Use of BnA Hybrid: We plan to observe the southern area ($\delta < -10°$) using the BnA hybrid to improve the point spread function. This would require observing 293 total hours in BnA per cycle (including 3% contingency). Note that the time is more heavily weighted towards BnA than the relative fractional area due to the compensation for sensitivity loss at low elevations which impacts VLASS observations only in the low-declination region.

4. Data Products

The VLASS data products are described below, along with risks and considerations in the production and assessment of these products.

Products are broken into classes of "Basic" and "Enhanced", with the former being simple enough to produce by NRAO's standard (or soon to be standard) data processing system. Enhanced data products will require domain expertise and/or extra resources, so they will be left for community members to define and produce. Both kinds of products will be curated and served to the public by the NRAO, as described below.

4.1. Basic Data Products

The Basic Data Products (BDP) of the VLASS consist of:

1. raw visibility data
2. calibration data and process to generate calibration products (current best version as well as past released versions maintained in archive)
3. quick-look continuum images
4. single-epoch images and image cubes
5. single-epoch basic object catalogs
6. cumulative "static sky" images and image cubes (made from single-epoch data for first epoch, multi-epoch data thereafter)
7. cumulative "static sky" basic object catalogs

The resources for processing, curating, and serving the data products will be provided by NRAO, as described in §4.3. Teams led by NRAO, but including external community members where possible, will carry out the activities required for the processing and Quality Assurance (QA) of the products. Table 13 summarizes the BDP.

Table 13: Summary of Basic Data Products

Product	**Timescale (Goal)**	**Timescale (Req.)**	**Notes**
Raw visibility data	immediate	immediate	in standard archive
Calibrated data	1 week	1 month	from standard archive
Quick-Look Images	48 hrs	1 week	I continuum only
Single-Epoch Images	6 mos.	12 mos.	Stokes I continuum
Single-Epoch Images	12 mos.	16 mos.*	Polarization and cubes
Single-Epoch Catalogs	w/Single-Epoch Images	w/Single-Epoch Images	by product
Cumulative Images	12 mos.	16 mos.*	Stokes I continuum
Cumulative Images	16 mos.*	16 mos.*	Polarization and cubes
Cumulative Catalogs	w/Cumulative Images	w/Cumulative Images	by product

*Warning: Delivery timescales beyond 12 mos. after end-of-cycle run into resource conflict with subsequent cycle QL.

Note that the polarization continuum images and the spectral cubes for the single-epoch and cumulative data products may be delivered on longer timescales than the Stokes I continuum intensity images. Information from the polarization and spectra cubes will appear in the catalogs on the timescale of the originating product.

Details of individual BDP are now described.

4.1.1. Raw Visibility Data

The raw visibility data for the VLASS will be stored in the standard VLA archive. These data will be available immediately after observation with no proprietary period. As the VLASS is being observed using standard data rates (25 MB/s maximum) there are no special resources required for the storage and distribution of these data. Data will be downloadable by users from the archive web pages as normal.

Risk: None. These is standard data comprising a volume that is normal for the amount of time spanned by the VLASS.

4.1.2. Calibrated Data

VLASS data will be processed using a modified version of the normal CASA-based VLA calibration pipeline. By the time of the VLASS observations, the VLA pipeline will have the requisite functionality to process VLASS data (full polarization, many individual target fields generated in OTF mode). The VLA pipeline is currently run on all VLA observations and is well tested. The VLASS will use a version specifically tested on VLASS pilot observations. See the description of the Calibration Pipeline below for more details.

In summary, the output of the pipeline will consist of:

- a set of final calibration tables
- (possibly) a set of source flux densities and polarizations, and/or sky models used in calibration
- one or more sets of flagging commands
- the final flag column (optional: currently output by pipeline)
- QA reports and plots
- the set of pipeline control instructions or script necessary to calibrate the raw data

Once the pipeline has run and after QA assessment, users will gain access to the calibrated data from the archive. Physically archiving the calibrated visibility data for long-term storage would double the amount of archive space required, which is too costly. Instead, the VLASS will archive calibration products and maintain scripts to generate the calibrated dataset. Scripts to apply calibration products will be based on CASA. Upon first processing of a Scheduling Block the calibrated data will be available for a short time (one to two weeks) for transfer to subsequent processing teams.

Risk: Low. The VLA Calibration Pipeline is in regular current operation, and its code is downloadable by users. We are currently upgrading this pipeline to use the infrastructure developed for the ALMA pipeline. Thus, by the time of the VLASS, this pipeline will have been in regular use and extensively tested. The addition of polarization calibration capability to the pipeline is the only significant addition, and this is expected to be available in the next year also.

4.1.3. Quick-Look Images

The identification of transient and variable objects is a key science goal of the VLASS. This requires the capability to process and image the data within a short period after the data is taken. We have set the

requirement on this to be 48 hours maximum, with a goal of 24 hours. If possible we will use the standard VLA Calibration Pipeline described above in a streamlined mode (highly parallelized where appropriate). As a fallback we can use a separate pipeline based on different software, such as the AIPS-Lite based pipeline developed and used by the Caltech group (PI: Hallinan) used for the S-band Stripe-82 observations taken and processed by that group (VLA Project 13B-370).

The output of the Quick-Look Calibration and Imaging Pipeline (QLP) will be continuum images (Stokes I) that can be used by the Transient Object identification teams (see below under Enhanced Data Products) to produce alerts for transient objects and arrange for follow-up studies. As these images will be constructed through mosaicking, there will also be a corresponding rms sensitivity (noise) image. Polarization images (Stokes QUV) are not part of the Quick-Look Basic Data Products.

There are thus a total of 2 images to potentially be produced by the QLP per trigger: an I image, and the corresponding noise map. As detailed in § 9.4 these images take 35TB and can easily be stored and served from the archive.

We do not plan to provide the higher-order MFS term images for spectral index (`tt1`) or curvature (`tt2`) per epoch, but it is planned to make tt1 images to reduce imaging artifacts. These could be made available as EDP. We do not plan to produce any image cubes in the QL pipeline as a BDP due to the high data volumes possible. This could also be part of a EDP proposal, most likely in a "processing on demand" (POD) service offsite. Also, no Quick-Look source or component catalogs will be produced as BDP.

The BDP Quick-Look images will be publicly available from the VLASS archive promptly upon production. Note that given this fast turnaround time and our staffing constraints only miminal QA will have been done on these images, which will likely contain artifacts from residual calibration issues and/or clean errors.

Risk: Medium Production of Quick-Look images will require prompt execution of a Calibration Pipeline, and if the main pipeline (see above) is not fast enough a separate one will need to be developed. Personnel will be needed to oversee running of the QLP and monitor this output, including astronomers and data analysts. Data storage needs are modest. A likely fallback is to relax the Quick-Look image production timescale from 48 hours to 1 week after data hitting the archive.

4.1.4. Single-Epoch Images

Within 6 months of completion of the observations of a given "epoch" (observations in a given configuration), fully calibrated and quality-assured continuum intensity images as detailed below will be produced and available in the archive. These will be generated using a specialized CASA-based Imaging Pipeline. This pipeline will be developed by the NRAO staff, with the involvement and guidance of the VLASS teams. The polarization images and the intensity and polarization cubes will be produced within 12 months of the end of an epoch. This delay is due to the added complexity and processing required.

The VLASS single-epoch wide-band continuum images will include:

1. Flux density calibrated beam-corrected Stokes I continuum intensity (band averaged) images covering the full mosaic area
2. Sensitivity (rms noise) images for the intensity I continuum image mosaic (the noise will vary over the mosaic)

3. Spectral Index and uncertainty images for Stokes I (generated using Multi-Frequency Synthesis)
4. Flux density calibrated beam-corrected Stokes QU continuum polarization (band averaged) images covering the full mosaic area
5. Sensitivity (rms noise) images for the QU polarization continuum images (the polarization is represented by a complex Q+iU image, and thus Q and U share the same rms noise image)

There are thus 7 single-epoch continuum image products (I, Irms, Ialpha, Ialpharms, Q, U, polrms). We do not plan to produce V (circular polarization) images for archiving, as these require different (and more expensive) processing options deal with instrumental effects.

Although the wide-band MFS imaging can produce spectral index (Ialpha) images, we suggest that instead of alpha, that the MFS "`tt1`" (Taylor-term order 1) image be natively stored, as this is effectively I*alpha and will not have the zeroes that come from dividing by I in noisy regions. The archive server can produce a masked alpha image from the native I and tt1 images.

Polarization: Due to the decorrelation effects of galactic and extragalactic Faraday Rotation on the linear polarization, the band-averaged Q and U images that the SEI pipeline produces will exhibit these issues. It will not be practical to construct the Q and U images using de-rotation from RM models or images, as these products are not available as BDP during the construction of the Q and U images. Comprehensive explanatory documentation will need to be provided to users about the limitations on using these products.

In addition to continuum images, there are spectral image cubes for each of:

1. Flux density calibrated beam-corrected Stokes IQU continuum per-channel image cubes covering the full mosaic area
2. Sensitivity (rms noise) cube images for I and polarization (Q+iU)

There are thus 5 potential image cube products at a given spectral resolution.

The spectral cubes will contain a wealth of information on the SED and polarization necessary for deriving RM and other computed products. In addition, these will be important for QA purposes and diagnosing RFI problems. Thus they will need to be generated with the processing of a given epoch. However, we note that it will be expensive to store these long-term in the archive for each epoch. In § 9.5 below, we describe the storage requirements for the single-epoch image cubes and propose to only store and serve coarse spectral cubes averaged over frequency to 128MHz (one plane per spectral window), and further restricted to 10% of the total sky area, likely through image cutouts around bright sources only. These cubes will still allow continuum polarimetry and rough rotation measure fitting to bright sources. However, full rotation measure synthesis will not be possible. The cumulative fine spectral images cubes, if available, would be used for this EDP science goal.

Given these limitations, it is attractive to consider a POD on-the-fly processing service for these cubes for ALL-SKY, as described above for the QL continuum images (§ 4.1.3), hosted on-site or externally (e.g. through XSEDE). In addition to efficiency, POD imaging will provide flexibility for choosing coarser frequency resolution in cubes, and the ability to control whether beam-corrections are done or not. In practice we have found that the channels in two or more entire spectral windows with 64 channels each will be entirely flagged, and so we assume we need cubes for only 896 channels maximum if uncompressed in

frequency. We assume that only temporary storage is required for the large full-resolution cubes for QA purposes and compression (see § 7.5).

Risk: Low to Medium. Currently, OTF imaging is done using special CASA scripts, with ongoing testing in development code. By the time of the VLASS, it is expected that all needed capability to produce the per-epoch images will be available and tested in a standard CASA release. The fallback is to continue to use development code. Processing for shallow to medium deep observations in ALL-SKY is of low risk. Development of a robust POD service for cubes is of medium risk, with a fallback to long-term archiving of the cubes. Storage of these images is of medium risk, with a number of fallbacks available using compression or reduced resolution. Investigation of acceptable spectral and spatial compression schemes are part of the Test & Development Plan.

4.1.5. Single-Epoch Basic Catalogs

There are many component finders used in the community for identification and classification of objects from images. It is expected from surveys such as the VLASS that basic component catalogs be produced and released along with the images. Over the next year, we will carry out a study of the available object finders suitable for use on the VLASS data and select and test one (or more if necessary) for production use by the team.

The output of the object finders will be a list of "components" in the image. It is beyond the scope of the BDP catalog production to associate multiple components of single astronomical sources together, or to cross-match with other wavelengths.

We consider the Basic Component Catalog entry for an "object" to contain:

1. Position, and uncertainty (likely centroid of I emission)
2. Peak Flux Density (continuum) in IQU, and uncertainty
3. Spectral Index at Peak (Stokes I) and uncertainty
4. Integrated Flux Density (continuum) in IQU, and uncertainty
5. Integrated Spectral Index (Stokes I) and uncertainty
6. Basic Shape information IQU (TBD, likely Gaussian fit parameters including deconvolved sizes)
7. Coarse Spectrum for Peak Flux Density and uncertainty in IQU measured at the I peak, tabulated for each spectral window
8. Coarse Spectrum for Integrated Flux Density and uncertainty in IQU integrated over the I source, tabulated for each spectral window

For the linear polarization Stokes Q and U values, we can instead report these as the more traditional polarized flux density (amplitude of Q+iU) and polarization angle ($0.5\ \tan^{-1}(U/Q)$).

Risk: Low. This has minimal requirements, and it is likely that object finder tools used for previous surveys such as NVSS, FIRST, and the Stripe-82 surveys will be sufficient, if not ideal. It is likely that the studies will identify a superior tool.

4.1.6. Cumulative Images

Within 12 months of the completion of observations of each epoch (16 months for polarization and cubes), continuum images for the cumulative "multi-epoch" data will be made. For the first epoch, this will be a minor extension of the corresponding single-epoch image. These will be largely the same set of images as described above for the single epochs. Accommodation for variable objects in the imaging will be across the multiple epochs is desirable.

The VLASS cumulative wide-band continuum images will include:

1. Flux density calibrated beam-corrected Stokes IQU continuum (band averaged) images covering the full mosaic area
2. Sensitivity (rms noise) images for the I and linear polarization (Q+iU) continuum images
3. Spectral Index and uncertainty images for Stokes I (generated using Multi-Frequency Synthesis)
4. Spectral Curvature and uncertainty images for Stokes I (generated using Multi-Frequency Synthesis)

There are thus 9 cumulative continuum image products. These are the images produced for the individual epochs (§ 4.1.4), with the addition of the next Taylor Term (tt2) in the MFS expansion for spectral curvature, plus its uncertainty.

Polarization: As in the single-epoch images, the Q and U continuum images will simply constructed using wideband single-term MFS imaging and thus will suffer decorrelation due to Faraday Rotation in some regions.

Tapered continuum images: At the VLASS Community Review, the panel determined that we should also provide tapered (lower resolution) images suitable for finding lower surface brightness extended emission than in the full-resolution images. To fulfill this request, we also plan to create tapered versions of the set of 9 images listed above tapered to a resolution 3x that for the standard images ($7.5''$), equivalent to that in C-configuration. This will take up 1/9 the storage of the high-resolution set and also require correspondingly less computational cost to create.

In addition to continuum images, there are spectral cubes for each of:

1. Flux density calibrated beam-corrected Stokes IQU continuum per-channel image cubes covering the full mosaic area
2. Sensitivity (rms noise) images for each of the cube images in I and Q+iU

There are thus 5 cumulative image cube products that can be made at a given spectral resolution.

The same considerations apply to the cumulative image cubes as for the per-epoch cubes (see § 4.1.4). Storage requirements are described below in § 9.7. The archive will store and serve only the most recent cumulative image cube. If the POD capability is available, users can request images from previous cumulative epochs (or possibly other selections). Note that the storage needs for these full-resolution cubes is considerable, and fallback options to reduced resolution or compressed cubes will be necessary to implement in the absence of enhanced archive resources. See the discussion of the required storage compression in § 9.7. In addition this this, there will be processing resource restrictions imposed upon these cubes. These

limitations will have to be explored as part of the test and development plan, but may involve restricting the imaging to a small (2.5% or less at full resolution) contiguous region(s) of the sky, and/or small cutout regions (possibly at increased rms noise level) around a subset of sources (possibly the brightest above some cutoff). At this stage we cannot define what these restrictions in BDP fine resolution cubes will be.

Tapered image cubes: As per the Community Review request, we will also produce tapered image cubes at 3x lower (larger) angular resolution.

Risk: Low to High. The cumulative ALL-SKY image rms will be only 58% of the single epoch image rms and thus low risk outside the Galactic plane, and has medium risk in the confused Galactic plane, bulge, and center region. Some test and development is needed for optimal combination for multi-epoch data in the presence of variable sources (see below). Development of a robust POD service for the cumulative data is highly desirable, but not critical as only the most recent cumulative images are of high scientific priority. Data storage for full-resolution cubes is of high (resource) risk. Fallback to reduced resolution or spatial coverage will have to be implemented in case additional archive resources (e.g. through EDP) are not identified.

4.1.7. Cumulative Basic Component Catalogs

As in the case of the single-epoch catalogs, these basic catalogs would be made available along with the cumulative images. These are components found largely based upon the continuum intensity images, we do not foresee searching the cubes for these. The cubes (intensity and polarization) will be used to derive the spectral and polarization information.

We consider the Basic Component Catalog entry for an "component" in the cumulative catalogs to contain:

1. Position, and uncertainty (likely centroid of I emission)
2. Peak Flux Density (continuum) in IQU, and uncertainty in I, Q+iU
3. Spectral Index at Peak (Stokes I) and uncertainty
4. Spectral Curvature at Peak (Stokes I) and uncertainty
5. Integrated Flux Density (continuum) in IQU, and uncertainty in I, Q+iU
6. Integrated Spectral Index (Stokes I) and uncertainty
7. Basic Shape information IQU (TBD, likely Gaussian fit parameters including deconvolved sizes)
8. Coarse Spectrum for Peak Flux Density and uncertainty in IQU measured at the I peak, tabulated for each spectral window
9. Coarse Spectrum for Integrated Flux Density and uncertainty in IQU integrated over the I source, tabulated for each spectral window
10. Fine Spectrum for Peak Flux Density and uncertainty in IQU measured at the I peak, tabulated for each fine spectral channel

11. Fine Spectrum for Integrated Flux Density and uncertainty in IQU integrated over the I source, tabulated for each fine spectral channel

Catalogs based on tapered images: As per the Community Review request, we will produce catalogs containing the same set of information based on the tapered images and cubes. As part of BDP we do not propose collate these with the high-resolution catalogs, nor associate components of the same astronomical source together, or cross-match to other catalogs.

Risk: Low to Medium. The main risk is in the imaging. Most of the ALL-SKY area imaging is low risk. Will need to handle increased object density and complexity for the Galactic regions and around bright sources (medium risk).

4.2. Enhanced Data Products

The Enhanced Data Products (EDP) are those that require more domain expertise, and so will be defined and produced by the VLASS community outside the NRAO. These data products will require external support to define, produce, and validate. However, these products are seen as essential to the VLASS science case, so both BDP and EDP will be curated and served by the NRAO.

The initial list of possible EDP are:

1. Transient Object Catalogs and Alerts
2. Full Spectral Resolution Image Cubes
3. Rotation Measure Images and Catalogs
4. Improved Object Catalogs
5. Matched filter source finding for extended objects
6. Light curves (intensity and polarization) for objects and/or image cutouts
7. Catalogs of multi-wavelength associations to VLASS sources

Beyond requiring extensive domain expertise, these areas are also ideal for nucleating multi-wavelength community groups and resources to work with and enhance the VLASS.

A special case of an EDP is the support for commensal observing at P-band (230–470MHz) using the VLITE system. There is no NRAO processing or archive support currently budgeted for VLITE data products, and thus use of VLITE with VLASS should be considered as an EDP (and Enhanced Data Services, EDS) provided in partnership with NRL.

Other areas for EDP will undoubtedly become apparent. Once the survey is approved, we will take proposals for new EDP to be included in the list above. Criteria for including EDP in the VLASS archive will be relevance to the VLASS science case and cost of curating and serving the products. As an incentive to include EDP in the VLASS archive, we ask that the NRAO encourage authors that use EDP to acknowledge groups that produced them.

4.3. Enhanced Data Services and the VLASS Archive

A comprehensive survey like the VLASS will produce a diverse set of data products and will require a full-featured archive to serve it to the public. A baseline plan is to serve products from a website hosted by the NRAO. This site will feature basic search capabilities of catalogs and products, as has been done for FIRST[8] and NVSS[9]. Previous VLA surveys only provided catalogs and images, so at a minimum the VLASS will extend that search capability to visibility data, calibration products, and deep/multi-epoch images. The NRAO will also provide data analysis scripts to apply calibration to raw data.

However, astronomy is increasingly a multi-wavelength discipline with a diverse set of tools for comparing observations from different observatories. If the VLASS archive exists only as a stand-alone NRAO-hosted service, it would not be as useful as one integrated with the tools available at places like IPAC[10] or the Virtual Observatory [11].

We are investigating options for having catalogs and/or images served by organizations outside the NRAO. This would extend the reach of the VLASS outside the radio community and open access to powerful tools for multi-wavelength analysis. The VLASS community, including the co-authors of the VLASS proposal, will be writing an NSF proposal to support VLASS data analysis and a more effective archive. These Enhanced Data Services (EDS) will greatly augment the utility of the VLASS and its basic and enhanced data products to the wider astronomical community.

Another area that would be greatly improved through EDS is the capability for "processing on demand" (POD) of images or image cubes. This would alleviate storage volume concerns, and enable more flexible angular and spectral resolution of the resulting products. We expect to utilize the NSF XSEDE network for modest use of POD-like processing for the pipeline. Fully enabled POD for VLASS could be carried out through partnerships with NSF supercomputing centers or with DOE science labs. Exploration of these options will commence upon approval by NRAO for VLASS.

As noted above, data archive and distribution support for commensal observing at P-band (230–470MHz) using the VLITE system is not currently budgeted for support by NRAO. Archive serving of commensal VLITE data taken at the same time as the VLASS should be considered an EDS provided in partnership with NRL.

4.4. Data Formats

We now describe the formats that we expect to use and serve as data products from the VLASS.

---

[8] `http://sundog.stsci.edu/cgi-bin/searchfirst`

[9] `http://www.cv.nrao.edu/nvss/postage.shtml`

[10] `http://www.ipac.caltech.edu`

[11] `http://www.us-vo.org`

4.4.1. Visibility Data

The VLA archive holds the raw data in the native SDM format. Users can request CASA MS format data that are produced from the SDM by the archive server.

Users of VLASS can also request the calibration products (tables, flags, pipeline instructions) that can be used to apply to a raw SDM or MS downloaded from the archive.

Calibrated visibility data will be served in CASA MS format upon request through application of the tables, flags, and pipeline instructions.

4.4.2. Images and Image Cubes

The most common image format in astronomy is FITS. CASA can recognize and use (for most operations) FITS images, although it has its own image format based on CASA tables.

The VLASS data services will need to provide the capability to serve FITS and CASA format images upon request for sub-areas (postage stamps, simple rectangular regions) from the available images.

The question of a "native" format in which to store images is more complex. The most straightforward approach would be to store a set of FITS (or CASA) images that tile the survey areas. Users could request sets of these directly, or ask for a region that would be assembled by the data server to one or more requested FITS or CASA images.

It might be advantageous to take more forward-looking approach and store the image data in a hierarchical data format such as HDF5 (e.g. in the context of LOFAR, Anderson et al. 2010, arXiv:1012.2266). Representation in HEALPIX might be useful also. Investigation of options such as these should occur in the year leading up to the commencement of VLASS.

4.4.3. Catalogs

Catalogs could be stored in some internal manner using flat ASCII files, in a relational database (RDB), or in a hierarchical data format (such as HDF5).

Users must be able to obtain catalogs in simple formats such as flat ASCII files, XML files, or other basic formats.

4.4.4. Plots

Where the data services have the capability of providing plots, these should be in standard formats such as PNG, JPEG, GIF, or even FITS in some cases.

5. Observing

This section describes the considerations for the real-time aspect of observing as carried out by the telescope system and observers.

- Correlator Resource Setup
- OTF Setup and Scanning
- The Antnena Pointing Table
- Sky Tiling
- Scheduling

5.1. Correlator Resource Setup

We will use the WIDAR correlator in the wideband mode (2MHz channels) with a total (maximum) of 2048MHz of bandwidth. The default setup has a 24MHz overlap of the two basebands at band center, but for the VLASS we have the option to place the basebands adjacent, e.g. covering 1976–4024 MHz. This will place the sub-bands on a regular grid for the coarse spectral cubes, and give a slightly wider frequency range for spectral and RM studies (the S-band has a 3db range of 1850–4150 MHz). Note that because of this the low end of the second baseband will be flagged and missing from imaging (without the overlap to cover this).

The options are:

1. *Default:* Use the default baseband setup of two basebands at 1984–3012MHz and 2084–4012MH, with 24MHz (12 channels) of overlap in the center at 3GHz, for a total span of 2028MHz from 1984–4012 MHz.
2. *Contiguous Centered:* Two adjacent basebands 1976–3000 MHz and 3000–4024 MHz, for a total span of 2048MHz from 1976–4024 MHz.
3. *Contiguous Low:* Two adjacent basebands 1964–2988 MHz and 2988–4012 MHz, for a total span of 2048MHz from 1964–4012 MHz. This is adjusted so that the low-dec RFI falls mostly in two SPW (spw 1 and 2 of first baseband).
4. *Contiguous High:* Two adjacent basebands 2092–3116 MHz and 3116–4140 MHz, for a total span of 2048MHz from 2092–4140 MHz. This is adjusted so that the low-dec RFI falls mostly in two SPW (spw 0 and 1 of first baseband), but the usable frequency range does not start until spw 2 at 2348 MHz.

We have decided to go with a slightly modified version of the Contiguous Low option. The combination of SEFD (sensitivity vs frequency) and integration time leads to this decision. The SEFD from EVLA memo 154 shows a sensitivity variation of 18% across the S-band receiver from 2–4 GHz, with better sensitivity at 4 GHz. However, the beam HWHM is approximately twice as large at 2 GHz compared to 4 GHz (EVLA memo 195), and therefore the integration time in OTF mode is four times greater at 2 GHz than 4 GHz.

Thus for a noise level of 1 [unit] at 4 GHz, the corresponding noise level at 2 GHz will be 1.18/sqrt(4) = 0.59 [units]. The better sensitivity at lower frequency means the Faraday transfer functions will be improved, and additionally this configuration allows a longer lever arm for spectral index measurement. Further, we adjusted to spw boundaries such that the strong RFI from the XM DARS satellite does not leak into a higher spw. Thus, we use the following boundaries for the two JVLA 8-bit basebands (designated AC and BD for historical reasons):

1. *AC*: 1965 – 2989 MHz
2. *BD*: 2989 – 4013 MHz

In this setup the first AC spectral window has low but acceptable sensitivity.

We will record in full polarization mode (four correlator products RR,RL,LR,LL).

We will employ a dump time of 0.45 seconds, which gives a nominal data rate (in the RCT page) of 26.32MB/s corresponding to 25MB/s using the equation in the OSS, but adding in the auto-correlations that are recorded by default.

Risk: Low We have observed the VLASS Pilot with this setup.

5.2. Mosaicking

In order to carry out the VLASS, we will need to observe the sky using a large number of mosaicked pointings of the VLA. At 2–4 GHz, the VLA has a field-of-view given by the primary beam response of the 25-meter diameter antennas as illuminated by the receiver and optics. This approximately follows a Gaussian response, with a measured full-width at half-maximum (FWHM) near the center of S-band given by the table in Fig. 1, and varies from 21.1′ near 2 GHz to 11.9′ near 4 GHz, with FWHM of $\approx 14'$ at 3 GHz mid-band. In order to optimally cover a given sky area in an efficient manner, the array must either conduct a raster scan using "on-the-fly" mosaicking (OTFM), or tile the area with a number of discrete pointings in a hexagonal packed configuration ("Hex-pattern Mosaicking"). The choice between these techniques is determined by the extent to which the extra overhead (from 3 to 7 seconds) needed to move the array and settle at each pointing in the discrete hex-pattern mosaic becomes a burden on the observations, and thus OTFM is favored.

The techniques of OTFM and Hex-pattern Mosaicking and the calculations and procedures needed to set these up are described in the Guide to VLA Observing: Mosaicking[1] section. The salient features are:

OTFM: There is very little move-and-settle overhead as the array is in continuous motion over a row of a raster with only a small start-up (∼10–15 sec) at the start of each row. In OTFM the phase center of the array is discretely stepped on timescales of a few seconds or longer, so no phase smearing of the images results. However, because the primary beam response pattern is moving with respect to the sky, there are errors introduced in the amplitudes by the moving beam in a single visibility integration time. Thus, the main cost of OTFM therefore is that for fast scanning rates the fundamental integration ("dump") times in the dataset must be short (10% or less) compared to time it takes to cross the FWHM of the primary beam. This in turn increases data rates from those that would otherwise be required (e.g. to avoid time-smearing of the loci in the uv-plane). The secondary cost of OTFM occurs in the imaging process, where the effects of the moving primary beam over the time at which the phase center is fixed must be compensated

for by the imaging algorithm at significantly increased computational cost over that required for a similar observation taken with a fixed pointing center. This is currently done by the CASA software package in its `clean` deconvolution task. Testing of the efficacy and efficiency of the use of the CASA imaging for OTFM is underway, and is part of the testing plan given below. For the purposes of this plan, we will assume that OTFM datasets can be imaged with sufficient accuracy to be practical for the ALL-SKY observations.

Hex-pattern Mosaicking: It takes the VLA 3–7 seconds (depending on the direction of motion in azimuth-elevation coordinates, usually around 6–7 seconds if not optimized) to move and settle between nearby pointings. Thus, if less than 28 seconds is spent integrating on each pointing, the overhead from this motion itself is 25% or higher in the worst case. For a hex-pattern, each field gets 67% of the total integration time desired on-sky, so observations where the VLA Exposure Calculator[12] indicates an on-source time of 42 seconds or less will incur significant overhead if not done with OTFM. For VLA S-band, the calculated exposure time is 7.7 seconds at a rms image sensitivity of $100\,\mu$Jy, and thus observations desiring a depth shallower than around $43\,\mu$Jy in a single pass will prefer OTFM. Thus, our ALL-SKY observations with single-pass depths $> 100\,\mu$Jy will require OTFM, and hex-pattern pointed mosaics will not be done for the VLASS.

Risks: Low to Medium OTFM has been used successfully for shallow (single-pass image rms $\sim 100\,\mu$Jy) in S-band in the Stripe-82 observations by Hallinan et al. (program 13B-370). Images with rms $\sim 60\,\mu$Jy from the three passes spanning 2 months are being made as part of the testing program, and current indications are that they are of acceptable quality. Furthermore, the VLASS Pilot is underway and producing single-epoch quick-look images of the expected rms noise level and quality. Thus, we deem the risk associated with using OTFM to be low overall on the basis of quality. The further consideration is the extent to which more expensive imaging costs are required in areas in which there are bright sources, particularly for polarimetry, and for accurate determination of fainter source spectral indices. This is also being assessed in the testing. As the new imaging algorithms are only recently available, we assign this as medium risk to resourcing for the VLASS, as extra computational power or longer processing times are likely to be required in some regions.

5.3. Antenna Pointing Table

During OTFM scanning, the array online system will produce and store in the SDM an Antenna Pointing table containing the direction towards which each antenna is pointed (as determined from the encoders and pointing model) on a fine time grid (currently 0.1sec). This will be used by the filler to populate the POINTING table in the MS, which CASA imaging can then use if requested during image reconstruction to mitigate smearing effects over the multiple (currently 2) integrations that comprise a phase center.

Risk: Low Although production of the pointing table is still in testing stage, and use during imaging is unproven, the VLASS observations have been set up such that the broad science goals can be met without using the pointing information.

---

[12] `https://science.nrao.edu/facilities/vla/docs/manuals/propvla/determining/source`

5.4. Sky Tiling

The VLASS will ultimately need to cover the sky $\delta > -40°$ using OTF scanning. As described above, we will do this through OTF stripes in RA (ascending or descending) at constant DEC. To carry this out logistically, we define a "tiling" of the sky to aid in the scheduling during the survey and for the pilot. It is desirable that:

- OTF stripes take at least 150s (preferably 180s or longer) to not cost too much overhead on row turnaround
- a given tile-set covered in a SB or sub-SB have OTF stripes that start and end at a given RA (with variable duration to fix the on-sky scan speed)
- the tiling be easily described to keep book-keeping simple
- the tiles can be fit into SBs of suitable length in units of one or more tiles
- there be a fixed set of tile row declinations and RA start and stop points for the survey

5.4.1. Example I: VLASS Full Sky Uniform Tiling

The goals of this tiling are to have SB durations around 4 hours with individual tiles that fill each block and are of nearly uniform size. We derive:

- Area around 80 deg^2 per tile (approx. $10° \times 8°$)
- Avg. OTF Target Dwell Time: 3.36hrs at 23.83 deg^2/hr
- Avg. OTF Duration: 3.47hrs at 3.3% OTF overhead (e.g. 6s for 180s scan)
- Avg. Block Duration: 4.16hrs at 20% CAL/Slew overhead
- Net Speed: 23.83 deg^2/hr / (1.033×1.2) = 19.22 deg^2/hr

Note that the actual tile SB durations will depend on the LST of observing and individual overheads when the schedule is constructed.

The trial tiling using this is shown in Table 14.

Features of this tiling include:

- A. Symmetric North and South, Tiers N01-N11 + S01-S05
- B. Tiles inclusive at S (low Dec) boundaries, exclusive N when row hits exactly
- C. Geometry of Tier 11 split TBD: assumed 3 sectors, could be 2 sectors + cap
- D. Rows at constant Dec. First and last Phase Centers half subscan inside edges.
- E. The sub-tile in a given Tier containing a specified RA is given by taking (RA/$\Delta\alpha$)+1.

Table 14: Tiling Example 1. Durations are computed for the stated areas using a net survey speed of 19.22 deg^2/hr.

Tier	δ_{low}**(deg)**	δ_{up}**(deg)**	**N tiles**	$\Delta\alpha$**(deg)**	**Area (deg^2)**	**Duration**
01	0	8	36	10	79.74	4.15
02	8	16	36	10	78.18	4.07
03	16	24	32	11.25	84.50	4.40
04	24	32	32	11.25	79.40	4.13
05	32	40	30	12	77.60	4.04
06	40	48	24	15	86.25	4.49
07	48	56	24	15	73.82	3.84
08	56	64	18	20	79.94	4.16
09	64	72	15	24	71.87	3.74
10	72	81	9	40	83.95	4.37
11	81	90	3	120	84.65	4.40

- F. This naming convention is for convenience of this table, e.g. (N/S)Tier.(Block 01-36). We will name the Source Catalog entries and scan names using positions including the center of the block, e.g. N01.01 as 0020+040 or similar.

Example: The COSMOS field at RA=150deg, Dec=+2deg is on the border between tiles N01.15 and N01.16. Thus, for COSMOS in the pilot test we might shift tiles 1/2 block to put in single one.

5.5. Scheduling Considerations

The Jansky VLA is normally operated using a "Dynamic Scheduling Queue" where the individual Scheduling Blocks (SBs) are created in the VLA Observing Preparation Tool (OPT) to be able to be executed in a prescribed range of LST, and submitted to the VLA Scheduler software (OST) to be queued up for observation by the array in a manner dictated by weather and priority.

For ALL-SKY, it would be advantageous to construct the schedules in large blocks to be observed at specific LST start times. This would allow maximum efficiency in calibration and control of slewing (e.g., telescope wraps). In practice, due to considerations such as the ability to allow interrupts for target-of-opportunity observations, and fault tolerance (e.g., for power outages, weather, etc.), the schedule will need to be broken in to modestly sized blocks. Ideally, the VLA Scheduler software would be able to handle sets of SBs that are linked (e.g., in a particular order or in alternate sets). However, this capability does not currently exist, and there may not be resources in the software group to allow this. Instead, the most straightforward plan is to make sets of SBs for submission (see below) and submit only a day ahead. This will require an "Astronomer on Duty" (AoD) for VLASS who will keep track of what SBs are ready to observe, make sure they are submitted, make sure that they run, and make any modification necessary (e.g., due to TOO or weather interrupts).

Target-of-Opportunity Interrupts: For long-block observations, provision would need to be made for the possibility that observations will be interrupted for time critical TOO programs (e.g., for triggered transient observations). There is currently no mechanical provision in the way schedules are constructed or

executed for the suspension and restarting of schedule blocks. Therefore, the most straightforward implementation is to break all schedules into blocks of 2–3 hours in length, and to allow TOO interrupts to simply stop the execution of the current schedule and possibly pre-empt the execution of the following one or more SBs. After TOO observations are complete, the VLASS schedule would resume with the next appropriate block. The AoD would be informed of this interruption, and would examine the archive record to determine the missing observations and construct a "make-up" SB to be run at the first appropriate opportunity. The plan for the construction of schedules (see below) will take this need into account.

Risk: Medium The VLASS scheduling and observation monitoring will be a vast book-keeping exercise. As described above we believe this is controllable, either through some modest improvements in operations software, or at worst with some workarounds in the way we carry out the scheduling. There will need to be a pool of VLASS astronomers and data analysts to fulfill AoD staffing throughout the survey. This ideally might include students participating in the VLASS from the community. Some NRAO resourcing will be required to support these activities both directly and for supervision.

5.6. Schedule Construction

It will be impractical to use the VLA OPT in standard interactive mode to construct the thousands of hours of schedules for thousands of pointings that must be in the Source Catalog Tool. Instead, we will create some lightweight software in Python to construct the ascii lists that the OPT and SCT can read. This feature has been used by the 13B-370 Stripe-82 observers (mainly Caltech graduate student Kunal Mooley) with success to schedule those observations. Our plan is to similar Python code which will be made available to the community for their own use for similar surveys.

The VLASS Pilot SB is scheduled by generating a pair of text files containing the Scheduling Block and Source Catalog, which will be read into the OPT and submitted to the queue for observation. The procedure work-through is described in detail in an accompanying Authorea document (`https://www.authorea.com/users/92338/articles/113729/`). A brief summary of the current procedure is:

- Determine the tile name, boundaries, and calibrator sources for manual input (in the future, this will be automatic using the database)
- Use `OTF_scans_from_tile.py` to create a source definition file and a scan definition file. Manually add a header with the list of calibrators and a guess for the initial LST range.
- Use `scanrows2opt.py` to create the SB definition file.
- Upload the source definition file to the SCT and the SB definition file to the OPT.
- Manually tweak the SB to have appropriate scan lengths and LST start range.

Risk: Low We can build upon the process used by 13B-370 for the Stripe-82 survey and our process for the VLASS Pilot Survey for schedule and catalog construction. Some rules for keeping track of schedules and archiving will need to be devised and followed.

5.6.1. Hour Angle (HA) range

At a given Declination, there is an allowed hour angle range set by the allowable elevation range and the desired PSF elongation limits. At Declinations where the source passes near zenith at the VLA, there are also restrictions on low HA limits. We describe these below.

Figure 5 shows the contours of PSF axis ratio A/B in the Declination-HA plane for the array in the B configuration. Figure 6 shows the A/B for the VLA in the BnA hybrid.

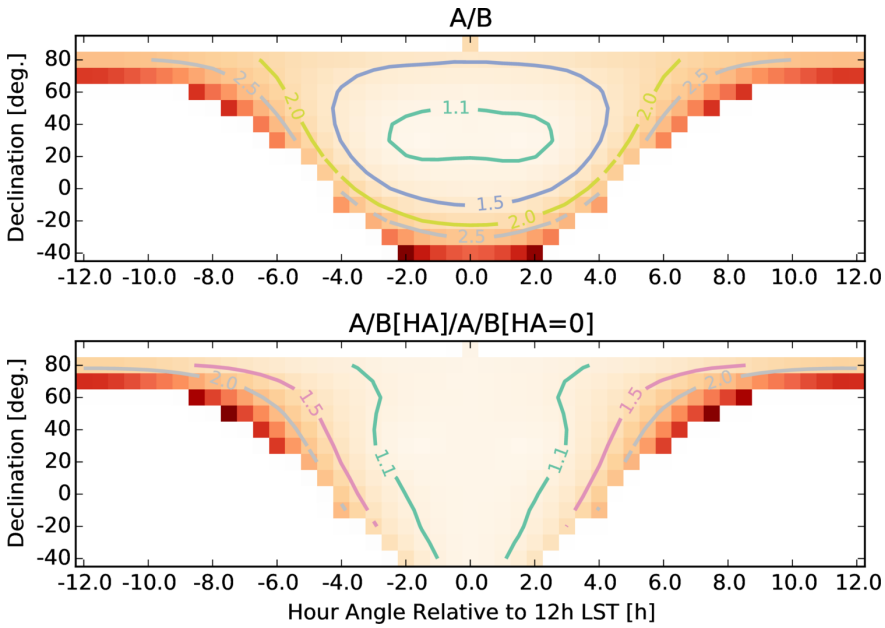

Fig. 5.— Contours of PSF axis ratio A/B as a function of Hour Angle and Declination, with the VLA in the B-configuration. The top panel shows the raw A/B, while the lower panel is the ratio of A/B to the value at HA=0h for that Declination. Most of our observations will likely take place at HA between the A/B=1.5 and 2.0 contours. Note that inside the HA=1.1 contour the Elevation starts to be too high, and these HA should also be avoided.

5.7. Overall Observing Schedule

The VLASS as proposed will be carried out over the course of at least 6 cycles of the VLA in its B (and possibly BnA) configurations, spanning a total of 7 years (84 months). We present here one possible schedule for observing the VLASS. Other scenarios are possible, should new constraints be imposed (e.g. based on design reviews).

5.7.1. 7-Year Schedule

We spread the VLASS over 7 years and 6 cycles (84 months: Table 15). In this scenario, the survey starts with B configuration in 2017B in Sep 2017, and completes in Oct 2024. Each configuration cycle gets

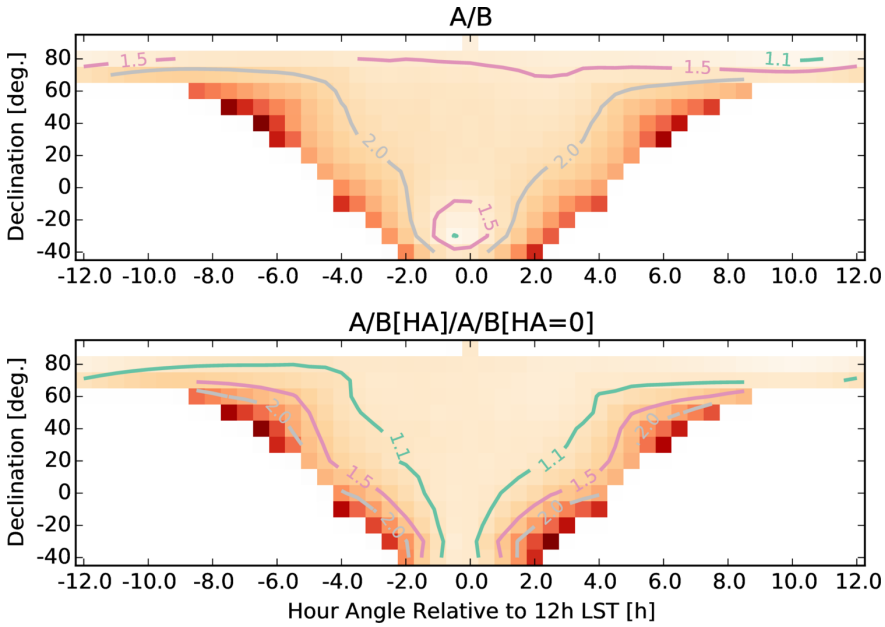

Fig. 6.— Contours of PSF axis ratio A/B as a function of Hour Angle and Declination, with the VLA in the BnA hybrid configuration. The top panel shows the raw A/B, while the lower panel is the ratio of A/B to the value at HA=0h for that Declination. The use of the BnA hybrid reduces the A/B beam elongation at low declinations ($\delta < -15°$) and the very highest ($\delta > 80°$).

Table 15: Distribution of VLASS observing hours by configuration and configuration cycle

Cycle	Nom. Start	B	BnA	Total
1	Sep 2017	627	293	920.0
2	Jan 2019	627	293	920.0
3	May 2020	627	293	920.0
4	Sep 2021	627	293	920.0
5	Jan 2023	627	293	920.0
6	May 2024	627	293	920.0
Total		3762	1758	5520

920 hours of scheduled VLASS, with 627 hours during the B-configuration and 293 hours dedicated in the BnA hybrid (§ 3.1).

5.8. Schedule Pressure by LST

Using the proposed schedule (§ 5.7.1) for 5520 hours spanning 6 configuration cycles over 7 years, we have estimated the total LST pressures in the B and BnA configuration for the various components. These pressures represent the average number of "passes" at a given LST needed to carry out the VLASS.

Formally, we approximate each component of the VLASS as a total time T broken into observing blocks

that can be observed in a "window" of length W starting at some LST H. All times from H to $H + W$ for that component are assigned a pressure $P = T/W$. We estimate the parameters in Table 16 for the VLASS:

Table 16: Mean LST pressure for components of the VLASS

Config	**T(hrs)**	**W(hrs)**	**H**	**P**
B	627.0	24.0	0^h	26.1
BnA	293.0	24.0	0^h	12.2

This scenario assumes that we spread the LST load evenly. In practice, there is less time available during the daytime and it is possible to shift the LST impact both during and between the two cycles comprising an epoch. A detailed scheduling plan will be devised for CDR.

5.9. Impact of VLASS on PI science

When spread over six configuration cycles the total number of observing hours that will be needed for the VLASS (920 hours per cycle) amounts to 13% of the total number of hours typically used for science observing (6937 hours per cycle), given the *current* observing efficiency of the VLA, which includes 50 hours per week for engineering, software maintenance, and other commissioning tests. Beginning semester 2016B (September 2016) the time for engineering, software maintenance and commissioning will go down to 42 hours per week, providing a total of 7434 hours for science per cycle. The impact of the VLASS averaged over a configuration cycle is therefore 12.4%.

Table 17 shows the current distribution of observing hours per configuration within a 16-month (487 day) configuration cycle (move time between configurations is not included), along with the approximate number of hours for PI science. It is important that the 16-month cycle be maintained, so that targets at a particular LST can be observed at night time at some point during three configuration cycles, for both the VLASS and regular PI science. However, it is clear from comparing column 3 in Table 17 with Table 15 that, if the timing of the VLA configurations within a configuration cycle were to stay the same during the VLASS, then the B/BnA/A configurations will be adversely impacted in terms of the number of hours available for PI science compared with the other configurations. In addition to these considerations, we note that NRAO is eliminating the hybrid configurations from the regular configuration cycle, because the usual proposal pressure as a function of LST for the hybrids is currently very skewed and poorly matched to the available hours at certain times of year.

We therefore propose that, while undertaking the VLASS, the configuration lengths within a configuration cycle be modified as shown in Table 18. In this model, the impact of the VLASS is spread over all configurations, rather than confining them to those used by the VLASS. It is assumed that except in the dedicated hybrid, science hours are 75% of the total clock hours. In the B-configuration, VLASS uses 27% of the available science hours, and the number of hours available in the B-configuration is still higher than in the past because of the extra 8 hours per week for science.

Table 17: Current configuration lengths and hours for PI science (70% wall-clock time for science)

Configuration	**Length (days)**	**Hours for PI science**
D	84	1411
DnC	18	302
C	80	1344
CnB	18	302
B	95	1596
BnA	18	302
A	100	1680

Table 18: Proposed configuration lengths and hours for PI science during the VLASS (75% wall-clock time for science)

Config.	**Length (days)**	**Total sci. hours**	**VLASS hours.**	**PI sci. hours**
D	87	1566	0	1566
DnC	0	0	0	0
C	88	1584	0	1584
CnB	0	0	0	0
B	131	2358	627	1731
BnA	17	306	293	13
A	101	1818	0	1818

6. Calibration

The goal of the VLASS Calibration process is to determine, on the basis of *a priori* factors and from observations of standard calibration sources, the corrections to the raw data amplitude, phase, and visibility weights to be applied to the data. This process also determines the flags that are needed to remove bad data due to instrumental faults, RFI, and other causes of error. When applied to the VLASS data, this calibration will allow the production of images in the next processing stage. This process only includes the derivation of the complex gain and bandpass calibration factors known through previous measurements or determined by the observations of calibrators and transferred to the VLASS target observations. The self-calibration of VLASS data is included in the imaging stage of processing.

VLASS data will be processed using a modified version of the normal CASA-based VLA calibration pipeline. By the time of the VLASS observations, the VLA pipeline will have the requisite functionality to process VLASS data (full polarization, many individual target fields generated in OTF mode). The VLA pipeline is currently run on all VLA observations and is well tested. The VLASS will use a version specifically tested on VLASS pilot observations.

The VLASS Calibration Pipeline will carry out

1. Application of initial online flags (off-source, focus error, subreflector error)
2. Determination and application of derived flags (RFI, bad antennas, shadowing, other)
3. Switched power amplitude calibration and antenna gain curves

4. Flux scale calibration (using standard sources)
5. Complex Delay and Bandpass Calibration
6. Complex Gain Calibration
7. Flux density bootstrapping (from primary to secondary calibrators)
8. Polarization On-Axis Leakage Calibration
9. Linear Polarization Angle Calibration
10. Interpolation and Application of Cumulative Calibration
11. Final Flagging of Data (insufficient or failed calibration, RFI)
12. Output of Quality Assurance (QA) information, plots, images

As mentioned earlier when discussing Data Products, it is more efficient to store the calibration tables, flags, and pipeline commands and then create the calibrated dataset upon request from the archive, rather than to store both raw and calibrated datasets. Should it be deemed appropriate and possible, we might consider also archiving off-site the full calibrated dataset (e.g. through Enhanced Data Services by a community partner).

Risk: Low to Medium The VLASS is well-suited to pipeline processing and will be able to make use of the VLA Calibration Pipeline as it is currently being developed. This pipeline is now being re-implemented in a new architecture based on the ALMA pipeline development, and by the time of VLASS will be well tested. Incorporation of polarization in this pipeline will be a primary goal over the coming year, and is necessary not just for VLASS. There are minor medium risk issues in the calibration for the Quick Look images.

6.1. Observations of Calibrators

The first concern for calibration is setting up the observing such that sufficient calibration can be performed on the data. The calibration of the entirety of ALL-SKY will require the availability of a "network" of suitable calibration sources spread across the entire visible sky with a spacing of one every few degrees — a density of around 0.05–0.25 deg^{-2} giving a list 1700–8500 in total. These will need to be compact (for the VLASS A and B configuration observations). Initially, the obvious starting place is the current VLA Calibrator Database, currently containing 1865 sources. Of particular interest is the VLBA calibrator database, with around 4700 sources in the VLASS area, as these sources are known to be compact and have astrometric precision positions. They will need to be verified as point-like to the VLA, with no source structure outside the VLBA delay beam.

Another good starting set is the CLASS catalog of compact sources measured at 8.4GHz in A-configuration Myers, Jackson, Browne et al. (2003). The CLASS database contains over 13000 distinct detected sources in the northern celestial hemisphere, a good fraction of which would be suitable as VLASS calibrators. There are extensions to the VLA-visible southern celestial hemisphere, including the compact calibrator catalog of Winn, Patnaik, & Wrobel (2003). These have some overlap with the VLA and VLBA calibrator databases but should yield a substantial number of excellent calibrators.

Prior to starting the VLASS, it would be prudent to observe candidate calibrators from these lists to identify those suitable for our survey. This could be carried out for 6000 targets with around 60 hours of observations. Ideally, this would be done at S-band in B or A configuration, but it may also be practical to carry out at C- or X-band in the C-configuration prior to the start of the survey.

Identification of calibrators for the VLASS in the Galactic Plane will be more difficult. Most of our known calibrators come from parent surveys that avoided the Galactic Plane and bulge. Some additional work will likely be required to find a good dense set of calibrators in this region. For example, one could contemplate a shallow fast-scanning survey covering the $\sim 3200\,\mathrm{deg}^2$ area in around 40 hours, sacrificing imaging quality and spectral bandwidth and sensitivity for scan speed within allowed data rates. This would also be of general benefit to VLA users.

Note that once the first epoch is complete, the survey itself will yield a full (unbiased) list of calibrators for use in subsequent epochs.

Identification and characterization of the VLASS calibrator list is a key item in the Test & Development Plan below (§ 10).

Risk: Low to Medium. There are viable paths to obtaining an initial calibrator database, although ideally verification of this database would require up to 100 hours of test observing prior to the VLASS.

6.2. Calibration Issues for the VLASS

Because the VLASS covers the entire sky usefully visible to the VLA, there are a number of issues related to calibration that require special attention and investigation. These are mostly related to the RFI known to exist at 2–4 GHz, but also include possible ionospheric issues.

6.2.1. RFI at S-band

As described above in § 2.1.2 substantial parts of the 2–4 GHz band are plagued by RFI. Some (though not all) of the most pernicious interference comes from geostationary satellites in the "Clarke" belt, which appears at Dec $\delta \approx -5.5^\circ$ from the VLA. This will affect VLASS observations near (within 10 degrees from our current estimation) this Declination. In addition to reducing the usable bandwidth, RFI can affect the calibration of the data. Investigation of this effect and the devising of observing and calibration strategies to mitigate RFI induced problems are part of the Test and Development Plan (§ 10.1.1).

Case Study: Stripe-82. The B-configuration S-band observations (12A-371, 13B-370) in Stripe-82 encountered calibration issues attributed to RFI. In the first set of observations in 2012 (12A-371) covering 50 square degrees, the sub-stripe was broken into two sections that were calibrated using different calibrators, one slightly north of the stripe (J2212+0152) and the other to the south (J2323−0317). During processing, it was noticed that the observed amplitudes on the southern calibrator J2323−0317 varied greatly as a function of time (azimuth), and that application of the gains derived from these scans to the target data introduced spurious variations in the flux densities and rms variations in off-source areas of the images. The observations of the northern calibrator J2212+0152 showed little or no variation. There did appear to be some variation in the Stripe-82 target observations, and thus the effect was still present on the equator. Some of the hour angles for J2323−0317 most strongly affected appeared to correspond to azimuths of known

geostationary satellites, and thus compression in the receiver system due to RFI from these satellites was strongly suspected. When the observations for the full 270 square degrees of Stripe 82 for 13B-370 were carried out, schedules were constructed avoiding the hour angles most strongly impacted in the 12A-371 data. In addition, calibrators to the south of Stripe-82 were not used. The discovery and mitigation of this effect in the 50 square degree sub-stripe are described in more detail in the paper by Mooley et al. 2015 (in preparation). More extensive tests on the full Stripe-82 from 13B-370 are still underway, and will also be part of the VLASS Test and Development Program.

Risk: Medium RFI is clearly going to be a problem near the Clarke belt, and possibly elsewhere. Observations in these affected regions will likely need to be treated specially during processing, with extra resources and personnel requirements.

6.2.2. The Ionosphere at S-band

There will probably be some times when ionospheric disturbances will impact the calibration and imaging of the data. Some of these can be avoided by use of dynamic scheduling, or re-observing of blocks damaged beyond repair. Use of pre-calibration (e.g. using the TECOR algorithm) and imaging/self-calibration iterative schemes coupled with global sky models (which will evolve as the survey progresses) will be employed as needed for the rest of affected data.

Risk: Low to Medium. The extent of this is unknown. Recent pilot observations and reduction of data from Stripe-82 and COSMOS at S-band do not appear to be strongly impacted by the ionosphere, although occasional times requiring careful self-calibration were encountered, and were possibly due to ionospheric issues. The main risk will be in the time and effort required to identify affected data and to re-process using mitigation techniques.

6.3. Algorithm and Software Development for the Calibration Pipeline

Only a modest amount of additional software development is required for the VLA Calibration Pipeline to handle the VLASS data. In particular, accommodation of OTF scans in the pipeline (e.g. suppression of flagging at beginning and end of scans for the short OTF scans, suppression of plotting for each of the > 10000 target fields) is the primary issue. Otherwise, the VLASS data can be treated as any other VLA dataset.

The other issue for use of this standard VLA pipeline for VLASS is its overall speed and efficiency. In particular, use of the pipeline within the Quick Look image production path will require it to process data promptly upon observation. The current VLA Calibration Pipeline is too slow, although bottlenecks have been identified (e.g. the speed of `applycal`, production of QA plots). It is likely that development of a version of the pipeline that streamlines processing for VLASS and/or uses extensive parallelization will be necessary. Exploration of options for speed-up for QL and for general use are part of the Test and Development Program.

Risk: Low to Medium The modest changes in the standard pipeline here should not require significant resources. Use of the pipeline for normal VLASS use is straightforward and low risk. Use for Quick Look processing might be medium risk if our efforts to speed it up are insufficient. Fall-backs include using more cluster nodes for parallel processing of single SBs, or use of the Caltech AIPS-Lite calibration pipeline.

6.4. Calibration Processing Requirements

Estimation of the processing resource requirements required for carrying out the VLASS operations outlined above is fairly straightforward. We now have experience running the current (script-based) JVLA Calibration Pipeline for all observed projects. In addition, the Stripe-82 and COSMOS programs have used custom calibration scripts as well as the standard calibration pipeline. All of these use CASA in the currently available (version 4.2.2 and earlier) standard "serial" processing mode. This forms the baseline for our processing time estimates.

6.4.1. Case Study: Calibration of Stripe-82 datasets

For the purposes of VLASS testing, we have created a custom crafted CASA calibration script for the 3-hour blocks of the 13B-370 program. This goes end-to-end from the importing of a raw SDM file to a CASA Measurement Set, through to the creation of a calibrated MS containing only the target data. As of this time, it does not include polarization calibration (though this should only increase the processing time by a small factor, perhaps 10%). It also does not create plots equivalent to the standard pipeline "weblog".

The test data set was one of the 3-hour blocks from the 13B-370 Stripe-82 program[13]. Running the custom calibration script took 10.8 hours of elapsed time, or a factor of 3.6 times the observing block duration of 3 hours. This implies that it is feasible to run a serial calibration process in less than 4 times the observing time, and thus it is practical to keep up with observing by running 4 independent calibration processes on a single cluster node (the memory footprint for calibration appears to be sufficiently small). For reference, the standard VLA Calibration Pipeline[14] took 66.25 hours to process this same 3 hour block (22 times the block duration), so some substantial efficiency improvements (including disabling of much of the plotting) would be required to employ this for the VLASS.

The calibration for Quick-Look imaging is the most constrained, as our specification is to fully process the data and make images available within 48 hours of the completion of an observation block, with a goal of 24 hours or less. If the serial processing of a block takes 4 times the block duration, then observing blocks would need to be 6 hours or less in duration to process within 24 hours (leaving 24 hours for imaging to meet the specification), or 3 hours if you want to process within 12 hours (half of the goal of 24 hours total). Implementation of an truly parallel calibration pipeline would allow use of longer observing blocks.

Risk: Low The modest changes in the standard pipeline here should not require significant resources. Use of the pipeline for normal VLASS use is straightforward and low risk. Use for Quick Look processing might be medium risk if our efforts to speed it up are insufficient, although custom scripts are clearly feasible. Implementation of intrinsic parallelization would be ideal and greatly beneficial, but is not required to meet our specifications.

---

[13]SB `13B-370.sb28581653.eb28626177.56669.781848645835`

[14]`https://science.nrao.edu/facilities/vla/data-processing/pipeline`

6.5. Temporary Storage Requirements for Calibration

Carrying out the calibration and quality assurance of the VLASS will require temporary storage of the calibrated data. This is through use of our Lustre filesystem, a highly parallel high throughput RAID array system. We expect that our Lustre system will have a total capacity of 1200TB in 2017, and 2500TB in 2020. We would like the total temporary VLASS Lustre usage during the survey to not exceed 10% of the capacity, or 120TB to 250TB total. As described below in § 9.2, the raw visibility storage volume of VLASS will be 82TB per configuration cycle (with only around 73TB on target after calibration backing out the overhead). In principle, we would be able to keep a full cycle worth of calibrated data on live disk during long-term processing (e.g. excluding the Quick Look imaging and analysis). Our goal is to stage the processing carefully and keep less than 33% live (e.g. two cycles), or around 25TB for the target data.

7. Imaging

The VLASS is at its heart a wide-band continuum imaging survey. The science goals of the survey are predicated on the ability of the instrument and data processing to deliver images of sufficient quality to be able to identify objects and measure the salient properties (e.g. flux density, position, spectral index, polarization, light curve).

Starting with calibrated visibilities output from the Calibration Pipeline, the Imaging Pipeline must:

1. Select a sub-region of the sky to image
2. Gather the visibility data that are relevant to that sub-region of sky
3. Carry out wide-band continuum imaging for that sub-region
4. Assess the quality of the imaging, determine whether further imaging, self-calibration and/or data flagging iterations are required
5. If required, perform iterative imaging steps
6. Output final images, sky models, and QA information and plots

We now describe the requirements on the VLASS Imaging Pipeline, discuss software development needed to carry this out, and estimate the processing resources that will be used to image the VLASS.

7.1. Imaging Requirements

In order to keep up with the observing, the Imaging Pipeline must be able to process the data at a rate commensurate with the observing rate. This will be effected through the parallel image processing of sub-mosaics on NRAO-based clusters or externally provided systems (e.g. through XSEDE).

There are three imaging product sets that need to be handled by the pipeline:

- Quick Look (QL) imaging triggered after every scheduling block is observed (e.g. for transient identification)

- Single-epoch (SE) imaging triggered after the last observation each configuration
- Cumulative (C) imaging incorporating all previous data (single-epoch after the first, multi-epoch after the second)

In turn, these will carry out two types of imaging based on the data required:

- Single-epoch imaging based on data taken in a single epoch
- Multi-epoch imaging based on data taken in multiple epochs (possibly with extra processing to deal with source variability and/or calibration variation)

Note that the Single-Epoch data products require only single epoch imaging, although single epoch imaging produces images for both Single-Epoch and Cumulative products.

For each of these, there are three kinds of images that may be produced:

- Wide-band continuum images (2–4GHz)
- Coarse-resolution image cubes (128MHz spectral windows or similar)
- Fine-resolution image cubes (nominally 10MHz spectral resolution)

Imaging is done in Stokes parameters IQU for linear polarization imaging capability.

Tapered Images: The Community Review panel requested that we produce tapered images at a lower angular resolution than that for the standard images. We propose to taper to a resolution 3x larger than that for the high-resolution images (7.5″). This would be triggered only for the cumulative images (not per-epoch) in BDP. This could either be totally independent of that for the above images or follow-on from them using them as a starting model. They will be 1/9 the size and thus significantly easier to compute and store.

Continuum imaging can include higher-order Taylor terms in the spectral dimension (e.g. spectral index, spectral curvature) depending on image depth (e.g. for processing beyond the Quick Look). CASA has algorithms for this that have been used in past programs, and further development of these capabilities is underway. Full-polarimetric imaging is a key part of VLASS, and the use of accurate polarized "primary beam" maps of the VLA field-of-view during imaging and analysis are critical to the production of science ready images. Self-calibration (through the use of previous sky models as well as true self-calibration from iterative imaging) is a part of the image processing if required (more likely in the cumulative imaging).

We assume for all image size calculations that in the ideal case (for single-epoch and cumulative imaging) the high-resolution images will be pixellated at a sampling level 0.4 of the (robust weighted) resolution at the highest frequency of the band (4 GHz), rounded to a convenient value. For B-configuration observations at mid-declinations, this is 0.6″ (resolution 1.58″ at 4GHz), or 36Mpix per square degree. *The tapered images will use correspondingly larger pixels, e.g.* 1.8″. Likewise, for the Quick-Look images, the pixel sizes will be larger (1″) to speed up imaging. In practice we will refine this based on imaging performance and we may be able to get by with less oversampling. In addition, individual sub-mosaics will need some amount of extra padding to accommodate all the data (see § 7.2 below). Overall we should treat these estimates as reasonably conservative, uncertain at the around the 25% level. However, this optimal level of resolution

leads to large image archive sizes (see § 9) and thus a key issue for testing is the determination of the lowest acceptable resolution in the images and image cubes that will still enable the key science with the Basic Data Products. It may be possible to reduce the image data volumes by significant factors (2–8) in this manner. In addition, image compression algorithms (lossless and lossy) can also improve storage efficiency and will be investigated in the Test and Development Program.

The image cubes are needed as input to more advanced processing for Rotation Measure determination, spectral line surveys, and more detailed SED modeling of sources. Most of these would be provided as Enhanced Data Products and Services. Note that the storage and distribution of the large full-resolution cubes will be a challenge for the archive (see § 9), and options for external hosting and "on-demand" image processing should be explored (e.g. as an Enhanced Data Service). As a fallback we would carry out compression through a combination of reduced angular resolution (e.g. $0.3''$, Nyquist at 3GHz) and spectral resolution (average 8 channels, 32MHz).

The imaging might be expected to be particularly challenging in the Galactic Plane, due to poorly-sampled extended emission. Here, we use the CORNISH survey as an example of what to expect Purcell, Hoare, Cotton et al. (2013). CORNISH was a 110 deg^2 continuum survey of the Galactic Plane from $10^\circ < l < 65^\circ$ carried out in the B and BnA configurations at 5 GHz in 2006–2008, before the WIDAR correlator was available. Purcell et al. reported that areas exhibiting imaging problems due to extended emission amounted to less than 2% of the surveyed area, and that these problems could be dealt with through special weighting schemes and manual inspection of the uv data. The CORNISH survey did not include the complex Galactic Center region, but the service monitoring of this region for the Sgr A*/G2 encounter in 2014[15] showed that snapshot imaging in the B-configuration is relatively straightforward, helped by the increased fractional bandwidth of the JVLA and MFS imaging algorithms. We can therefore expect that some of the Galactic Plane imaging will require manual intervention, but that the fraction of the data requiring such attention will be small. In these regions imaging may be dynamic range limited, rather than sensitivity limited.

Finally, imaging of multi-epoch data may require mitigation of time-variable effects from calibration and source variation in order to produce suitable quality images.

Risk: Medium to High Previous Jansky VLA programs (e.g. Stripe-82 and COSMOS observations) have been imaged using scripts and software tailored to the individual projects. As of this time, there is no standard CASA-based JVLA imaging pipeline available. The development of this capability is a high priority for NRAO in the next two years, and thus the VLASS can build upon and help pioneer this effort. We expect this to take substantial resources (design, development, implementation, execution, and QA), some of which will need to take place also as part of the normal JVLA operational plan. Due to their similarity to Stripe-82 processing, we expect the pipelining of extragalactic imaging to be only medium risk, with the possibility of falling back to the processing used for 13B-370. We assess the risk for imaging in the Galactic Plane to be higher, due to the considerably more stringent dynamic range constraints, the complexity of the emission in the Galactic fields, and the relative lack of previous experience in automated image processing for large deeper mosaics. These risks will be mitigated through the VLASS Test and Development Program (§ 10) using existing data taken in similar modes of observing.

[15]https://science.nrao.edu/science/service-observing

7.2. Imaging Mosaic Definition

To construct a full imaging survey of the sky, one must divide the sky into areas that can each be imaged in one mosaic imaging operation. These "sub-mosaics" can be no smaller than a single primary beam area, but should not be so large that data from most of the pointings have impact on only a very small portion of that sub-mosaic image. This suggests that the sub-mosaic area be only a few primary beam diameters in span at most.

To estimate the useful size of the primary beam, we used the radius R_g to reach a given level g in the Gaussian approximated response,

$$g = 2^{-\left(\frac{2R_g}{\theta_P}\right)^2} \qquad \Leftrightarrow \qquad R_g = \theta_P \sqrt{-\frac{\ln g}{4 \ln 2}} \tag{77}$$

where θ_P is the FWHM of the beam at the frequency of interest. For example, for $g = 0.2$, $R_g = 0.76\,\theta_P$. We will adopt $R_g = 0.8\,\theta_P$ at which the Gaussian response is $g = 0.17$.

In Figure 7 we illustrate the size of a sub-mosaic of side length L_{sub} relative to a primary beam of representative radius R_g. The data to be imaged must include fields with centers within a distance R

$$R < R_{fld} \qquad\qquad R_{fld} = 0.5\,L_{sub} + R_g \tag{78}$$

of the sub-mosaic center in each dimension (R_{fld} defines the bounding box of field centers). Strictly speaking, for OTFM these should be individual visibility pointing centers, but for simplicity in selection we will restrict this to field phase centers and select $R \leq R_{fld}$. This diagram also illustrates that the maximum image size that can/should be made for this data is of length $L_{img} = L_{sub} + 4\,R_g$. In practice, we will truncate this a bit to $L_{img} = L_{sub} + 2\,R_g$, which in most cases will be large enough to clean out sources outside of the edge of the sub-mosaic.

For the VLASS, the largest beam size is $\theta_P = 21.1'$ near 2 GHz (Figure 1), and thus we use $R_g = 0.8\,\theta_P = 1000''$ rounding to a convenient value. Thus, for a sub-mosaic of $L_{sub} = 2\,R_g = 2000''$ we find all the fields within $R_{fld} = 2\,R_g = 2000''$ and make an image of larger size $L_{img} = 4\,R_g = 4000''$.

7.2.1. Tile and Sub-mosaic Definition

For a given tiling of the sky (§ 5.4), each tile will in turn be subdivided into "sub-mosaics" for imaging as described above. The exact sizes of the sub-mosaics will be set so that there are integer numbers of these in the RA and Dec directions within the tiles. For the full survey final imaging, the sub-mosaics can cross Scheduling Block boundaries and can be made to be convenient sizes, while for the Quick Look images, and much of the Pilot survey, the subtile sizes will be set by the tile/SB shapes.

For a tile with center at $(\alpha_{tile}, \delta_{tile})$ divided into $N_{RA} \times N_{Dec}$ sub-mosaics each of length L_{sub} (also distance between centers), the center of sub-mosaic ij will be located at (α_i, δ_j) where

$$\alpha_i = \alpha_{tile} + \left(i - \frac{N_{RA} - 1}{2}\right) L_{sub}\,(\cos\delta_j)^{-1} \qquad i = 0, \ldots, N_{RA} - 1 \tag{79}$$

$$\delta_j = \delta_{tile} + \left(j - \frac{N_{Dec} - 1}{2}\right) L_{sub} \qquad j = 0, \ldots, N_{Dec} - 1 \tag{80}$$

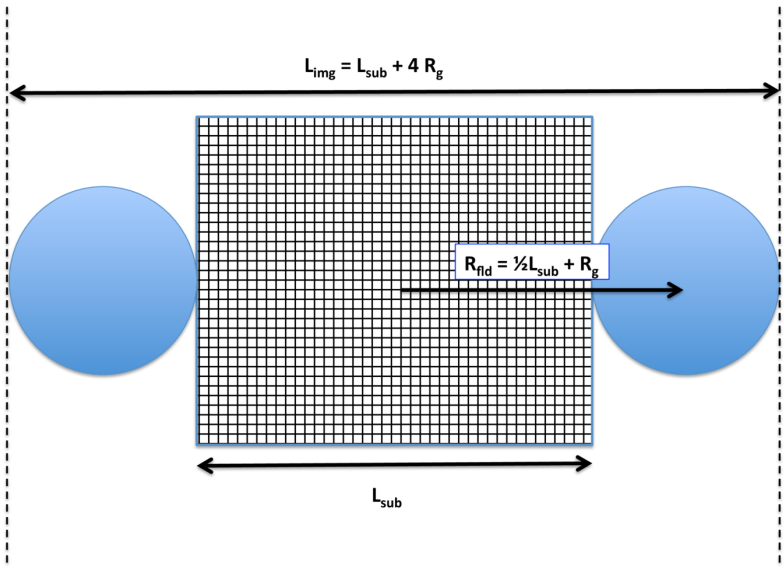

Fig. 7.— Illustration of the size of a sub-mosaic L_{sub} relative to the assumed radius R_g of the primary beam. Also shown is the maximum images size L_{img} containing support from data to be included in the imaging with pointing centers within a distance R_{fld} in each dimension of the sub-mosaic center.

7.3. Algorithm and Software Development for Imaging

The development and implementation of improved software in CASA for imaging is critical for the success of the VLASS. For example, the Quick-Look imaging is the most time-critical, Galactic Plane imaging and imaging near bright sources will be the most difficult from dynamic-range and image complexity perspectives.

The issues to be addressed (including some options that may need to be investigated) include:

- the robust parallelization (either through multiple-process submission or internal MPI/OpenMP parallelization) of imaging with minimal memory footprint (so multiple processes can be run on a single node) and optimal I/O (to keep disk access traffic to only what is required);
- the efficient joint mosaicking over a modest area ($\sim$ 1deg^2) with multiple Taylor terms, including A-projection (with average or more detailed-beams, and with W-projection if necessary), multi-scale, for full polarimetry;
- handling of primary beam effects during imaging (e.g. A-projection) and for correction of the final mosaic images ("`wfpbcor`") at the appropriate level and accuracy for the VLASS components;
- the use of pre-boxing (based upon other catalogs or evolving VLASS global sky models) and auto-boxing;
- incorporation of self-calibration during imaging, likely by a separate step after first imaging to determine gain (phase, possibly also amplitude) calibration tables for fields containing bright ($S >$

25 mJy/beam) point sources near field centers using the first-pass sky model, application of self-cal gain tables to data, and re-imaging;

- possibly use of "peeling" or other technique to deal with bright sources appearing far out in some of the mosaic beams;
- possibly the use of temporal fitting or synthesis to deal with time-variable sources in the field for multi-epoch data;
- ability to carry this out in a semi-automated pipeline that includes fault detection and handling, robust and frequent check-pointing of the run to allow restarting of the imaging upon failures or crashes.

Note that most of these are also general development targets needed to fully realize the potential of the JVLA and ALMA for high-quality imaging. The needs of the VLASS are not special but the large volume of data and the requirement to produce science capable images on our schedule do place constraints on the timescales for this work, and thus require substantial resources for the software development and testing. Naturally, aspects of this work are part of the Test & Development Plan (§ 10.2.

7.4. Processing Requirements for Imaging

The imaging of the VLASS data will clearly be the computational bottleneck for processing. However, it is also the most straightforward part of the processing to run parallel serial scripts on, as individual fields or sub-mosaics can be processed independently and combined together in a final linear mosaic (or left as "postage stamp" sub-images). Careful benchmarking using representative test data will be required to obtain accurate estimates of required resources. This will be a critical task under the Test & Development Program, and will require significant effort to carry out.

As an illustrative example, we consider a simple test case based upon existing data.

7.4.1. Test Case: Imaging of Stripe-82

A custom simple imaging script for the same observing block used for the calibration benchmarking (§ 6.4.1) was run alone on a single cluster node. The observations contained in this 3 hour observing block covered approximately 22.5 square degrees of the sky reaching a depth of $\sim 90\,\mu$Jy/beam rms for the full band. On average, it took 145 seconds per field, or 81.56 hours for all 2025 OTF phase center fields. Thus, the basic imaging for our 3 hour observing block took approximately 27 times the block duration. Thus, imaging could keep up with observing by running the imaging of individual fields in parallel using 7 nodes with 4 processes per node.

Note that the script used for this test only did very basic imaging of each OTF phase center as if they were single fields. No joint mosaicking was employed, nor was any self-calibration carried out. This did a single MFS Taylor term and single scale deconvolution, did not include any auto-boxing, but did use W-projection to deal with the wide-field aberrations. The cell size employed was $1''$ matched to the band center, rather than the more optimal $0.6''$ proposed for VLASS (§ 9.4), so the VLASS images would have 2.8 times the number of pixels compared to images generated in this test. Our test thus provides a lower limit on the processing required for the imaging, and an approximation of the requirements for Quick-Look

imaging. Given the above considerations, one might conservatively extrapolate that VLASS imaging will require around 4 times the resources indicated by this test, requiring around 30 nodes (with 4 processes per node) to image in the same time as observing (e.g. 6 hours to image a 6 hour block).

These preliminary estimates carry significant uncertainty, and more careful studies are required to provide accurate projections of resources needed for VLASS imaging. In particular, detailed tests using the deeper COSMOS data and test observations in the Galactic plane, are needed to give reliable estimates for the imaging of the galactic plane.

7.5. Temporary Storage Requirements for Imaging and Analysis

In § 6.5 we estimated that we could handle keeping around 25TB of the calibrated target data live on Lustre storage at any given time for further processing. We also argued that we wanted VLASS to use no more than around 120–250TB (from 2017–2020 onward) at any given time. The image data products will likewise take up temporary storage, in particular for further analysis and production of catalogs, as well as for quality assurance before ingestion into the NGAS archive.

The following numbers are derived from the archive space requirements given in § 9 below:

Quick-Look Images: The Quick-Look images will take on 29TB total, or only 5TB per cycle, and thus are easily accommodated. We plan to keep all 5TB for a given cycle live.

Single-Epoch Images: There are 202TB of single epoch images and cubes to be archived in the VLASS (§ 9.5) or 67TB per epoch (3 epochs), produced at a rate of 34TB per configuration cycle. If we assume that two cycles (previous and current) are on disk at a given time for processing and comparison, that requires 67TB live.

Cumulative Images: There are 184TB of cumulative images to be archived (§ 9.7), with 43TB for continuum images and 141TB for spectral cubes. We assume that we carefully stage the processing and that at most all of the continuum, and 33% of cubes (47TB), need be on disk at a given time, and thus require a total of 90TB. Note that the cumulative imaging does not kick in until after the second epoch observing is complete in 2019.

The total temporary storage for imaging and analysis estimated above is 162TB.

General Scratch Space: In processing all of the above, some amount of scratch space will be required to handle trials of processing options and comparisons, as well as higher resolution spectral cubes before compression. Note that the quick-look, single epoch, and cumulative processing described above will be naturally staggered in time (though with some overlap), and thus we will not need the full 162TB live all the time. Thus the 162TB can accommodate a 67% of that total steady state plus a 50% extra for scratch. Thus we do not add extra for scratch.

The 162TB for imaging is to be added to the 25TB estimated in § 6.5 for calibration. Thus, we estimate that **a total of 187TB of temporary Lustre storage** will be sufficient to carry out the VLASS. This fits comfortably within the long-term envelope of 10% of predicted Lustre storage reached in 2020 (250TB).

7.6. Preliminary Design Specification for Imaging Pipeline(s)

We now propose a preliminary design for the imaging pipelines that will be used by the VLASS.

7.6.1. Quick-Look Imaging Pipeline (QLIP) Design

The goal of the QLIP is to produce images and QA products for wide-band Stokes I continuum images of the sky. These would be imaged using *clean/tclean* with:

- MFS with 2 Taylor terms (tt0 and tt1) in Stokes I (only tt0 for intensity will be used/archived). *Fallback: tt0 only.*
- single scale (0 pixel delta function)
- no W-projection using *mosaicft* gridding *Option: if shown not to image with sufficient quality, use w-projection with small number of w-planes (4–8).*
- A-projection using an average beam for joint mosaicking *Fallback: single field imaging plus linear mosaicking at lower sensitivity.*
- PSF calculation: Clark *Option: Clark performs sufficiently in testing, though further testing may indicate use of Hogbom in high dynamic range cases.*

We envision that the QLIP will carry out the following sequence of actions:

1. Gather (and calibrate if necessary) the visibility data from a given processed SB, and determine the set of sub-regions ("sub-mosaics") to be imaged from this SB. *For Quick-Look Imaging all sub-mosaics will be made with data only from a single SB.*
2. Define the set of sub-mosaics to image from this block. We expect each sub-mosaic to encompass a (square) contiguous area of $\sim 1\mathrm{deg}^2$(7.2). Submit the processing of the sub-mosaics to the cluster. We envision that triggering of this would be carried out by the "astronomer of the day" and the Survey Operations Team based on knowledge of what has been observed and reference to an observational status database and visualization tools, but the process control of all the sub-mosaic imaging would be autonomous.
3. For each sub-mosaic, select and split off relevant data to a working MS for this process, using the critera in 7.2.
4. Imaging and deconvolution will be carried out on this subset data. Working copies of the calibrated MSes containing only the fields to be imaged will be made (e.g. with *mstransform* and used in imaging. This will allow for multiple re-runs of imaging if needed, avoiding damage to the calibrated MSes themselves.
5. Identify bright sources in the sub-image area and perform initial deconvolution restricted to boxes around these sources. This identification would be on the basis of previous imaging (e.g. from previous epochs) or from preliminary images made of the field to identify sources for boxing and cleaning (necessary for first epoch). Note: if there is an extant implementation of an automated "auto-boxing"

algorithm in clean that can be used to efficiently box and clean in a single pass, then this would be employed instead of the two-step process outlined here. *Fallback: if initial boxing takes too long or proves unhelpful, then proceed with cleaning without boxes.*

6. Proceeding from the initial cleaning, carry out deconvolution of the residual datasets until the nominal threshold limit of L-σ with respect to the expected thermal noise level is reached. The value of L will need to be determined through tests and studies, but will likely be around the value of 1.5–2 based on past experience. The procedure used to determine the stopping criterion for cleaning will also need to take into account image complexity in crowded regions and around bright sources.

7. Carry out quality assurance (QA) of the imaging result, based on automated and visual examination of the image and of QA products that may include: images of the rms residual over the area, plots of cleaned flux density versus iteration. If the imaging fails the QA, then the team will need to manually assess the problem and carry out any re-reduction, additional self-calibration and re-imaging, or possibly re-observation, required.

8. If required, perform iterative imaging steps by carrying out a self-calibration followed by re-imaging following the previous steps.

9. Output final images, sky models, and QA information and plots, to a staging area for access by the team, including community team members producing the Enhanced Data Products. These products will be larger than the subset that will uploaded to the archive.

10. Upload the BDP to the archive. This will require sub-selection (e.g. cutouts of image cubes) on the staged products.

7.6.2. Single-Epoch Imaging Pipeline (SEIP) Design

The goal of the SEIP is to produce images and QA products for data from a single epoch. These would be imaged using *clean/tclean* with:

- Continuum images and spectral cubes, consisting of:
  - Continuum Stokes I Image: MFS with 2 Taylor terms (tt0 and tt1) over full band. *Option: in some cases it may be necessary to image tt2 in addition to create reliable tt1 images, if shown by testing.*
  - Continuum Stokes QU Image: single Taylor term (tt0) over full band. Due to Faraday Rotation, sources will be de-polarized in moderate RM regions but it is beyond the processing envisioned for BDP to correct for this.
  - Coarse Spectral IQU Cube: 128MHz resolution (avg per spw) for spectral windows not lost to RFI (usually 14). These will be constructed over the full sky due to bright source density, but currently budgeted for storage for only 10% of the sky as part of BDP. We expect to image each plane and Stokes parameter separately for maximum parallel processing.
  - Fine Spectral IQU Cube: No fine cubes are stored and served as SE BDP, however for the first epoch these will will be created as cumulative cubes.

- Spectral cubes will be made and labeled in the LSRK frame for deterministic imaging, though there are small offsets due to Doppler motion ($\sim$ 0.4MHz at 4GHz) in frequency labeling over the course of an epoch. For coarse cubes these differences are smaller than the channels lost between spectral windows, so selection for imaging in a single spectral window is sufficient.
- Multiscale: single scale (0 pixel delta function) *Option: multi-scale with 2 or 3 additional extended scales may prove beneficial in galactic regions or other areas with bright extended sources.*
- W-projection with a minimal number of w-planes (4–8) *Fallback: no w-projection with some losses due to smearing.*
- A-projection using an average beam for joint mosaicking *Fallback: single field imaging plus linear mosaicking.*
- PSF Calculation: Clark. *Option: it may prove beneficial to use Hogbom to deal with high-dynamic range issues near bright sources, not currently an option in the tclean code.*

We envision that the SEIP will carry out the following sequence of actions:

1. Define a contiguous sub-region ("sub-mosaic") of the sky to image. It is expected that this sub-mosaic will encompass an area of $\sim$ 1deg^2 (§ 7.2). We envision that triggering of this processing for a batch of such sub-mosaics would be carried out by the "astronomer of the day" and the Survey Operations Team based on knowledge of what has been observed and reference to an observational status database and visualization tools.
2. Gather the visibility data that are relevant to that sub-region of sky. We envision that this will be carried out by query of a database containing the contents of observed blocks from the program to identify those containing the scans needed. Based on the results of this query, the datasets and required calibration products would be obtained from the archive and calibrated measurement sets (MSes) would be assembled for the target fields needed for imaging.
3. Imaging and deconvolution will be carried out on this subset data. Working copies of the calibrated MSes containing only the fields to be imaged will be made (e.g. with *mstransform* and used in imaging. This will allow for multiple re-runs of imaging if needed, avoiding damage to the calibrated MSes themselves.
4. Identify known sources in the sub-image area and perform initial deconvolution restricted to boxes around these sources. This identification would be on the basis of previous imaging from the Quick-Look imaging or from preliminary single-epoch images made of the field to identify sources for boxing and cleaning. Note: if there is an extant implementation of an automated "auto-boxing" algorithm in clean that can be used to efficiently box and clean in a single pass, then this could be employed instead of the two-step process outlined here.
5. Proceeding from the initial cleaning, carry out deconvolution of the residual datasets until the nominal threshold limit of L-σ with respect to the expected thermal noise level is reached. The value of L will need to be determined through tests and studies, but will likely be around the value of 1.5–2 based on past experience. The procedure used to determine the stopping criterion for cleaning will also need to take into account image complexity in crowded regions and around bright sources.

6. Carry out quality assurance (QA) of the imaging result, based on automated and visual examination of the image and of QA products that may include: images of the rms residual over the area, plots of cleaned flux density versus iteration. If the imaging fails the QA, then the team will need to manually assess the problem and carry out any re-reduction, additional self-calibration and re-imaging, or possibly re-observation, required.

7. If required, perform iterative imaging steps by carrying out a self-calibration followed by re-imaging following the previous steps.

8. Output final images, sky models, and QA information and plots, to a staging area for access by the team, including community team members producing the Enhanced Data Products. These products will be larger than the subset that will uploaded to the archive.

9. Upload the BDP to the archive. This will require sub-selection (e.g. cutouts of image cubes) on the staged products.

7.6.3. Cumulative Imaging Pipeline (CIP) Design

The goal of the CIP is to produce images and QA products for wide-band Stokes I continuum images of the sky. The CIP operates on both single-epoch data (after the first epoch) and multi-epoch data (from the second epoch onward). These would be imaged using *clean/tclean* with:

- Continuum images and spectral cubes, consisting of:
  - Continuum Stokes I Image: MFS with 3 Taylor terms (only terms tt0, tt1 for intensity will be used/archived). *Fallback: tt0, tt1 only.*
  - Continuum Stokes QU Image: due to RM decorrelation, standard continuum imaging techniques will be inadequate to image in QU over 2–4GHz, therefore these will likely be constructed by processing the QU Coarse Cubes to de-rotate.
  - Coarse Spectral IQU Cube: 128MHz resolution (avg per spw) for good spw (usually 14). These cubes will be processed covering the full sky due to bright source density, but storage is budgeted for only 10% of the sky as part of BDP.
  - Fine Spectral IQU Cube: $\sim$ 10MHz resolution for science goals (8MHz or 16MHz will likely be used for practical reasons, TBD). Storage for BDP is only budgeted to cover 2.5% of the sky at 10MHz resolution. Preliminary processing estimates suggest we can only support processing of 10% of the full sky at this spectral resolution (more detailed benchmarking is underway).
- Spectral cubes will be made and labeled in the LSRK frame, as there are only small offsets due to Doppler motion ($\sim$ 0.4MHz at 4GHz) in frequency labeling over the course of the survey. Mostly relevant for fine cubes, but data from a given spw can be split for all epochs and combined and sub-selected at imaging for a particular LSRK fine channel.
- Tapering: untapered and tapered versions (to 3x the untapered PSF size).
- Multiscale: MS using minimum of 3 scales from 0 pixels to 3 times the PSF size. *Fallback: single scale (0 pixel delta function)*

- W-projection with a minimal number of w-planes (4–8) *Fallback: no w-projection with losses due to smearing.*
- A-projection using an average beam for joint mosaicking. *Option: in dynamic-range limited regions, and particularly for polarization, it may be necessary to use properly rotated (with PA) beams at higher processing cost. Fallback: single field imaging plus linear mosaicking.*
- PSF Calculation: Clark. *Option: it may be necessary to use Hogbom in dynamic-range limited regions, though this is not currently an option in tclean for joint mosaics.*

We envision that the CIP will carry out the following sequence of actions:

1. Define a contiguous sub-region ("sub-mosaic") of the sky to image. It is expected that this tile will encompass an area of $\sim$ 1deg^2 (§ 7.2). We envision that triggering of this would be carried out by the "astronomer of the day" and the Survey Operations Team based on knowledge of what has been observed and reference to an observational status database and visualization tools. Note for the CIP this should be triggered after all fields for all epochs to be summed are complete.
2. Gather the visibility data that are relevant to that sub-region of sky and the given spectral channel to be imaged. We envision that this will be carried out by query of a database containing the contents of observed blocks from the program to identify those containing the scans needed. Based on the results of this query, the datasets and required calibration products would be obtained from the archive and calibrated measurement sets (MSes) would be assembled for the target fields needed for imaging. For the CIP, this will include previous epoch data.
3. Imaging and deconvolution will be carried out on this subset data. Working copies of the calibrated MSes containing only the fields to be imaged will be made (e.g. with *mstransform*) and used in imaging. This will allow for multiple re-runs of imaging if needed, avoiding damage to the calibrated MSes themselves.
4. Identify known sources in the sub-image area and perform initial deconvolution restricted to boxes around these sources. This identification would be on the basis of previous imaging from the single-epoch orcumulative images made of the field to identify sources for boxing and cleaning, or for Q and U and cubes would come from the corresponding current cumulative I continuum image. Note: if there is an extant implementation of an automated "auto-boxing" algorithm in clean that can be used to efficiently box and clean in a single pass, then this could be employed in between the two-step process outlined here.
5. Proceeding from the initial cleaning, carry out deconvolution of the residual datasets until the nominal threshold limit of L-σ with respect to the expected thermal noise level is reached. The value of L will need to be determined through tests and studies, but will likely be around the value of 1.5–2 based on past experience. The procedure used to determine the stopping criterion for cleaning will also need to take into account image complexity in crowded regions and around bright sources.
6. Carry out quality assurance (QA) of the imaging result, based on automated and visual examination of the image and of QA products that may include: images of the rms residual over the area, plots of cleaned flux density versus iteration. If the imaging fails the QA, then the team will need to manually assess the problem and carry out any re-reduction, additional self-calibration and re-imaging, or possibly re-observation, required.

7. If required, perform iterative imaging steps by carrying out a self-calibration followed by re-imaging following the previous steps.

8. Output final images, sky models, and QA information and plots, to a staging area for access by the team, including community team members producing the Enhanced Data Products. These products will be larger than the subset that will uploaded to the archive.

9. Upload the BDP to the archive. This will require sub-selection (e.g. cutouts of image cubes) on the staged products.

7.7. Polarimetric Imaging

Imaging of the linear polarization Stokes Q and U pose no special challenges for the VLASS BDP, other than the option for including source variability during imaging. This section gives our current plans for approaching this problem. Further testing using the Pilot data will be needed to refine this processing.

7.7.1. Continuum Polarimetric Imaging

For the SEIP and CIP, continuum Q and U images will be made by single Taylor-term MFS, with no correction for Faraday Rotation across the band. These Stokes images will nominally be made separately in parallel imaging processes rather than in a QU cube (separately from I). They will use initial deconvolution masks determined from the corresponding continuum I imaging, followed by deconvolution without any masking.

Multi-Epoch Imaging: If a process for measuring or correcting for source varibility (through use of the singe-epoch models or through temporal synthesis) is available, these can be used on the Q and U images in a similar manner to take out polarization intensity and angle variability.

7.7.2. Spectral Cube Polarimetric Imaging

For the SEIP and CIP, continuum Q and U images will be made by single Taylor-term MFS, with no correction for Faraday Rotation across the plane (coarse or fine). These Stokes images will nominally be made separately in parallel imaging processes rather than in a QU channel cube (separately from I). They will use initial deconvolution masks determined from the corresponding continuum I imaging, followed by deconvolution without any masking.

Multi-Epoch Imaging: If a process for measuring or correcting for source varibility (through use of the singe-epoch models or through temporal synthesis) is available, these can be used on the Q and U cube images in a similar manner to take out polarization intensity and angle variability.

8. Image Analysis and Sky Catalogs

The main image analysis task for the VLASS is the production of the basic object catalogs for the Quick-Look and standard images.

A good study of the performance of radio continuum image source finders is Hancock, Murphy, Gaensler et al. (2012), which considers the available options in the context of ASKAP. The upshot is that there are options available that should have acceptable performance for the basic catalogs for VLASS. Note that inclusion of the spectral index images and polarimetric images from VLASS will likely require some extensions to these source finders, which in turn will require some developer or astronomer time.

Also available as a proof of concept is the source finding carried out for the JVLA Stripe-82 surveys by Mooley et al. (in preparation). There is also a comprehensive discussion in Mooley, Frail, Ofek et al. (2013) in the analysis of archival VLA ECDFS multi-epoch data. It is our current assessment that one or more of these methods will be suitable for the basic catalogs from the VLASS.

More advanced catalogs and source finding algorithms could be developed and produced as an Enhanced Data Product.

Risk: Low to Medium There are a number of options available which will do some of what we want, if not all. We are currently testing PyBDSM as a source finder with the pilot images. Dealing with the wide-band spectral index and polarimetric data products of the JVLA will likely require some amount of extra work.

9. Archiving and Data Distribution

The primary interface that the user community will have to the VLASS is through the archive and data distribution system. Raw data will be served via the normal JVLA archive, available with no proprietary period as soon as it has been ingested into the archive system.

The archive, or at least some archive, will have to also serve the VLASS data products as described above. It is the responsibility of NRAO and the VLASS to make the Basic Data Products available through this archive mechanism. Enhanced Data Products may be made available through the NRAO-hosted VLASS archive, this will need to be negotiated and is largely dependent upon resources required. The VLASS products, either in basic form or further processes, may also be made available via alternative Enhanced Data Services, as described above.

9.1. Estimated Archive Space

The estimated ideal data volumes required for storage of the VLASS data and data products are:

1. raw visibility data — 523TB
2. calibration data — not significant
3. quick-look continuum images — 29TB
4. single-epoch continuum images — 101TB
5. single-epoch coarse image cubes — 101TB
6. single-epoch basic object catalogs — not significant
7. cumulative “static sky” continuum images — 43TB

8. cumulative "static sky" tapered continuum images — 5TB
9. cumulative "static sky" coarse image cubes (compressed) — 34TB
10. cumulative "static sky" tapered coarse image cubes (compressed) — 4TB
11. cumulative "static sky" fine image cubes (compressed) — 107TB
12. cumulative "static sky" tapered fine image cubes (compressed) — 12TB
13. cumulative "static sky" basic object catalogs — not significant
14. **Total: 959TB with 523TB of data, 436TB of images** (continuum images — 178TB; image cubes — 258TB)

These volumes have been calculated assuming the angular and spectral resolutions defined in § 7 with compression in some cases as noted below, for the data products listed in § 4.1. We consider for the above calculation that the storage needed for the calibration data and catalogs to not be significant compared to the imaging and visibility data, and should be less than 10TB total. These estimates also now include the tapered images and cubes requested by the Community Review panel.

The 800TB of data storage is slightly above what we expect for normal science data use (it uses the maximum allowed data rate of 25MB/s for the ALL-SKY observations), and thus will be accommodated within the normal JVLA archive data storage plans. The required storage volume of nearly 500TB for the images, however, is significant, but can be accommodated in storage expansion plans. Based on information provided by James Robnett, the JVLA NGAS archive is planned to have the capacity for around 3300TB in 2017 (1 year after start of VLASS) and 5700TB in 2020. Thus, our image data will use less than 10% of the total NGAS storage in 2020. The NRAO support for storage beyond this level would require extremely strong recommendation by the VLASS science review based on strong science drivers. Beyond this, partnerships with the community and other agencies will be necessary (see § 4.2).

Risk: Medium to High Details of the overall NRAO archiving plan as they extend into the future are yet to be developed fully and resourced. The VLASS archive should fit in with this overall plan, and perhaps be used as a testbed to explore options. The risk is mainly due to this uncertainty in overall NRAO data management strategy at this time. As noted above, the clear high (resource) risk issue is the large volume taken by the image cubes, and the current plan relies upon significant (spatial and frequency) compression. We believe the proposed compression schemes can be carried out without unduly impacting the science goals (spectral intensity, polarization and rotation measure studies).

We now provide details on our estimates of the data volumes required for storage of each of the individual VLASS data products.

9.2. Raw Visibility Data

The VLASS will take a total of 5520 hours of observing time, observed at a data rate of 26.32MB/sec (94.75GB/hr). **the total visibility data volume for the VLASS is 523 TB**. We observe 920 hours per configuration cycle, taking 87TB of storage per cycle.

Note that if it is necessary for us to reduce data rates and volumes further, we could employ frequency averaging in the correlator backend or archive. This has potential undesirable effects due to delay losses and

loss of instantaneous field of view which could complicate processing, as well as limiting the usefulness of the data products for Rotation Measure analyses, and we do not recommend taking this approach unless truly necessary.

9.3. Calibration Data

The total primary and secondary calibration data for VLASS must come from the assumed overhead time not on target, and in practice will be only around 10% of the total data volume. Furthermore, the calibration and flagging tables derived from this data will be significantly smaller than this (being per antenna rather than per correlation), comprising much less than 1% of the total data volume. Thus we conclude that calibration data is an insignificant contributor to archive volume.

As noted earlier, the archive will need the facility to store, retrieve, and apply this calibration data to raw visibilities when requested by users and further processing pipelines.

9.4. Quick-Look Continuum Images

These images are produced for every scheduling block for purposes of QA and transient object detection. We assume for all image size calculations that the images will be pixellated at a sampling level 0.4 of the (robust weighted) resolution at the highest frequency of the band (4 GHz), rounded to a convenient value. For B-configuration at moderate declinations, this is $0.6''$ (resolution $1.58''$), or 36Mpix per square degree. In practice we will refine this based on imaging performance and we may be able to get by with less oversampling. In addition, individual sub-images will likely need some amount of extra padding to accommodate odd shapes. Overall we should treat these estimates as reasonably conservative, uncertain at the around the 25% level.

For QL production images, we assume 2 BDP images for Stokes I plus an uncertainty map. See § 4.1.3 for a description of these products.

The 33885 square degrees of ALL-SKY will be mapped in B-configuration (or BnA in the south) in three epochs. An all-sky image comprises 1.2Tpix, with size 4.8TB assuming single precision storage. For a single epoch of the ALL-SKY, the 2 QL images will take 9.6TB per epoch, with 28.8TB required for all three epochs.

The total storage required for the QL images is 29TB.

9.5. Single-epoch images and cubes

After each epoch, we can potentially produce refined images and cubes for the following:

Continuum Intensity Images: For these we assume there will be 2 Taylor terms (`tt0` and `tt1`) and uncertainty maps for each, giving a total of 4 wide-band continuum images (I, Ialpha, plus uncertainty maps).

Continuum Polarization Images: We assume that only 3 images are required, Q, U, and an uncertainty (rms) map (valid for both Q and U). We do not plan to create V circular polarization images for VLASS as a BDP, due to the required care of careful gain calibration and added expense of beam squint corrections

during imaging.

There are thus a total of 7 continuum image products.

Coarse Spectral Cubes: As a compromise, we can store coarse cubes (in the 14 viable spectral windows, each 128MHz wide). These would be for the 5 standard images (I, Q, U, plus uncertainty maps for I and polarization) resulting in a total of 70 image cube planes. This takes 1/64 the storage of the full cubes. Note that we cannot as BDP store the "full" coarse cubes, and offer only a compressed (10:1) version. This is most straightforwardly done as "postage stamp" cutouts around identified sources.

Full Spectral Cubes: As described in § 4.1.4, the image cubes can potentially have 1024 channels at full resolution (2MHz per channel), of which expect to only have unflagged data in a maximum of 896 channels (2 spectral windows totally lost and dropped). We would expect to create 5 cubes (I, Q, U and uncertainty maps in I and polarization) for the 896 channels, producing 4480 total image cube planes. Storage of cubes this size will be prohibitively large to store and serve as a BDP.

An all-sky image in B-configuration comprises 1.2Tpix, with size 4.8TB assuming single precision storage. This requires a total of 14.4TB for the 3 epochs.

Continuum Images: The 7 continuum images (4 intensity, 3 polarization) will take 100.8TB total storage.

Full Spectral Cubes: For the 4480 total cube planes (5 cubes, 896 channels) this would require 64.5PB total (10.75TB per cycle). *We do not plan to store or serve these ALL-SKY full spectral cubes as part of the BDP.*

Coarse Spectral Cubes: The coarse spectral image cubes with 70 planes total (5 cubes, 14 windows) will take a total of 1008TB for all 3 epochs (336TB per epoch, or 168TB per cycle). *We do not plan to store or serve these ALL-SKY coarse spectral cubes as part of the BDP.* Because polarization science requires some form of spectral cubes, we will provide an even more compressed (10:1) coarse cube, most likely by providing "postage stamps" around identified sources. This would require 100.8TB.

Total storage required for single-epoch images and coarse spectral cubes for BDP is 202TB, or 67TB per epoch. The continuum images require 101TB and (coarse and compressed) cubes use 101TB.

9.6. Single-epoch basic object catalogs

The data volume for catalogs will not be significant. Flat catalog files in simple formats can easily be served from the archive. If served by a Relational Database (RDB), the number of entries may be large and may need consideration in implementation.

9.7. Final cumulative "static sky" images and image cubes

After each epoch after the first, we will produce refined images and cubes summed over the preceding decades, eventually arriving at the "final static-sky image". For these we assume there will be potentially:

Continuum Images: For these refined deeper images we can make 3 Taylor-Term images, for 9 total (I, Ialpha, Icurv, Q, U and uncertainty for I, Ialpha, Icurv, and polarization).

Coarse Spectral Cubes: For these we make 5 cubes (I, Q, U, plus uncertainty maps for I and polarization) in each of 14 spectral windows, or a total of 70 image planes. As with the single epoch images, we plan to provide compressed (10:1) coarse cubes, likely as cutouts in regions containing sufficiently bright emission. The delivery of the uncompressed coarse resolution cubes is a possible target for an Enhanced Data Product or Service (§ 4.2).

Full Spectral Cubes: For these we make 5 cubes (I, Q, U, plus uncertainty maps for I and polarization) in each plane. There are potentially 896 channels in a 14 spectral window dataset, giving a total of 4480 image planes. As noted below this requires more storage than we expect to be available, so some channel compression will be necessary for the BDP cubes. The delivery of full spectral resolution cubes (even in "postage stamp" cutouts around bright sources) is a target for an Enhanced Data Product or Service (§ 4.2).

Highly Compressed Spectral Cubes: Given that full resolution spectral cubes are too large to store with projected resources, we entertain the possibility of providing compressed cubes at sufficiently high spectral resolution to carry out the primary spectral science goal of rotation measure studies. The most likely approach is a combination of spatial compression (cutouts around bright emission regions) and frequency compression. The frequency channel compression will need to be done carefully, likely with the higher frequency channels compressed more. There may also be lossless compression schemes that can reduce the lossy compression required. We assume that a total compression factor of 200:1 is possible. The possible compression factors and optimal scheme is a Test & Development Plan item. We need to archive these only for the latest cumulative release.

Tapered Images and Cubes: As requested by the Community Review panel, we will produce tapered versions of the cumulative images and cubes listed above at a resolution 3x larger ($7.5''$) than the standard high-resolution images. These will take 1/9 the storage space of the full resultion images and cubes.

There is a total of 1.2Tpix in ALL-SKY or 4.8TB per plane.

Continuum Images: A total of 43.2TB required for the 9 images.

Tapered Continuum Images: A total of 4.8TB required for the 9 images.

Coarse Spectral Cubes: A total of 336TB would be required for 70 planes. Thus, we propose to provide compressed (10:1) coarse cubes as in the single-epoch image case. This requires 33.6TB.

Tapered Coarse Spectral Cubes: A total of 3.7TB is required for for tapered versions of the compressed (10:1) coarse cubes.

Fine Spectral Cubes: For full resolution cubes with 4480 total planes (5 images, 896 channels) a total of 21.5PB would be required. This is well above our projected storage available (§ 9.1). *Full spectral resolution cubes for ALL-SKY will not be provided as a BDP.* We propose to provide highly compressed (200:1) high frequency resolution spectra around objects as described above and/or by averaging to lower frequency resolution (e.g. 10MHz). This will require 107.5TB of storage.

Tapered Fine Spectral Cubes: It will require 12TB to store the tapered versions of the 200:1 compressed high spectral resolution cubes.

The cumulative image storage total for VLASS is 204TB. The continuum images take up around 43TB, the compressed coarse spectral cubes 34TB, and the highly compressed full resolution cubes will require 107TB. The tapered images (19.4TB total) take 4.8TB for continuum, 3.7TB for coarse cubes, and 12TB for fine cubes.

9.8. Cumulative "static sky" basic object catalogs

The data volume for catalogs will not be significant. Flat catalog files in simple formats can easily be served from the archive. If served by a relational database, the number of entries may be large and may need consideration in implementation.

10. Test and Development Plan

There are a number of issues related to the VLASS that must be addressed before the survey can be observed on the telescope. We feel that none of these are "show-stoppers" that are likely to prevent the survey from being carried out at all, and most have obvious work-arounds. Fundamentally, these are schedule and resource risks rather than functionality risks, in that it will take longer and will be more costly in computing and human resources to process the survey, impacting the data product delivery schedule. However, they do need to be addressed, and in the TIP as submitted for review we proposed a VLASS Test and Development Program leading up to and through the survey start. Test or larger pilot observations are indicated in some areas, while analysis of archival data from previously observed projects such as Stripe-82 13B-370 or COSMOS will serve in others. These require significant astronomer resources to carry out, and thus we were unable to fully execute this program even by the time of PDR. Below we summarize only the most important testing areas, as the most comprehensive testing comes through the full analysis of the VLASS Pilot and test observations (see the VLASS Memo 2: Pilot Survey Definiton[16]).

10.1. General Flagging, Calibration, and Imaging Tests

The main tests to be performed are related to RFI, calibration, and wide-field polarimetric imaging performance of the JVLA. These are issues that are important for VLA observers in general, not just the VLASS. The VLASS provides us an opportunity for directed testing of these issues, with the results to be made available to the user community (e.g. through VLA memos and improved software tools).

Also to be studied in this area are the trade-offs that can be made in the image and image cube sizes (angular and spectral resolution) in order to reduce archive and distribution costs but still maximize the science capabilities of the survey. Also under investigation are the utility and limitations of more general lossless and lossy compression algorithms on the images.

We highlight a few of the key challenges below.

10.1.1. RFI, Bandwidth, and Sensitivity

As described in § 2.1, the main contribution to the sensitivity of the JVLA for continuum observations is the effective useable bandwidth that one must enter into the radiometer equation or the Exposure Calculator Tool. Past experience has shown that good (automated) imaging can be carried out with fairly brutal flagging of affected sub-bands, leaving around 1350 MHz of effective bandwidth. On the other hand, past careful reductions have shown that 1500 MHz should be achievable, and this is what we recommend to users. As this

[16] https://safe.nrao.edu/wiki/pub/JVLA/VLASS/VLASS_Memo_002_Pilot_Definition.pdf

difference is equivalent to 11% in observing time or 5.4% in sensitivity, this issue constitutes a medium risk for the VLASS and will required significant testing as well as the development of automatic RFI heuristics (and possibly new algorithms).

An example RFI sweep in S-band carried out as part of VLASS testing is shown in Figure 8. This was carried out at Declination $\delta = -5°$ which is located in the heart of the "Clarke" geostationary satellite belt as viewed from the VLA. The declination range around this is likely to be the most highly affected by satellite generated RFI, and further tests will be required to show that imaging in this region is viable using standard observing, or whether special approaches are needed (e.g. by adjusting the baseband edges to exclude the worst RFI and recording only the good spectral windows). More such scans are needed covering the full range of Declinations of the VLASS.

Risk: Medium. Data can easily be obtained particularly in the pilot, but requires careful testing to establish the performance at all Declinations. Initial Pilot imaging shows it is possible to reach the rms sensivity goal of 0.12mJy/beam over much of the sky, but there is significant losses at the equator through the satellite belt at many hour angles, resulting in significant non-uniformity in the imaging rms. Mitigation could involve loss of data and sensitivity, or development of more complex heuristics or algorithms.

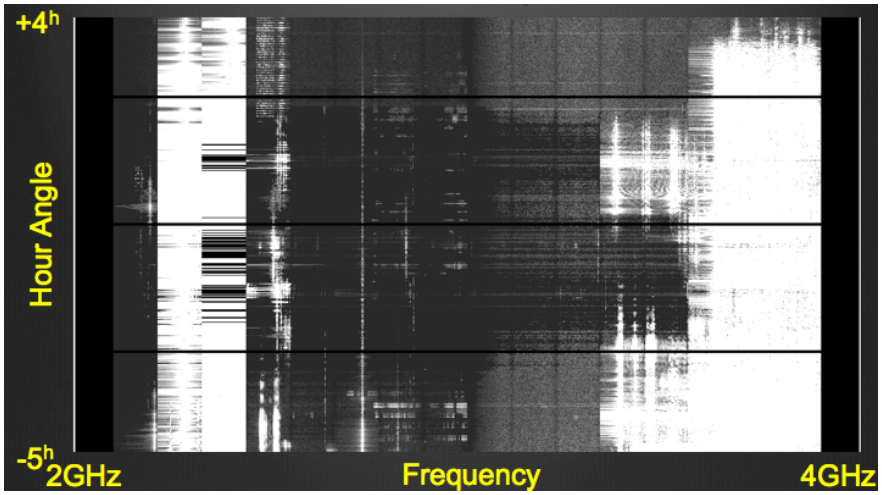

Fig. 8.— A sweep using fast OTF scanning across the sky at Declination $\delta = -5°$ where the geostationary satellite appears from the VLA. The horizontal axis is frequency channel from 2–4 GHz, and the vertical axis is time, covering hour angles from −5 hours to +4 hours. At the lower and upper ends of the spectrum we clearly see strong satellite interference at all azimuths, and over wider areas of the spectrum at certain hour angles corresponding to specific satellites. Sweeps like this will need to be done at various declinations of interest.

10.1.2. Wide-band Wide-field Continuum Imaging

The substantial increase in the continuum survey speed for the JVLA comes from the greatly increased instantaneous bandwidth provided by the upgrade. However, in order to produce a continuum image from this bandwidth, the system response and the source spectrum must be folded in to the calculation. This includes effects such as:

- the system response over the full bandwidth (e.g. the complex bandpass and system noise spectrum);
- the antenna primary beam responses (in the R and L polarizations) over the field-of-view (initially in the main beam only, but ultimately out into the near sidelobes);
- the array synthesized beam (PSF) as a function of frequency, for extended sources, possibly changing (rotating) during the course of the mosaic observing;
- the intrinsic source spectrum over this band (intensity, spectral index, spectral curvature, etc.);
- the amount of flagged channels (e.g. for RFI) as a function of frequency over the band;
- the distribution of visibilities (and weights) in the uv-plane after gridding.

These effects will all contribute to the final continuum image rms, resolution ("synthesized beam width", sidelobe level and structure, response to extended emission, and reconstruction of the source spectrum (through the multi-Taylor-Term imaging).

The default way of dealing with the source spectrum over the bandwidth is to break the band into smaller coarse channels, such as imaging each 128 MHz spectral window separately as a sub-band. In this approach, the spectral index can be fitted across these sub-bands, and incorporated into the model. This can be done iteratively during imaging, until no more emission is detectable above the noise in each sub-band. The drawback is that deconvolution is limited to what is detectable in a sub-band rather than the combined full-band image.

In principle, the technique of Multi-Frequency Synthesis (MFS) can be used to image the Taylor expansion terms (TT) with frequency over the full band. This is implemented in CASA as part of the `clean` task, with the performance as described in Rau, Bhatnagar, & Owen (2014). However, very recent tests using simulated point sources and the L-band CHILES data (Gim et al. private communication) may indicate at low signal-to-noise ratios (SNR) there may be a bias in the recovered spectral indices at SNR < 20. In this event, we would have to fall back to using the sub-band imaging approach described above.

Another aspect of wideband continuum imaging performance to be evaluated is the mosaic sensitivity to sources of different sizes and spectral indices. In a mosaic, the effective survey speed as a function of frequency goes as the area of the primary beam, which varies by a factor of 4 over 2–4 GHz. Thus, the lower end the band gets more integration time when summed up over the mosaic than the upper end. When combined with weighting of the spectrum taking this factor into account, this moves the effective mean frequency of the wideband continuum flux density downward from the nominal 3 GHz band center, giving more sensitivity to steep spectrum sources than one would otherwise expect. However, the exact weighting function and thus the magnitude of this effect also depends upon the relative instrumental noise (SEFD) and amount of channel flagging done over the band. In addition to this purely spectral effect is the fact that the synthesized beam also varies as a function of frequency in the same way, and thus more extended sources also get more sensitivity at the lower end of the band. Thus, careful test measurements will be needed before we can establish the true sensitivity to sources as a function of size and spectral index.

Risk: Medium to High The tests should be straightforward, and if software or algorithm flaws are identified CASA will need to apply bug fixes or re-engineering as necessary. The fall-back to sub-band imaging will incur penalties in the achievable imaging rms. As of the time of the Pilot observations and PDR, this is still in CASA 4.7 development and will likely be pushed into the next release (5.0) after that at earliest for many features, with some features that might be needed in worst cases possibly not

available in time for first epoch Single-Epoch processing. Accurate wide-band flux density and spectral index reconstruction has yet to be demonstrated beyond the Quick-Look level.

10.1.3. Polarimetry

A key aspect of the VLASS as compared to previous surveys is the capability for wide-band polarimetry at sub-mJy flux density levels. This science case was highlighted in the VLASS White Paper "A Wideband Polarization Survey of the Sky at 2–4 GHz" Mao, Banfield, Gaensler et al. (2014).

The use of the Jansky VLA for deep wide-band polarimetry is being pioneered through several RSRO programs. For example, graduate student Preshanth Jaganathan is carrying out C-band observations in Elais-N1 that will inform our development of VLASS processing. The CHILES-ConPol L-band processing is also ongoing (C. Hales, NRAO). Of more direct interest are the COSMOS S-band observations (PI: Smolcic). These programs have identified issues and paths forward, in particular the need for high-quality full-Stokes primary beam measurements and models. Observations obtaining these and the processing are underway.

Special care will be taken in investigating strategies for dealing with variable polarized sources when combining passes and epochs in VLASS imaging. It is possible that this may push us towards observing fields at the same LST and thus with the same uv coverage on each occasion.

Risk: Medium to High. Given the unique science that polarimetry brings to the VLASS makes this a high science priority issue. That this JVLA capability is only recently being fully explored, makes this medium to high risk at the current time. Mitigation of this risk over the next year is a top priority test and development target.

10.1.4. Transients and Variability

Exploring the time domain is a key science frontier for the VLASS. The survey has been designed to survey the sky in several epochs with sufficient cadence to identify candidate varying sources. The requirements on, and pitfalls of, a transient survey are described by Frail, Kulkarni, Ofek et al. (2012). Previous and current JVLA programs (12A-371, 12B-158, 13B-370) are employing this capability and provide us a set of on-sky test cases. We will work with these groups to carry out the required tests for the VLASS.

As part of the Test & Development Program, the choice of cadences for classes of transients and variables will be investigated. For example, if the VLASS is broken into two regions of the sky (say N and S) then the three epochs spread among 6 cycles would uniformly sequence as NSNSNS giving 32-month cadence between epochs of a given region. It may be advantageous to sequence this to NNSNSS so there are 16-month and 32-month separations sampled between epochs.

Risk: Low Existing pilot programs are underway. No obvious show-stoppers. The main need is modest personnel time to investigate and document.

10.2. ALL-SKY OTFM Processing and Testing

The VLASS science case is built around the efficiency of OTF mapping. The overhead time during OTF mapping is driven by time to slew to calibrators, which scales with time on sky. Overhead for pointed mapping scales with the number of points visited on the sky (beams times visits), so shallow and/or repeated visits to the same part of the sky would be very costly. However, OTF imaging has until recently been considered an experimental observing mode, so more work is needed to confirm in detail that the VLASS science goals are achievable in this mode. Here we describe the open questions to achieving the full VLASS science case (particularly transients) via OTF mapping and a plan to resolve these questions.

The assumptions and calculations for setting up the OTFM parameters are detailed in § 2. Given these, we outline the current testing results and further tests needed to address remaining questions:

1. Quantify the imaging errors introduced by fast OTF slewing
   - We have test data taken at a range of slew rates that will define the magnitude and scaling of imaging artifacts for OTF mode.
   - This test will give us a maximum safe slew rate for a given required image sensitivity.

   Status: No imaging artifacts attributable to OTF scanning are seen at VLASS speeds (3.3′/s), as expected from the calculations of smearing.

2. Evaluate whether the sensitivity of three co-added 120 μJy epochs scales down to 69 μJy
   - Pilot data has been taken for 3 "epochs" in 3 regions, and 10 passes in another.

   Status: processing and imaging of these has not yet been done.

3. Confirm whether the correlator can observe with 16 spectral windows and a dump time of 0.45s
   - Early testing was done to identify and fix issues.
   - Pilot data has been taken in VLASS mode in 2016 B-configuration.

   Status: Pilot data successfully observed. No issues seen after early issues fixed.

4. Investigate whether certain spectral windows are consistently hit by RFI for large regions of the sky
   - Search of archival data for S-band RFI.
   - If a spectral window is unusable for a large fraction of the sky, we will exclude it and recalculate the minimal single-epoch sensitivity.
   - Pilot data now available over a significant sky area.

   Status: Pilot data near equator showing issues, working to identify best hour angles for observing to reduce the losses.

5. Verify increase in integration times needed to reach uniform depth for low-declination fields
   - Test and pilot data now taken for southern fields and at low elevations.
   - For the survey, a choice should be made by the SSG on level of allowd rms noise non-uniformity (decision was $\sqrt{2}$ in rms, equivalent to 2x in time $\times$ bandwidth).

Status: analysis underway.

6. Quantify polarization bias/uncertainty is introduced by OTF mapping, focusing on answering the following questions:

   - Are observations of polarization calibrators in OTF and pointing mosaic mapping modes required?
   - What is the polarization bias as a function of frequency and pointing location? Polarimetric mapping in both OTF and pointed mosaic modes may require further algorithm development to accommodate large fractional bandwidths.
   - Are more observations of the in-beam polarization required to support polarimetric calibration in general?

   Status: Pilot data taken including polarization calibration. Not yet processed, polarization calibration pipeline and scripts not yet available.

7. Determine whether avoidance or corrections for ionospheric effects (TEC and/or Faraday Rotation) are necessary, and if so devise strategies for mitigation

   - Are TEC forecasts and models with sufficient accuracy for avoidance and correction available? If not, what additional information is needed and how do we get it?
   - Is the CASA code (`gencal` task with `tecim` mode) sufficiently accurate to use if corrections are necessary?
   - How would one, if needed, incorporate ionospheric diagnosis and correction into the calibration and/or imaging pipelines?

   Status: Initial tests by F. Schinzel after sunset on a moderately active day do not show any measurable effects. Further testing will be done, but at this time we do not foresee having to incorporate ionospheric correction into the calibration or imaging pipelines.

8. Investigate strategies for handling time-variable sources for intensity and polarization imaging when combining the 3 epochs

   - The CNSS data (13B-370 PI: G. Hallinan) can be used for this, and Pilot data is also available in same areas of Stripe-82.
   - It is likely that the best performing strategy will involve observing using fixed LST scheduling, so that each epoch has exactly the same uv-coverage and thus will average during gridding, but this is not possible over all of the survey.

   Status: processing and analysis for multi-epoch imaging in CNSS and in VLASS Pilot not done, pending effort allocation.

9. Evaluate more accurately the calibration and slewing overheads, in order to optimize the scheduling

   - Construction, observation, processing and analysis of realistic VLASS test blocks is needed.

   Status: scheduling software was made for the pilot by A. Kimball and successfully used. Revised overhead estimates given above were based on this.

10. Finalize estimate of computing resources are needed for image processing

- The (13B-370 PI: G. Hallinan) data and CASA scripts used to estimate the processing time given in § 7.4.1 above can be used for this.
- Pilot Survey observations will be the most reliable for this.
- This test will guide, test, and track speed and performance (e.g. memory footprint) improvements in CASA imaging code as they are implemented.

Status: Pilot survey imaging now underway using custom scripts. First results available and used in PDR resource estimation.

11. Quantify sensitivity degradation of imaging complex structures in the Galactic Plane and Bulge region

    - Archival data (e.g., the service monitoring of the Galactic Center) can be used for this test, but test observations in OTFM mode will also be required
    - Pilot survey observations in Galactic plane, center, and inner bulge made.

    Status: imaging and analysis of the pilot data underway. Initial indications are that indeed galactic regions are more crowded and have more extended sources causing greater imaging artifacts.

12. Quantify imaging issues around bright sources where dynamic range limitations will be substantial

    - Archival data can be used for this test, but test observations in OTFM will also be required.
    - Pilot and test data include regions near bright (J2130+0040 in Stripe-82, plus Cygnus-A and 3C84 areas).

    Status: There clearly are issues in initial images, more effort is needed to quantify the area that will need manual intervention.

The timescale on which the answers to some of these questions is needed is quite extended, as the second epoch does not start until the third configuration cycle of the VLASS.

Risk: Medium No show-stoppers yet identified, but availability of personnel to carry out the detailed analysis of test data has been very limited until new staff (Kimball, Schinzel) hired in Spring 2016.

10.3. Other Logistical Tests

In addition to the tests already described, the following will need to be investigated:

1. Calibrators for VLASS

    - In order to optimize the observing schedule nearby calibrators are needed; the VLA calibrator catalog has several areas of the sky where the density of calibrators could be significantly improved, and some effort will be needed to compile a set of calibrators for the VLASS from other catalogs

2. Data storage and image cube compression

    - Determination of optimize vs. practical options for image cube pixel and spectral resolution compression (needed for archival storage planning)

3. Source finding algorithms

- Assessment of source finding algorithm performance is needed, and any needed improvements identified

Risk: Low. Investigation of these issues is underway post-pilot and only modest resources are needed to carry out.

10.4. Pipeline development

The following modifications are expected to be needed for the VLA calibration pipeline to support the VLASS:

1. Polarization calibration

   - The addition of polarization calibration, based on user-defined scan intents, will be needed. These calibration heuristics are expected to be the same as is needed for standard VLA observations, although may need modification pending the outcome of the polarization tests described in § 10.2.

   Status: heuristics now available by C. Hales, not yet implemented.

2. Imaging

   - A modified version of the VLA calibration pipeline is already in use for 13B-370 that includes Stokes I imaging, so automated production of polarization products will need to be developed and tested

   Status: not yet ported to CASA pipelines for SEIP and CIP use. Only QLIP proto-pipeline scripts currently available.

3. Quick-look calibration and imaging pipeline

   - A stripped-down version of the full CASA-based calibration and imaging pipeline has been developed and tested as the Quick-Look pipeline. If this proves to be too slow for transient detection we may have to use the AIPS-Lite pipeline already developed for 13B-370. This item will primarily comprise timing tests.

   Status: QLI proto-pipeline using Python scripts developed by S. Myers and undergoing testing. Results promising. Used for resource estimation.

4. Source catalog production

   - The output of source finding algorithms will need to be cataloged and integrated into the NRAO archive system

   Status: testing of PyBDSM source finder on Pilot data by summer REU student A. Cavanaugh with promising results. Further testing underway.

Risk: Medium to High Significant work on pipeline needed, paricularly for imaging, with resources for testing required also.

10.5. Data Product & Archive Design Issues

There are a number of issues related to the data products and archive that need to be worked out before the full survey commences. These include:

1. Spectral resolution for Fine Spectral Cubes

   - The science goals require $\sim$ 10MHz resolution, but resolutions that divide evenly into the 128MHz spectral window width are advantageous for processing (as data from a single spectral window can be used to process those fine channels within with no boundary effects, and these channels can be directly related to the coarse cube planes) and for analysis (gaps at spectral window boundaries are in predictable channel boundaries). A decision of resolution (8, 10, 16, or other MHz) in consultation with the SSG should be made. *Impact: This has only modest impact on imaging pipeline design.*

2. Native Data Format for Images

   - In § 4.4.2, the question of the choice of native data format for image products was raised. Options include: CASA images, FITS, HDF5, and HEALPix. Note that whatever the native format, the archive will need to have the capability to serve the user images in one or more standard formats, and do a conversion if not the native format. A decision of format should be made. *Impact: This has some impact on image pipeline and archive design.*

3. Production & Storage of Cube channels

   - In our data products description, we talk in various places about production and storage of "spectral cubes" (coarse and fine) and "Stokes cubes" (IQU). However, whether these are created or stored as cubes or as individual images (per plane/channel/Stokes), or a mixture (a cube of fine channels in a given coarse cube spw) has not been specified. Note that the choice for image processing also has impact on the efficiency and parallelization (in-house and on AWS/EXCEDE). It is likely users will desire the capability of constructing a cube either from the archive on request or using a simple CASA task/recipe. Note that due to RFI losses, spectral channels will be missing and gaps in cubes must be accounted for. Research into requirements and limitations on cube formats for FITS (or HDF5 or other) format will need to be done, as well as on the availability of 3rd party software to handle these. *Impact: This has some impact on image pipeline and archive design.*

11. Project Schedule

The key high-level milestones and operations deliverables for the VLASS Project are given in Table 19 below.

12. Acknowledgements

The authors of this document would like to acknowledge the hard and effective work done by the VLASS Survey Science Group (SSG) and the numerous White Paper authors and working group participants who

Table 19: Proposed schedule for VLASS Project and operations deliverables

Begin date	**End date**	**Activity or deliverable**
2016 June	2016 September	VLASS Pilot observing
2016 September		Preliminary Design Review
2017 March		Critical Design Review
2017 September	2018 February	Epoch 1 config cycle 1 observing (covers 1st half of sky)
2018 March	2018 August	Single epoch Stokes I BDPs delivered for epoch 1/cycle 1
2018 September	2019 February	Single epoch Stokes QU+coarse spectra BPDs delivered for epoch 1/cycle 1
2018 September	2019 February	Cumulative (epoch 1) Stokes I BPDs delivered for 1st half of sky
2019 January	2019 June	Cumulative (epoch 1) Stokes QU+coarse/fine spectra BPDs delivered for 1st half of sky
2019 January	2019 June	Epoch 1 config cycle 2 observing (covers 2nd half of sky)
2019 July	2019 December	Single epoch Stokes I BPDs delivered for epoch 1/cycle 2
2020 January	2020 June	Single epoch Stokes QU+coarse spectra BPDs delivered for epoch 1/cycle 2
2020 January	2020 June	Cumulative (epoch 1) Stokes I BPDs delivered for 1st half of sky
2020 May	2020 October	Cumulative (epoch 1) Stokes QU+coarse/fine spectra BPDs delivered for 1st half of sky
2020 May	2020 October	Epoch 2 config cycle 1 observing (covers 1st half of sky)
2020 November	2021 April	Single epoch Stokes I BPDs delivered for epoch 2/cycle 1
2021 May	2021 October	Single epoch Stokes QU+coarse spectra BPDs delivered for epoch 2/cycle 1
2021 May	2021 October	Cumulative (epoch 1+2) Stokes I BPDs delivered for 1st half of sky
2021 September	2022 February	Cumulative (epoch 1+2) Stokes QU+coarse/fine spectra BPDs delivered for 1st half of sky
2021 September	2022 February	Epoch 2 config cycle 2 observing (covers 2nd half of sky)
2022 March	2022 August	Single epoch Stokes I BPDs delivered for epoch 2/cycle 2
2022 September	2023 February	Single epoch Stokes QU+coarse spectra BPDs delivered for epoch 2/cycle 2
2022 September	2023 February	Cumulative (epoch 1+2) Stokes I BPDs delivered for 2nd half of sky
2023 January	2023 June	Cumulative (epoch 1+2) Stokes QU+coarse/fine spectra BPDs delivered for 2nd half of sky
2023 January	2023 June	Epoch 3 config cycle 1 observing (covers 1st half of sky)
2023 July	2023 December	Single epoch Stokes I BDPs delivered for epoch 3/cycle 1
2024 January	2024 June	Single epoch Stokes QU+coarse spectra BPDs delivered for epoch 3/cycle 1
2024 January	2024 June	Cumulative (epoch 1+2+3) Stokes I BPDs delivered for 1st half of sky
2024 May	2024 October	Cumulative (epoch 1+2+3) Stokes QU+coarse/fine spectra BPDs delivered for 1st half of sky
2024 May	2024 October	Epoch 3 config cycle 2 observing (covers 2nd half of sky)
2024 November	2025 April	Single epoch Stokes I BPDs delivered for epoch 3/cycle 2
2025 May	2025 October	Single epoch Stokes QU+coarse spectra BPDs delivered for epoch 3/cycle 2
2025 May	2025 October	Cumulative (epoch 1+2+3) Stokes I BPDs delivered for 2nd half of sky
2025 September	2026 February	Cumulative (epoch 1+2+3) Stokes QU+coarse/fine spectra BPDs delivered for 2nd half of sky

contributed to the proposal for which this is but a supporting document. We also acknowledge the input from SSG member Jim Condon, who pointed out the issues of setting survey limits and sensitivity to extended sources and sources with non-flat spectra, and provided many of the calculations presented in § 2.6. Finally, we would also like to acknowledge the constructive input given by the NRAO reviewers of this plan and the VLASS proposal.

REFERENCES

Condon, J. 2015, ArXiv e-prints. 1502.05616

Frail, D. A., Kulkarni, S. R., Ofek, E. O., et al. 2012, ApJ, 747, 70. 1111.0007

Hancock, P. J., Murphy, T., Gaensler, B. M., et al. 2012, MNRAS, 422, 1812. 1202.4500

Mao, S. A., Banfield, J., Gaensler, B., et al. 2014, ArXiv e-prints. 1401.1875

Mooley, K. P., Frail, D. A., Ofek, E. O., et al. 2013, ApJ, 768, 165. 1303.6282

Myers, S. T., Jackson, N. J., Browne, I. W. A., et al. 2003, MNRAS, 341, 1. astro-ph/0211073

Purcell, C. R., Hoare, M. G., Cotton, W. D., et al. 2013, ApJS, 205, 1. 1211.7116

Rau, U., Bhatnagar, S., & Owen, F. N. 2014, ArXiv e-prints. 1403.5242

Winn, J. N., Patnaik, A. R., & Wrobel, J. M. 2003, VizieR Online Data Catalog, 214, 50083